Master's thesis

NTNU
Norwegian University of Science and Technology
Faculty of Engineering
Department of Geoscience and Petroleum

Rehema Kivuyo

Droplets Analysis and Model Development for Oil-water Pipe Flow Experiments

Master's thesis in Petroleum Engineering
Supervisor: Heiner Schumann and Milan Stanko
August 2019

NTNU
Norwegian University of
Science and Technology

Rehema Kivuyo

Droplets Analysis and Model Development for Oil-water Pipe Flow Experiments

Master's thesis in Petroleum Engineering
Supervisor: Heiner Schumann and Milan Stanko
August 2019

Norwegian University of Science and Technology
Faculty of Engineering
Department of Geoscience and Petroleum

NTNU
Norwegian University of
Science and Technology

Abstract

Among other things one of the major challenges in production of crude oil is the associated water that tugs along with oil. The results of the simultaneous production of oil and water is the formation of different flow regimes. These flow regimes can range from as simple as totally separated phases to totally complicated regimes like mixed (dispersed) flow. Different flow regimes are associated with different potential pressure drops over the production line. Precise prediction of the pressure drop along the line is of vital significance during both the design and production phase.The advancement of technology in the Petroleum industry, have been of much input to the industry in development of numerous commercial flow simulators. Unfortunately, these flow simulators have only been accurate for some types of flow. The prediction of flow regimes involving oil-water dispersions is rather unreliable and requires further model studies and improvements. The correct representation of rather complex flow regimes in a simplified way is not always clear. While most models are able to handle the extremes of stratified and fully dispersed flow, the in-between situation of partly or inhomogeneously dispersed flow is often not considered.

This thesis has thus dedicated in two parts. First part is the modelling of the pressure gradient in the two phase stratified flow and the three layers flow. The three layers flow involves two continuous oil and water layers which are separated by dense packed layer of droplets in the middle. The three layers model was extended from the two fluid model by an addition of a homogeneous dispersed layer between the oil and water continuous layers. Both models were Implemented in MATLAB. The models were then tested with the provided data from two different experiments performed in SINTEF laboratory hall. The experiments were conducted in a 220m test section with 4" diameter at different times. The first experiment was conducted with low oil viscosity of 1.43 cp and the later with a medium oil viscosity of 35 cp. The provided data comprised of pressure drops, video recordings, phase fraction profiles and in-situ droplet measurements at different positions along the pipe.

The two fluid model resulted in good predictions of pressure gradients with the predictions that were very close to the experimental measurements. The deviation of modeling predictions and experimental measurements resulted an average absolute error of 1.78% and average relative error of 2.35%. These results were improved by the use of hydraulic diameter in the modeling which reduced the average absolute error to 1.64% and average relative error of 2.14%. The three layers model predicted the pressure drop for very few among the identified three layers flow patterns. The prediction results for such few patterns were good and The model looked okay. The deviation of the model and the measured pressure gradient resulted an average absolute error of 1.02% and average relative error of 1.27%. The three layers model was not improved when the hydraulic diameter was used but performed well when the pipe diameter was used instead. For experiments which were identified to have three layers flow patterns but were not well predicted by the the model, It was proposed that the large deviation in the input phase fractions and the insitu phase fractions could be

the reason to such deviations. Including the effect of slip between the phases was suggested to be a measure to improve these predictions in the three layers flow pattern.

The second part of the report involved the analysis of the droplets sizes from the experiments with medium viscosity(35cp) oil. Flowrate and the pressure drop over a choke valve at the test section inlet were varied to simulate flow disturbance so that at different flow conditions, the droplets behaviours can be captured and interpreted. The comparison was then made between the analysis of experiments with low oil viscosity (were previously analyzed in the Project report) and the medium viscosity oil. Droplets from medium viscosity oil, were found hard to coalesce and to settle at the bottom of pipe during the flow unlike when the oil viscosities were low. The two oils also composed different types and different concentrations of surfactant which was also a contributing factor to the the less development of droplets in the medium oil viscosity experiments.

Declaration

I solemnly declare that the thesis titled DROPLETS ANALYSIS AND MODEL DEVELOPMENT FOR OIL-WATER PIPE FLOW EXPERIMENTS is based on my own work carried out during the course of my study under the supervision of Mr. Heiner Schumann. I further declare that the work contained in this report is original and I have done it under the supervision of my supervisor. Whenever I used materials and information from other sources, I have given due credit to the owners in the text of the report and giving their details in the references.

Acknowledgements

I would like to express my sincere gratitude to God Almighty for being with me through it all,

Special mention to ANTHEI program for offering me a master's degree scholarship, my coordinator Prof Richard Rwechungura, and my supervisor Heiner Schumann of SINTEF, for his enormous knowledge, guidance and mentorship in accomplishing this thesis, I can't imagine bringing about this work without your aid.

Moreover, I would like to thank the whole SINTEF Laboratory staff for all the help and access to their laboratory, along with my college mates especially my best friend Beatrice for the best two years of my intellectual expedition.

Finally saving the best for last, it's no competition but my family is the best family one can possibly be graced with, I'm so humbled to have you for a family. I literary don't deserve you! To my fiance, my parents, brothers and sister, your spiritual, emotional, material and all the support have been felt all along.

Contents

Abstract . . . . . **i**

Acknowledgement . . . . . **iv**

Table of Contents . . . . . **vi**

List of Figures . . . . . **viii**

List of Tables . . . . . **ix**

1 Introduction **1**
1.1 Background 1
1.2 Problem Statement and Objectives 2
1.3 Expected Results 3

2 Literature Review **4**
2.1 Oil-Water Flow Regimes 4
2.2 Pressure Drop 9
2.2.1 Effects of Flow Pattern on Pressure drop 9
2.2.2 Effects of fluid properties on pressure drop 9
2.2.3 Influence of pipe characteristics 10
2.2.4 Pressure drop Calculations 10
2.3 Phase Fraction and Slip 11
2.3.1 Gamma Densitometry 11
2.3.2 Phase fraction and holdup estimation 12
2.3.3 Oil Water Droplets 13
2.4 Droplet Size Distribution 13
2.4.1 Droplets Size Representation 15
2.4.2 Droplets Mechanism 16
2.5 Modelling of oil water flows 17
2.5.1 Homogeneous Model 18
2.5.2 Two fluid model 18
2.5.3 Three Layers Model 19

3 Experimental Overview **21**
3.1 SINTEF flow loop section 21
3.2 Instrumentation 21
3.2.1 Pressure Transducers 21
3.2.2 Optical section 22
3.2.3 Traversing Gamma Densitometer 22
3.2.4 CANTY InFlow Particle Sizer 23

3.3 Fluid System . . . 24
3.4 Data Collection . . . 24

4 Flow Characteristics . . . 26
4.1 Identified flow patterns . . . 26
4.2 Pressure drop . . . 31
4.2.1 Effect of Pressure Drop Across the mixing valve . . . 31
4.2.2 Effects of Water Cut and Flowrate on the pressure gradient . . . 31

5 Oil Water Flow Modeling . . . 33
5.1 Oil water flow modeling . . . 33
5.2 Two fluid model . . . 33
5.3 3 Layers model . . . 38
5.3.1 Comparison of the Model and the Experimental Data . . . 41

6 Droplets Analysis . . . 44
6.1 Droplets Measurement . . . 44
6.2 droplets distribution and sizes . . . 45
6.2.1 Effects of Viscosity on droplets size . . . 47
6.2.2 Effects of Surfactants on Droplets Size . . . 48

7 Conclusion . . . 50

Bibliography . . . 51

A Useful Tables and Charts . . . 56

B Histogram Plots . . . 64

C Normal Distribution Plots . . . 70

D Matlab Codes . . . 72
D.1 Three Layers flow . . . 72
D.2 Two fluid Simple . . . 78
D.3 Histograms, Normal distribution and Mean Sizes . . . 81

List of Figures

2.1 Horizontal oil water flow patterns (Trallero et al., 1997) 6
2.2 Horizontal oil water flow patterns Vedapuri (1999) 7
2.3 Horizontal oil water flow patterns (Vedapuri, 1999) 8
2.4 CANTY Inflow Particle sizer 15

3.1 An Image captured by an optical section to describe the flow pattern 22
3.2 An example of a Phase fraction Profile produced from local Phase fraction data 23
3.3 Positioning of a Sampling point at different water cuts(Fossen & Schümann, 2017) 24

4.1 Homogeneous oil dispersion (Do-H) 26
4.2 Inhomogeneous oil dispersion (Do-I) 27
4.3 Inhomogeneous water dispersion (Dw-I) 28
4.4 Oil continuos dispersion with a dense packed layer of water droplets (Do-DP) 28
4.5 Stratified mixed flow with oil droplets in the water phase (SM) 29
4.6 Stratified wavy flow (SW) 30
4.7 Oil dispersion with the dense packed layer plus water layer 30
4.8 Effect of different mixing on the pressure gradient along the test section . . 31
4.9 Oil dispersion with the dense packed layer plus water layer 32

5.1 2018 Experimental v/s model pressure gradient with pipe diameter used . . 35
5.2 2019 Experimental v/s model pressure gradient with the pipe diameter used 36
5.3 2018 Experimental v/s model pressure gradient with hydraulic diameter used 37
5.4 2019 Experimental v/s model pressure gradient with the hydraulic diameter used 37
5.5 Comparison of the models on the use of pipe diameter and hydraulic diameter 38
5.6 Comparison of the models on the use of pipe diameter and hydraulic diameter 38
5.7 Three layers flow along and across the pipe 39
5.8 Relationship between the circle geometry and the pipe cross section occupied by 3 layers of phases 40
5.9 experimental v/s model prediction pressure gradient 42
5.10 Pressure gradient versus input water fraction for different mixture velocities. 42
5.11 Comparison of the models on the use of pipe diameter and hydraulic diameter 43

6.1 Manual counting of droplets by image j 45
6.2 Normal distribution plots for Pressure drop of 0.1, 0.2, 0.35, 0.5 and 1 bar at the mixing valve respectively 46
6.3 The Sauter mean diameter for different oils and pressure drops across the mixing valve 47
6.4 Maximum droplets diameter for different oil viscosities and Pressure drops across the valve 49

A.1 2019 experimental data 58
A.2 2019 experimental data 59
A.3 2019 experimental data 60
A.4 2019 experimental data 61
A.5 2019 Identified Flow Patterns 62
A.6 Piping and instrumentation diagram 63

B.1 Histogram plots for experiment ce19027,002: WC=0.2, Umix=1m/s, DP=0.1 bar 65
B.2 Histogram plots for experiment Ce19027,000: WC=0.2, Umix=1m/s, DP=0.2 bar 66
B.3 Histogram plots for experiment Ce19027,001: WC=0.2, Umix=1m/s, DP=0.35bar 67
B.4 Histogram plots for experiment Ce19027,003: WC=0.2, Umix=1m/s, DP=0.5bar 68
B.5 Histogram plots for experiment Ce19027,004: WC=0.2, Umix=1m/s, DP=1bar 69

C.2 Normal distribution plots for 0.1, 0.2, 0.35, 0.5 and 1 bar respectively 71

List of Tables

A.1 Dmax and Sauter mean diameter: Umix=1m/s, WC=0.2, DP=0.1bar 56
A.2 Dmax and Sauter mean diameter: Umix=1m/s, WC=0.2, DP=0.2bar 56
A.3 Dmax and Sauter mean diameter: Umix=1m/s, WC=0.2, DP=0.35bar . . . 56
A.4 Dmax and Sauter mean diameter: Umix=1m/s, WC=0.2, DP=0.5bar 56
A.5 Dmax and Sauter mean diameter: Umix=1m/s, WC=0.2, DP=1bar 57

Acronyms

A	Cross-sectional area of the pipe
D	Internal pipeline diameter
D10	Arithmetic mean
D32	Souter mean
D43	De Brouckere mean
Dmax	Maximum droplet's diameter
Do-DP	Oil continuous dispersion with a dense packed layer of water droplets
Do-H	Homogeneous oil dispersion
Do-I	Inhomogeneous oil dispersion
DP	Pressure drop
DPvalve	Pressure drop across the valve
Dw-DP	Water continous dispersion with dense packed layer of oil droplets
Dw-H	Homogeneous water continuous dispersion
Dw-I	Inhomogeneous water continuous dispersion
f	Friction factor
Hw	Local water fraction
k	Phase
MI	Stratified flow with mixing
n	Number of particles
O-W	Oil in water emulsion
Qo	Oil flowrate
Qw	Water flowrate
R	Radius
Re	Reynolds number
S	perimeter
SM	Stratified mixing

SS	Stratfied smooth
ST	Stratified flow
SW	Stratified wavy
Umix	Mixing velocity
Uso	Superficial oil velocity
Usw	Superficial water velocity
WC	Water cut
W-O	Water in oil emulsions
y	Position in pipe cross-section
ρ	Density
α	Phase Fraction
τ	Shear stress
μ	Viscosity
ε	Insitu Phase Fraction
θ	Inclination Angle
Nw	Weber number

Chapter 1

Introduction

1.1 Background

Regardless of the fact that oil is the desired fluid to be produced in petroleum industry, existence of oil/water flows during production and transportation phases of oil in petroleum industry is a rather common phenomenon. There are few cases in which water production is helpful, for instance during production of more viscous oil whereas water is injected in the reservoir and produced with oil to facilitate the transportation to the surface and to the processing facilities Hasan et al. (2010). Here the oil is dispersed in water forming droplets that are transported in water as continuous phase. The flow then has properties more similar to those of pure water, avoiding the high pressure loss that would be experienced with a high viscous oil. It was also mentioned by Arirachakaran et al. (1989) that the methods of transporting heavy crude oil, was made possible by introducing water in predetermined ratios to form the mixture that can easily be transported through pipelines.

During production, the produced water along with Oil usually increases as the life of the producing fields increases. Sometimes the volume of produced water climbs rapidly and exceed the volume of produced oil. This is because the fields have been almost depleted and the little remaining oil in the reservoir, is produced with water that was initially present in the reservoir or the injected water to enhance the oil recovery Petrowiki (2012). Massive water production limits the production of oil in a number of ways, and may pose a great threat to the field's economy if poorly forecasted. The excessive production of water in petroleum fields requires that the available water producing, handling and disposing facilities have enough capacity and ability to handle these water, which is usually very costly. Production of oil associated with water could also cover very large distances as it is produced from the reservoir to the platform, to the shores and finally to the processing facilities. Large distances are associated to large loss in pressure in the pipeline such that, boosters and pumps could be required to aid the transportation. The installation and operation of these equipment is costful and over a long run they could be uneconomic. Water production could also form strong stable emulsions with oil in the presence of natural surfactant, which later brings complexity in separation processes.

The distribution of oil and water when flowing together usually takes different forms, as they flow from the reservoir to the surface and during surface transportation. These distributions ranges from totally separated phases to totally mixed phases. The distribution of these phases is termed as flow regimes or flow patterns. Different flow patterns have been identified

by many researchers but the main patterns include, Smooth stratified flow (SS), Stratified mixed(SM), Inhomogeneous dispersion(could be oil in water or water in oil (Do-I, Dw-I)), Dual dispersion(D O/W & W/O) and Homogeneous dispersed flow(could be oil in water or water in oil dispersion (D W/O)). The flow patterns have large influence on the flow parameters since different flow regimes causes a different flow behaviorsAngeli & Hewitt (2000). The variation and complexity of these flow patterns which is caused by the low difference in oil and water densities Brauner (2002), have brought a big interest in the oil industry. The flow patterns and their respective hydrodynamic characteristics thus requires enough attention and consideration in the petroleum field.

1.2 Problem Statement and Objectives

Different flow regimes from oil water flows, causes different potential pressure drop in the flowlines. The accurate predictions of pressure drop is essential for the production monitoring itself and designing of the production facilities. Different models and Commercial simulators have been designed to predict the pressure drop of multiphase flows through the lines. These models and simulators are however very few and are not reliable in the predictions of oil water flow parameters. The available models often only consider the two extreme situations of fully separated (stratified) flow or fully and homogeneously dispersed flow, but do not consider the in-between situation of partly or in-homogeneously dispersed flow.

The main objective of this thesis is to study oil-water flow behavior based on data from two experimental campaigns, and use these data to test and/or improve the models that covers the stratified and three layers flow for the prediction of pressure gradient along the pipe. The secondary objectives are:

- Relate observed flow patterns with the measured pressure gradient
- Test and if necessary improve the provided flow models against the data.
- Produce droplet size information from the available sampling data.
- Compare the two experimental campaigns and conclude on the effect of viscosity

This report will therefore generally cover two main parts. The first part is based on the modelling of oil water flow patterns, specifically the stratified and the intermediate flow between stratified and dispersed flow (Three layers flow patterns). The flow patterns were identified from the 2018 and 2019 experimental data provided by SINTEF conducted in a 220m test section in the laboratory hall. The provided data included the flow video recordings from the transparent part of the test section, the phase fraction profiles from the traversing gamma densitometers, pressure recordings from nine pressure transducers and the droplets images taken by a CANTY Inflow particle sizer. Other data can be seen in table A1 to A3 in the Appendix A. A sketch of the test section can be found in Appendix A. A choke valve mounted at the test section inlet was used to produce different states of pre-mixing of the flow.

This thesis also focus in the assessment of the effects of oil viscosity and presence of surfactant on the flow behaviour by using data from the two different experiments conducted on 2018 and 2019 in SINTEF. The previous data of 2018 were from the mixture flow of water and low viscosity oil (1.43cp) with a known type and concentrations of surfactant added to facilitate the stability of emulsions. The new experiment composed the flow mixture of water with

a blend of an old used oil containing the surfactant and a new light oil without surfactant. The resulted oil measured an oil viscosity of 35cp with a Span80 surfactant of unknown concentration.

1.3 Expected Results

By the end of this thesis therefore, two models, a two fluid model and a three layers model are expected to be reported to provide with the good pressure drop predictions for the stratified and three layers flow patterns. The effect of oil viscosity on the flow pattern maps, pressure drop and droplets setting and growth will also be reported. Finally the influence of surfactant on the flow pattern will also be discussed and presented.

Chapter 2

Literature Review

2.1 Oil-Water Flow Regimes

During the flow of two immiscible liquids, there is a tendency of liquids to distribute themselves inside the flowline forming different flow patterns. The forms in which these liquids distributes inside the flowline depends on different factors. Elseth (2001) mentioned these factors as the flow rate of the mixture (flow velocity), the ratios of input phases, density and viscosity ratios, the geometry of the transporting pipe and the interfacial tension between fluids and the pipe. Ibarra et al. (2014) categorized these factors as the three basic parameters namely; flow velocity, fluid properties(density, viscosity, wettabillity and the surface tension) and the pipe characteristics(pipe diameter, wall roughness and the geometry of the pipe). Angeli & Hewitt (2000) summarized the previous research works in section 2.2 that were conducted to identify how the fluids viscosity, density and the wetting properties of the wall influence the flow patterns and the pressure drop in the pipes.

Understanding flow regimes is essential in multiphase flow studies since each flow pattern influence the flow parameters differently. It is vital therefore that these flow patterns are categorized in a way that the important flow parameters such as pressure drop and phase fractions can be correctly deducted. A number of methods are currently employed to identify the flow patterns but the most common method is based on visualization of flow through transparent pipes. This method however was observed to be subjective and affected by reflections of light (Elseth, 2001; Angeli & Hewitt, 2000) leading to the introduction of other methods that will complement these observations. Other methods involved the use of conductivity probe by Nädler & Mewes (1995), High frequency impedance probe Vigneaux et al. (1988) and gamma ray densitometers as they were used by Elseth (2001) and Schümann (2016) to obtain the distribution of phases in the flow and finally predict the flow regime.

Most researchers have classified the flow patterns by giving them different names and different definitions based on their observations but the most common flow patterns will be mentioned here under:

- Stratified Smooth: This flow pattern occur when the two immiscible liquids completely separate by their density differences forming two continuous phases with a clear interface. Normally this type of flow happens for low velocity flows in horizontal pipes, where the two immiscible liquids naturally segregate themselves with the less denser liquid on-top of the denser liquid, following the gravity force that is acting perpendicu-

lar to the direction of flow Trallero et al. (1997). It was also observed by Elseth (2001) and Schümann (2016) that this flow patterns appear at low velocity with intermediate water cuts.

- Stratified wavy; Slight increase of mixture velocity, creates some disturbance at the interface of the liquids forming a wavy like plane in between the two layers. Angeli & Hewitt (2000) observed this pattern at slightly increased of flow velocity in the experiments she conducted in an acrylic pipe. Elseth (2001) also observed the stratified wavy pattern at slightly higher velocity and at lower and higher water cuts.
- Stratified mixed; This type of flow pattern includes two continuous layers of oil and water phases with either of the two phases suspending the droplets of the other phase Soleimani (1999). At slightly higher flowrates, Elseth (2001) and Trallero et al. (1997) observed the formation of droplets near the interface of the two phases from the stratified wavy flow pattern. The droplets increased as the flow rate increased because of the break-up of interfacial waves. Elseth (2001) mentioned that these droplets were kept so close to the interface because the phases couldn't have enough energy to suspend these droplets.
- Three layers flow; In this type of pattern, flow generates a separate layer of oil or water droplets at the middle just like in a stratified mixed pattern. The only difference here is that both the top and bottom of the pipe remains with continuous oil and water with an addition of a third layer which is a dispersed layer. Vedapuri (1999), Angeli & Hewitt (2000) and Soleimani (1999) observed and reported this type of flow pattern in their experiments. The generation of droplets at the interface is usually attributed by the mixture velocity, oil viscosity or even the pipe inclination. Vedapuri (1999) analyzed the pipe cross section for the three layers patterns as it can be observed in figure 2.3 and 2.2.
- Dispersed flow; In dispersed flow, the flow is characterized by a single continuous layer of one of the phases, with the other phase homogeneusly or inhomogeneouly distributed in form of droplets in the other phase Angeli & Hewitt (2000). This type of flow patterns mostly appear at higher flow velocities and low water or higher water cuts. Different forms of dispersions have been observed and reported by several researchers but will not be covered in this thesis work.

The figure below shows different flow patterns as they were identified by different researchers in their experimental works.

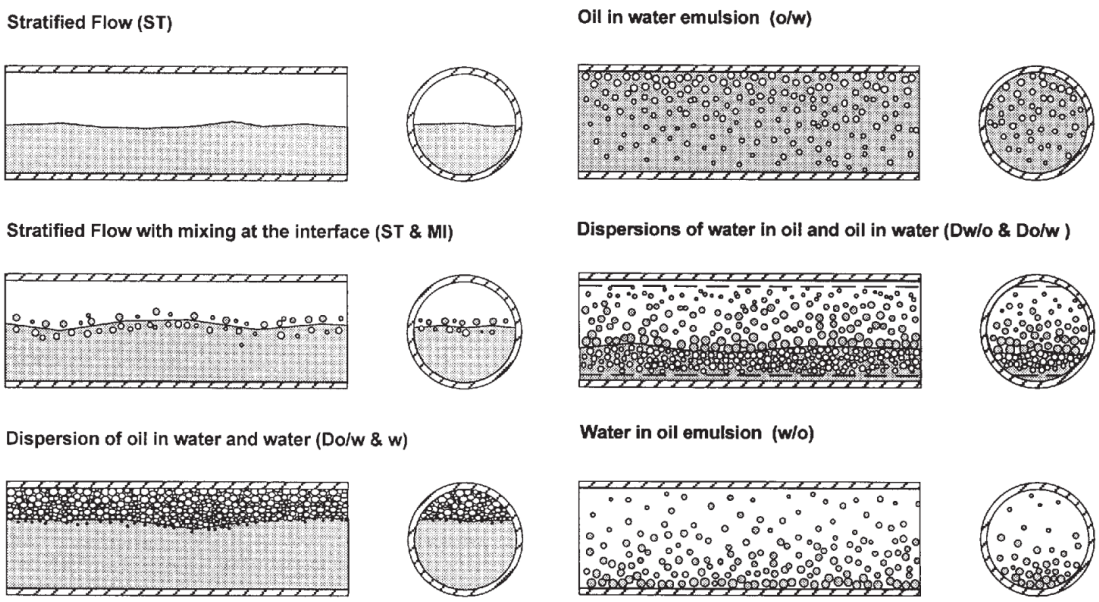

Figure 2.1: Horizontal oil water flow patterns (Trallero et al., 1997)

Figure 2.2: Horizontal oil water flow patterns Vedapuri (1999)

Figure 2.3: Horizontal oil water flow patterns (Vedapuri, 1999)

2.2 Pressure Drop

Pressure drop is a very significant parameter in the oil industry as it plays a major role in field designing and operational cost. Before production, the effective design of production and processing facilities requires the selection of proper materials and parameters (diameter and thickness) capable of sustaining the allowable pressure ratings restraints and pressure drop when transporting liquids from one point to another. Knowing how the pressure drops are calculated through the flowlines and other facilities is the first step towards predicting how pressure will behave in a flowline. This will be explained in the next section.

Pressure drop in oil-water flows is greatly influenced by the flow patterns, fluid properties(viscosity and density) and pipe characteristics(roughness, diameter, inclination).

2.2.1 Effects of Flow Pattern on Pressure drop

In the variation of pressure gradient with velocity and water cut, Soleimani (1999) related these variations with flow patterns where he found a characteristic peak in pressure gradient at the the phase inversion point in dispersed flow. The phase Inversion point refers to the phenomenon that occurs when oil water dispersion reverts its form oil in water dispersion to water in oil dispersion. Trallero et al. (1997) observed the decline in pressure loss when the flow was changing from stratified flow to dispersed flow. Al-Moosawy et al. (2008) also experienced the changes of pressure drop with the changes of flow regimes. In his experiments, the increase in water flow rates led to a substantial increase in pressure gradient which he mentioned that it was attributed by the larger fraction of pipe wall being covered by a rough oil-water interface which increases the frictional factor and the pressure gradient. Al-Moosawy et al. (2008) also mentioned that increased oil flow rates also led to the increased pressure drop. Angeli & Hewitt (1999) found a peak in pressure gradient at higher mixture velocity where the dispersed flow patterns dominated at the phase inversion point in the experiments she conducted in an acrylic pipe. Most studies and observations suggests that, for low flowrates where the flow is mostly stratified, the frictional drop dominates the flow Al-Moosawy et al. (2008). Increasing flowrates increases the dispersion and entrainment resulting in to higher pressure drop in the pipesAl-Moosawy et al. (2008).

2.2.2 Effects of fluid properties on pressure drop

The main fluid properties that are likely to influence the pressure drop are fluid viscosity and density. The internal frictional force that liquids exhibits when flowing is called Viscosity. This frictional force exist in different layers of the liquids as they move past each other. The viscosity of liquids exists from the cohesive forces that bounds the same molecules together. A more viscous liquid means more internal friction and so will the pressure drop be. Most oil water experiments involve water with different oils in varying temperature conditions. Different temperature conditions allow for investigation of viscosity effect in flow. Arirachakaran et al. (1989) found that the pressure drop in the pipe is a function of viscosity, input water fraction and mixture velocity. He reported that the temperature and viscosity have a small effects on the mixture pressure drop for an oil in water dispersion when oil viscosity is higher than the water viscosity. For the water in oil dispersion however, Arirachakaran et al. (1989) mentioned that the pressure drop is highly affected by temperature since the viscosity of the

oil is largely affected by temperature. Vuong et al. (2009) studied the effect of viscosity on oil water flow, keeping the superficial oil and water velocities constant and found that the increase in oil viscosity increased the pressure gradient in the horizontal pipes.

The segregation of two immiscible liquids is aided by the differences in their density. Dispersing one fluid in the other fluid greatly depends on the difference of densities between the two fluids. If the density difference is small however, it will be more difficult to disperse these liquids. Charles et al. (1961) studied the effect of density on flow patterns using liquids of the same densities but did not find any stratified flow. He found that small density difference of liquids were easy to disperse while the large density difference were hard to disperse.

2.2.3 Influence of pipe characteristics

Here the characteristic properties such as pipe geometry, pipe material, pipe roughness and diameter are highly likely to affect the flow characteristics and pressure drop at large. For the diameter and the surface roughness these are the common pipe properties that affects the pressure gradient through the pipelines. Other properties such as wettability and pipe inclination have not extensively been studied despite their contribution in drop of pressure especially in the oil and gas pipelines through rough terrains. Soleimani (1999) highlighted about the effect of pipe material on the wetting properties of the fluid. He mentioned that the degree of wall wetting is the function of wall pipe material and all the dynamics of the flow motion close to the pipe wall. Angeli & Hewitt (1999) performed the experiments in steel pipe and acrylic pipe only to discover that the two pipe material gave out different results which could not be explained based on wall roughness only. She found out that the wetting characteristics of the two different pipes was responsible for the difference in their results.

Amundsen (2011) conducted her experiments in horizontal and inclined pipes from $-10°$ to $+10°$. She generally found out that, the frictional pressure gradient in upward flows is lower compared to downward flows at medium to low water cuts due to the gravity forces acting opposite to the flow in the upward direction resulting in the accumulation of high density water phase. she also found that,for the horizontal, downward and upward flow at medium to high water cuts, the pressure gradient in two phase flow is larger than in single phase flow. Between the downward, horizontal and the upward inclined flows, Amundsen (2011) reported that the normalized frictional pressure gradient were similar in terms of trends and the absolute values.

2.2.4 Pressure drop Calculations

The calculations of pressure drop in a pipe with two fluids (liquid-liquid) is not so much far from those of single phase. Understanding the type of flow pattern before attempting to estimate the pressure drop is the key to these estimations. For a single phase fluid flowing fully inside a cylindrical pipe of uniform diameter, the pressure drop is calculated from the common Darcy Weisbach equation below,

$$\frac{\Delta P}{L} = f_D \frac{\rho}{2} \frac{v^2}{D} \tag{2.1}$$

where

f_D - friction factor

ρ - Density of the liquid

v - velocity of the fluid

D - Pipe diameter

Estimations of friction factor is from different published correlations such as Colebrook (1939), Moody (1944), Haaland (1983), Blausius (1911) etc, which mostly requires the estimation of a Reynolds number to know if the flow is laminar or turbulent. Reynolds number is calculated using the formula below

$$Re = \frac{\rho v D}{\mu} \tag{2.2}$$

For a single phase flow, the density ρ and the viscosity μ of the fluids are those of single phase fluid. for two phase flow, the viscosity and densities are calculated following the respective flow patterns. For a homogeneous dispersed two phase flow, the density of two phase flow(Oil water flow) without considering slip between the phases is calculated as shown below

$$\rho_m = \rho_w \alpha_w + \rho_o (1 - \alpha_w) \tag{2.3}$$

The effective or apparent viscosity of two phase flow typically for dispersed flow is calculated based on different models suggested by different researchers. Mooney (1951), Brinkman (1952) and Pal & Rhodes (1989) proposed models for the determination of the effective viscosity of the liquid mixtures in form of dispersion. For the stratified flow, the pure viscosities of each phase is used in the calculations since each layer of fluid is treated and calculated separately then the total pressure drop for all the layers is estimated from the individual layers. The holdups for the estimation of velocities for each layer have to be present and can either be obtained from experiments or closure laws. These closure laws can be used to calculate the slip (velocity difference) between the two phases but they are very tricky and still not completely understood. When inside the pipe, the two separate layers are calculated as the whole pipe flows but with hydraulic diameters.The calculations of two phase flow pressure gradient for the stratified and dispersed flows will be covered well in the models section.

2.3 Phase Fraction and Slip

When oil and water distributes themselves differently and occupy different flow regimes, at every point in a pipe cross section there is insitu water and oil volume ratios occupying that cross section of the pipe. The input volumetric ratios of water and oil to the total volumetric flow is called phase fraction of the phases. Phase fraction are usually known since they are set points for the designed experiments. The insitu local fractions however, are unknown and can be obtained from special measurement devices such gamma ray densitometer, impedance probe, and conductivity probes or can be calculated from the formulas.

2.3.1 Gamma Densitometry

Gamma densitometry is a technique used to determine void fractions for multiphase flows and was used for measurements of the data analyzed in this work. It is applicable for liq-

uid - liquid flow and gas - liquid flows. Gamma densitometers are also employed for field measurements of phase fractions in offshore pipelines that are important for multiphase flow metering (Elseth, 2001). The gamma instrument contain a radioactive source from which the incident unidirectional photon flux is given. This is employed normal to the test section through the pipe wall to the two phase mixture then goes through pipe wall, again to the detector collimator and finally to the detector itself. There is an exponential relationship between the incident beam and the thickness of the absorber plus the local intensity of the beam which depends on the absorption coefficient of the two fluids (Elseth, 2001). The system was regularly calibrated by using the single phase oil and single phase water in order to obtain the absorption coefficients of oil (γ(o)) and water (γ(w)). The absorption thickness could be determined from the knowledge of the gamma beam intensity. For a known thickness of absorption, the amount of material can be calculated. Therefore the fraction of water in an oil water flow can be measured for every point in the pipe. In For the experiments conducted in SINTEF, the water fraction in the pipe was measured by traversing the gamma densitometer in vertical direction. At the same time only a thin photon beam penetrated the pipe. Thus, vertical phase fraction profiles were produced (side view)

2.3.2 Phase fraction and holdup estimation

Local/insitu phase fractions also known as holdup is the ratio of the cross-sectional area occupied by one phase relative to the total cross-sectional area of the pipe at that particular point.The determination of local phase fraction is important for the accurate prediction of pressure drop and and the volumetric flow of phases. Equation 2.4 and 2.5 below shows how the volumetric phase fraction and the local(insitu) phase fractions are calculated respectively.

$$\alpha_w = \frac{Q_w}{Q_w + Q_o} = \frac{U_{sw}}{U_{sw} + U_{so}} \tag{2.4}$$

with,

$$\alpha_w + \alpha_o = 1$$

$$H_w = \frac{A_w}{A} \tag{2.5}$$

The components of multiphase flows, usually flows with different velocities. Depending on the amount of the water cuts, flow rates of liquids, the liquids properties and the orientation of the pipe one of the two phases might be moving at a higher speed than the other. The difference between the flowing liquids velocity is what is known as slip. Slip is the result of shear vs gravity forces battles acting on the flow inside a pipeline. The ratio between the insitu oil velocity to the water velocity is the slip ratio. When slip ration equals 1, it means the two phases are moving at the same speed. when slip is less that one, it mean that water is the fastest moving liquid and vice versa when slip is larger than unity. Slip ratio can also be obtained from the insitu volume fractions averaged over pipe cross section and input volume fractions data as shown in equation 2.7

$$S = \frac{U_o}{U_w} \tag{2.6}$$

$$S = \frac{\frac{\alpha_o}{\alpha_w}}{\frac{Ho}{Hw}} \tag{2.7}$$

2.3.3 Oil Water Droplets

When Crude oil is produced along with water in the production lines, fluids may be flowing as two separate layers (stratified flow) or take the form of dispersion. Flow induced dispersions require sufficiently high velocities. However, in a production system, the presence of high shear devices, such as pumps and valves, can efficiently disperse the flow. For the case where the viscosities of fluids varies greatly, the dispersion are difficult Pergushev & Tronov (1998). After a long run in the pipeline these flows may again separate to form a stratified flow if there are no/too low emulsion/dispersion stabilizers. Low oil and water cuts can also cause dispersion for typical field flowing speeds. Dispersion are stabilized by the presence of natural surfactant and added production chemicals that can act as surfactants that are present in the produced fluids especially oil. The composition of crude oil varies between different oilfields and so does the amount of surfactant in the oil. Heavy oil contains a lot of Asphaltenes and resins which are very good surfactant Schlumberger (2016). Solutions with a lot of surfactant will of course be more stable hence create more challenges in the separation process, increased pressure drop along the transporting lines and, causes trips and upsets in the wet crude transportation and processing facilities.

During the turbulent dispersion flows, where oil water droplets exist especially, continuous process of droplet coalescence and breakup usually takes place. Better understanding of behaviours of these droplets during the oil water flow can therefore provide an understanding of the flow and its dispersive processes. The best way to explore the behaviour of these droplets is through the in-situ measurement and analysis of their sizes. Liu & Li (1999) stated that the continual breakup and coalescence of droplets do not only determine the distribution of droplets sizes which is an equilibrium process but also have a profound influence on the mass transfer. To accurately investigate and understand the droplet sized data, all the important variables such as fluid properties, types of droplet measurement techniques, type of measurement equipment, sampling process, data analysis and presentation should be well understood as they all have a strong influence on the sizes of droplets Schick (1997).

2.4 Droplet Size Distribution

Generally, oil water flows have droplets ranging between 0.1 μm to 100 μm in diameter Petrowiki (2012). Droplet size distribution in oil water flows is a function of inter-facial tension, shear, nature and amount of emulsifying agents(surfactant), presence of solids, and bulk properties of oil and water. Special instruments have been engineered to analyze liquid droplets in the flow under varying conditions of flow-rates, pressure and temperature. Amongst many methods used for droplets characterization, the most common recently used methods are mentioned here under Liu & Li (1999)

- Measurement of a number of different sized droplets by using image analysis software (Microscopy and image analysis)
- Focused-beam reflectance measurement (FBRM)

- Laser diffraction (LD)
- Ultrasonic attenuation spectroscopy (UAS)

Microscopy and Image Analysis

Microscopy is the most direct method that is used to acquire images of droplets in dispersed fluids. Real-time capturing of videos/images of the droplets enable the changes in the droplets size to be detected by the aid of Image Processing technology. CANTY Inflow Particle analyzer, is an example of a microscopy and will only be explained in this chapter since it was used for the present experiments.

Acquiring Droplets Images

CANTY Inflow Particle analyzer seen in Figure 2.4 provides real time measurements of oil in water or water in oil droplets. It can be placed inside the flow providing an inline measurements or outside the flow system with a small sample tube directing fluids towards it. On one side it has a Camera that is used to capture the videos of the droplets with the light source on the other side to illuminate the droplets to be captured. CANTY provides the fluid sample or the continuous flow a microscopic non destructive and a two dimensional view system of the output in form of video camera recordings or pictures which later will be analyzed separately Schlumberger (2016). Counted droplets demands to be very representative of the actual sampled fluid and for that reason it is recommended that the size of the sampling probe directing fluids towards the CANTY should be larger than the droplets themselves. This will ensure that large droplets do not break up to form smaller droplets which will later affect the results. CANTY Inflow particle sizer has a gap which can be varied to allow easy and non destructive passage of droplets to be captured by a video Camera. The size of the gap varies between 0 to 0.5". The identified droplets in the video Camera/picture need to undergo counting process in which each droplets size will be measured

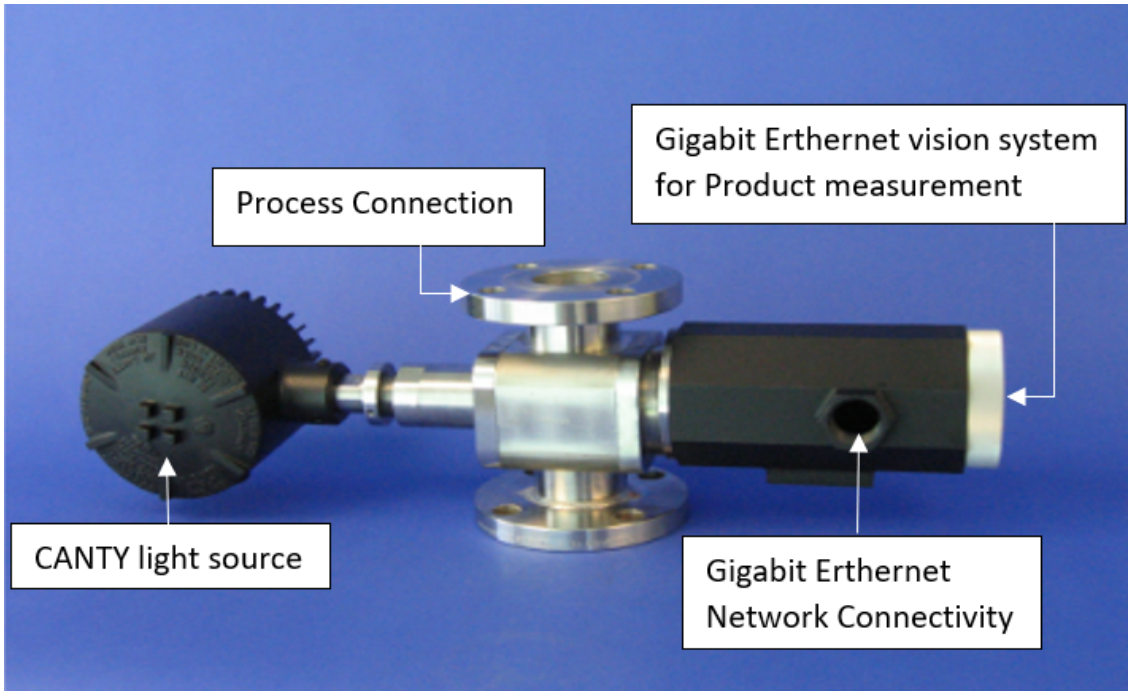

Figure 2.4: CANTY Inflow Particle sizer

2.4.1 Droplets Size Representation

A large number of droplet sizes obtained from the measurements are collected and analyzed in a way that the important information can be deducted from it. Different statistical methods are used to represent the size distribution of droplets from a set of hundreds and thousands data in to a single number or a single diagram with a physical meaning. A number of statistical ways have been used to represent the droplets sizes such as calculating different types of averages, plots of histogram, cumulative distributions and normal distributions. Different averaging methods such as arithmetic mean, geometric mean and harmonic mean are available. When dealing with droplets the most common ways of finding average as discussed by Malvern (2012) have been mentioned below;

- Arithmetic mean (D10): Also known as the number length mean is the normal average for all the droplets, taken as a sum of all the droplets sizes divide by the total number of droplets. This number is important when the total number of particles/droplets is of interest. This type of averaging is limited to the number of particles available as it requires the total number of particles to be known.
- Volume mean diameter (D30): This is the diameter's droplet which when it's volume is multiplied by the number of droplets results in the total volume of droplets. This method also require the total number of particles or droplets to be known.

$$D30 = \frac{\sum_{i=1}^{n} n_i \cdot {D_i}^3}{\sum_{i=1}^{n} n_i} \tag{2.8}$$

- Sauter Mean Diameter (D32): Also known as surface-volume mean, is the averaging method defined as the diameter of a sphere that has the same volume/surface area ratio as the particle of interest Filippa et al. (2012). For a collection of different sized spherical objects, sauter mean diameter is equal to the diameter of identical spherical

objects forming an equivalent collection of spheres. This means that the whole system has different sized spherical objects whose total surface area and total volume is equal. This is a mostly common method used in the characterization of bubbles, droplets Atkinson & Strauss (1978), Fossen & Schümann (2017), Liu & Li (1999) and sediments Filippa et al. (2012). This type of mean is mostly sensitive to coarse particles as it has been discussed by Filippa et al. (2012).

$$D32 = \frac{\sum_{i=1}^{n} n_i \cdot {D_i}^3}{\sum_{i=1}^{n} n_i \cdot {D_i}^2} \tag{2.9}$$

- De Brouckere mean diameter D43: Also known as volume mean diameter is the diameter that reflects the size of particles that usually constitute the bulk of the droplets size. This method is sensitive to droplets of large diameter size Malvern (2012).

$$D32 = \frac{\sum_{i=1}^{n} n_i \cdot {D_i}^4}{\sum_{i=1}^{n} n_i \cdot {D_i}^3} \tag{2.10}$$

Different charts/figures through which the numerical data can be presented resulting to a significant meaning is another way of presenting the the droplets sizes. Figures are the best representation as they can show different droplets size distribution at a particular position in relation to what they represent inside the flow. There are many graphical ways of representing the droplets sizes such as Normal distribution curves, histograms, cumulative distribution plots, scattering data as well as fitting curves and lines on the scattered data Malvern (2012). In this work normal distribution curves, histograms and fitting lines on scattered data were the graphical methods of representation used.

2.4.2 Droplets Mechanism

The most researched droplets mechanisms that have been observed in most research works involves droplets formation, droplet coalescence, droplet breakup, droplets flocculation and escape Amundsen (2011). Droplets coalescence and breakup are the most common mechanisms that occur in turbulent dispersionLiu & Li (1999). The generation of droplets starts at the oil water interface where the instabilities of flow are likely to attack. The formation of droplets were studied by Roumpea et al. (2019) in a flow focusing microchannel with the presence of surfactant and he identified three stages that the droplet formation can occur. These stages were expansion, necking and pinch-off of part of a suspended liquid. Lignel et al. (2017) also studied the droplet formation in a flow focusing micro-system by using pressure and flowrate driven pumps. She found out that droplets are generated within a certain range of pressure difference between the inlet and the outlet(thus flowrate).

Chesters (1991) studied the mechanisms of droplets coalescence and stated that the whole process starts with the deformation of the droplets. After deformation, the film of the continuous phase will be trapped by the droplets and then the inertia, interfacial and the gravity forces will cause the film drainage until it raptures and form a new bigger droplet. Amundsen (2011) highlighted that the droplets coalescence occur when droplets collide, remain in contact for some period of time until it is sufficient for them to merge. The formed droplet results in a smaller surface area making it energetically stable. Droplets break-up usually occurs when the droplet has reached it's maximum size Pergushev & Tronov (1998). The process of droplet breakup usually occurs at the mixers, pumps, bends, other restrictions

and by the flow itself. Based on the hydrodynamic Taylor theory, Hinze (1955) made an analysis of droplet break-up and obtained an equations which represent the dimensionless numbers for which the process of droplets breakup will occur. The first dimensionless number in equation 2.11 which is a Weber number shows a critical number above which the droplets breaks. This happen when the surface forces overcome the inertia forces. Hinze (1955) concluded in his studies that the forces from the continuous phase were responsible for the deformation of the droplets. The second number in 2.12 varies in a wide range depending on the ratio of viscosities. He also concluded that the interfacial tension and viscosity of the dispersed phases stabilizes the droplets.

$$N_w = \frac{\mu_c S_v d}{\sigma} = \frac{Viscous force}{Surface force} \tag{2.11}$$

$$N_{vi} = \frac{\mu_d}{\sqrt{\rho_d \sigma d}} \tag{2.12}$$

General distribution of droplets in the flow

Lovick & Angeli (2004) studied the droplets size in dispersed liquid-liquid flows. They found in the most appeared dual continuous flow pattern that the size and the concentration of droplets decreased at each side from the oil water interface. They also found a very small variation of sizes of oil droplets contained in the water continuous layer and those of water contained in oil continuous layer. At different mixture velocities, Lovick & Angeli (2004) did not find any significant effect on the droplet sizes of either phase. This was explained from the observation that even in higher velocities where the flow would result in smaller droplets, they were accompanied by the increased entertainment of one phase dispersed in to the other phase that favoured the larger drops.

Fossen & Schümann (2017) studied the effects of pressure drop, flow rate and phase fractions on the droplets size produced on the mixing valve. They found that there was a systematic trend in the data that showed the production of lower maximum droplets attributed by the increasing pressure drop across the mixing valve. They also found that the flow rate has a very little effect on the droplet size when passing the valve and keeping other properties, such as pressure drop constant. Fossen & Schümann (2017) also reported that upon changing the water cuts from 5% to 95%, 30% and 70% showed the same trend as that of pressure drop that low maximum droplets were produced in these water cuts. Pal (1996) studied the effects of droplets size on the rheological behaviour of oil in water and water in oil emulsions on the controlled stress Rheometer. His results showed that the fine emulsions resulted in to high emulsion viscosity and the storage moduli while the coarse emulsions were associated with lower viscosities. He explained his results based on the shear thinning effect that is much stronger on fine emulsions than in coarse emulsion.

2.5 Modelling of oil water flows

During the flow of oil and water, many processes happen within the flow. It is important to be able to predict the unexpected variations in the flow so that the whole system is properly controlled. There are two types of models, Empirical models and Mechanistic (Phenomenological) models. Empirical models are models that are constructed from relations

that are based on experimental data. Mechanistic models are models based on the physics of flows such as forces, turbulence, mass and momentum transfer. Models have a wide range of applications when it comes to oil and gas. They can be used to predict the mass flow rate of fluids(multiphase) flowing in the pipes, the flow regime, phase fractions and pressure drop within the length section of a pipe. This thesis will focus in the modeling of pressure drop associated to their respective flow regimes.

2.5.1 Homogeneous Model

The homogeneous model consider the mixture flow of oil and water as a single phase that is flowing in a pipe. The mixture contains oil droplets dispersed in a continuous water or water water droplets in oil continuous phase. The properties of the mixture such as density with no slip is calculated as indicated in equation 2.3 while the effective viscosity of the mixture can be obtained from different models such as that of Pal (1988) models. The pressure drop for the homogeneous is only contributed by the frictional pressure drop since the gravitational force disappear. Equation 2.13 is used to calculate the pressure gradient of a homogeneous dispersed flow

$$-\left(\frac{dP}{dx}\right) = \frac{f_m \rho_m U_m^2}{2D} \tag{2.13}$$

2.5.2 Two fluid model

The two fluid model is a suitable model in the prediction of holdups and pressure drops in separated flows. The relationship between the walls, the fluids interfacial relations and the momentum equations for each fluid phase is the basis for the formulation of this model. The model is a one dimensional model which assumes the isothermal, incompressible, fully developed and a steady state flow. The model also assumes that there is no momentum change due to mass transfer between the oil and water and the radial velocity is equal to zero. Most researchers Arirachakaran et al. (1989),Angeli & Hewitt (1999), Charles et al. (1961), assumes the smooth interface when dealing with two fluid model. Trallero et al. (1997) and Brauner (2002), proposed the two fluid models with curved and wavy interfaces. The two fluid model is the balance between the pressure gradient and the interfacial shear forces which are normally defined and expressed differently by different researchers. The two fluid model for each fluid phase in a horizontal and inclined pipes is presented in equations 2.14 and 2.15 below (Vedapuri, 1999)

$$-A_w(\frac{dP}{dx}) - \tau_w S w - \tau_i S_i + A_w \rho_w g \sin\alpha \tag{2.14}$$

$$-A_o(\frac{dP}{dx}) - \tau_o S_o - \tau_i S_i + A_o \rho_o g \sin\alpha \tag{2.15}$$

Dividing each equation by total cross sectional area, the water holdups can be inserted in the equations as they are calculated as

$$\varepsilon_w = \frac{A_w}{A} \tag{2.16}$$

where ε_w is the water holdup, dP/dx is the pressure gradient, τ_o, τ_w and are the wall oil and water shear stresses respectively, τ_i oil and water interfacial shear stress, A is the cross

sectional area of a pipe, S_w and S_0 are the circumferences of pipe wetted by water and oil respectively, ρ is the density, g is gravitational constant and α is the pipe inclination angle. The elimination of pressure drop in the two equations, will leave only the two unknowns (Holdup and heights of the phases which is included in the oil and water wetted perimeters) which can be calculated iterativelly. Since other parameters are known from fluid properties and pipe characteristics one will end up with two possible solutions. A closure relation is usually used to solve this problem. For the case where the local phase fractions have been measured from the experiment, the height of interface can be calculated explicitly and finally the pressure drop can be predicted from the model. In this work, among the provided data, the insitu holdups were also available. From their works, Arirachakaran et al. (1989), Vedapuri (1999), and Schümann (2016) reported how the water, oil interfacial shear stresses and wall shear stresses can be calculated as indicated in equations 2.17,2.18 and 2.19.

$$\tau_w = \frac{1}{2} f_w \rho_w U_w^2 \tag{2.17}$$

$$\tau_o = \frac{1}{2} f_o \rho_o U_o^2 \tag{2.18}$$

$$\tau_w = \frac{1}{2} f_o w \rho_o (\, U_o - U_w) \mid U_o - U_w \mid \tag{2.19}$$

f_w and f_o are water and oil friction factor, f_{ow} is the friction factor of the oil water interface, U_o and U_w are oil and water velocities respectively. The pure oil and water friction factors can be calculated as the friction factor for single phases while the frictional factor for oil water interface can be taken as that of single phase oil in smooth pipes. As an often used simplification, calculations of the single phase oil and water friction factors assumes the fluids to be flowing independently in the pipe. The hydraulic diameters however, can be used to account for the presence of the other fluid inside the pipe. There is a number of correlations for the estimation of friction factor such as Colebrook (1939), Moody (1944), Haaland (1983) and Blausius (1911).

2.5.3 Three Layers Model

From the phase fraction data and flow video recordings in transparent sections, the segregated flow patterns may be observed to have a disturbed interface. The interface might be wavy, curved, or with droplets distributed over a certain height at the interface. The Prediction the phase fractions or pressure gradient of these flow patterns using a model that assumes a smooth/plane interface has not resulted in to proper predictions (Vedapuri, 1999). To solve for the three layers, He introduced a separate equation 2.22 and added it in to the two fluid model equations with each layer with its own defined properties and equations. The equations become;

$$-A_w \left(\frac{dP}{dx} \right) - \tau_w S w - \tau_{i1} S_{i1} + A_w \rho_w g \sin \alpha \tag{2.20}$$

$$-A_o \left(\frac{dP}{dx} \right) - \tau_o S_o - \tau_{i2} S_{i2} + A_o \rho_o g \sin \alpha \tag{2.21}$$

$$-A_m\left(\frac{dP}{dx}\right) - \tau_m S_m - \tau_{i1} S_{i1} + \tau_{i2} S_{i2} - A_m \rho_m g \sin\alpha \tag{2.22}$$

A_m is the pipe cross section occupied by dispersed/mixed layer, τ_m is the mixture shear stress, the sub scripts i1 and i2 represents water mixture interface and oil mixture interface respectively. ρ_m is the mixture density at the interface and it can be calculated as shown in 2.3 if there is no slip within the dispersed layer. With Slip, the mixture density can be calculated as shown in equation 2.23Amundsen (2011)

$$\rho_m = \sum \frac{(\,\rho_w \varepsilon_i + \rho_0(1-\varepsilon_i))\,A_i}{A_{tot}} \tag{2.23}$$

The shear stresses at the interface are calculated as indicated in equations 2.24, 2.25 Vedapuri (1999)

$$\tau_{i1} = f_{i1}\frac{\rho(U_m - U_w) \mid U_m - Uw \mid}{2} \tag{2.24}$$

$$\tau_{i2} = f_{i2}\frac{\rho(U_o - U_w) \mid U_o - Uw \mid}{2} \tag{2.25}$$

Chapter 3

Experimental Overview

3.1 SINTEF flow loop section

As it can be observed in figure A.6 in appendix A, the experiment was conducted by SINTEF laboratory in a low pressure, 220 m long, and 4" diameter pipe. The pipe configuration was such that four 48 m pipe sections were joined together by three 180° bends of 2.25 m radius with the two pairs of pipes placed on top of each other. The test section was inclined at 0.1°. The fluids used in the experiments were water and a medium model mineral oil blend consisting of the two oils "Exxsol D60" and "Primol 352". Two different pipelines extending from the 3 phase separator were leading oil and water each towards the common pipeline for the experiment. Right after the joint of the two pipes, a mixing butterfly valve was placed to blend the two mixed fluids with the designed pressure drops through it. The pressure drop across the mixing valve was measured between the tap in the water inlet pipe and 40cm downstream the mixing valve. There were no other intrusive devices so any mixing inside the pipe were from the mixing valve and from the hydrodynamics of the flow.

All the measurements for oil water flows were conducted at four mixture velocities (0.5m/s, 1m/s, 1.5m/s and 2m/s). The water cuts were varied from 0.1 to 0.9. Single phase oil and water experiments were also conducted at different flow velocities.

3.2 Instrumentation

The main pipeline instruments in the loop system includes TEN differential pressure meters which were placed for pressure measurements at 10 different positions in a loop, two traversing gamma densitometers mounted on the pipe for vertical density profile measurements and two pairs of optical sections for video recordings. There was also a particle sizing camera known as CANTY InFlow particle sizer for which a mini flow was bypassed by a sample probe leading the fluids towards it for capturing droplets videos inside the flow.

3.2.1 Pressure Transducers

8 pressure transducers were placed on the pipeline with 2 transducers at the beginning and end of every 48 m approximately pipe sections and another one added at 14.09 m from the

mixing valve, observe figure A.6 in appendix A. Another transducer was placed 40 cm just after the mixing valve for measuring the pressure drop across the mixing valve making a total of 10 pressure transducers in the system. All transducers measures pressures at each point relative to the atmospheric pressure except for the one that measures pressure drop across the mixing valve.

3.2.2 Optical section

Two optical sections placed in pairs at two different positions in the hall were used to capture the video recordings of the flow in all the transparent sections of the pipe. The Optical sections were placed at 1.6 m, 106.0 m, 113.9 m and 218.6 m from the mixing valve. Always two optical sections were positioned such that one camera could cover both sections. Figure 3.1 shows an example of a picture captured in the experiment be18227 by camera 2.

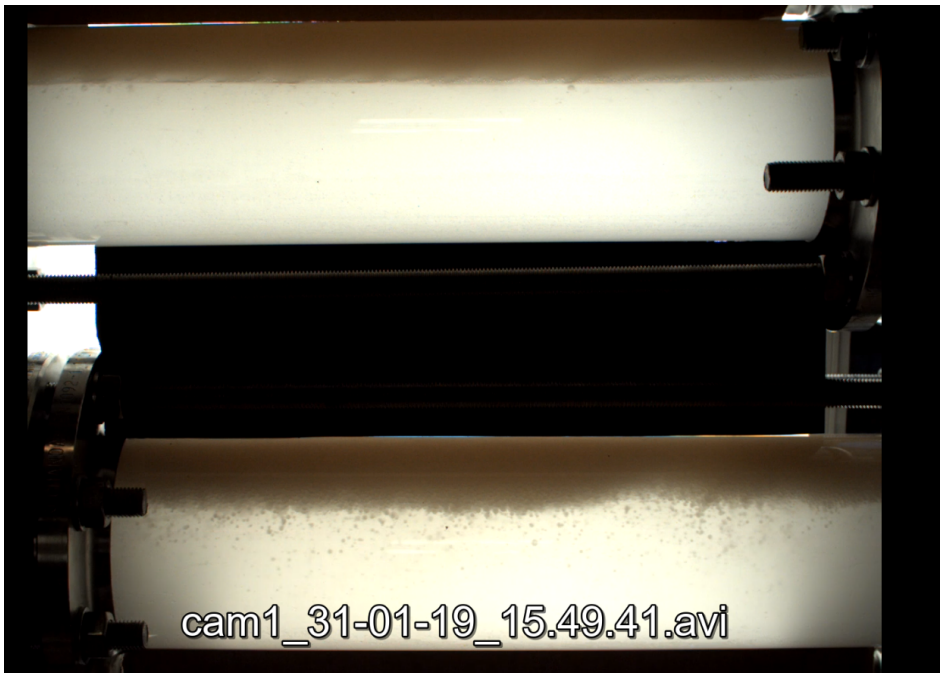

Figure 3.1: An Image captured by an optical section to describe the flow pattern

3.2.3 Traversing Gamma Densitometer

Two traversing gamma densitometers were used to determine the fraction of water in a pipe cross-section. The placement of pipe sections on top of each other enabled the two pipe sections to be scanned by one traversing gamma densitometer making it possible to scan a total of 4 different positions for the 2019 experiments and 6 positions for the 2018 experiments. The data obtained from the gamma densitometer included the water fraction for every normalized pipe position (y/D) where 0 corresponds to bottom of the pipe and 1 corresponds to top of the pipe. This data was used to construct the phase fraction profiles seen in figure 3.2 that were useful in the identification of the flow patterns.

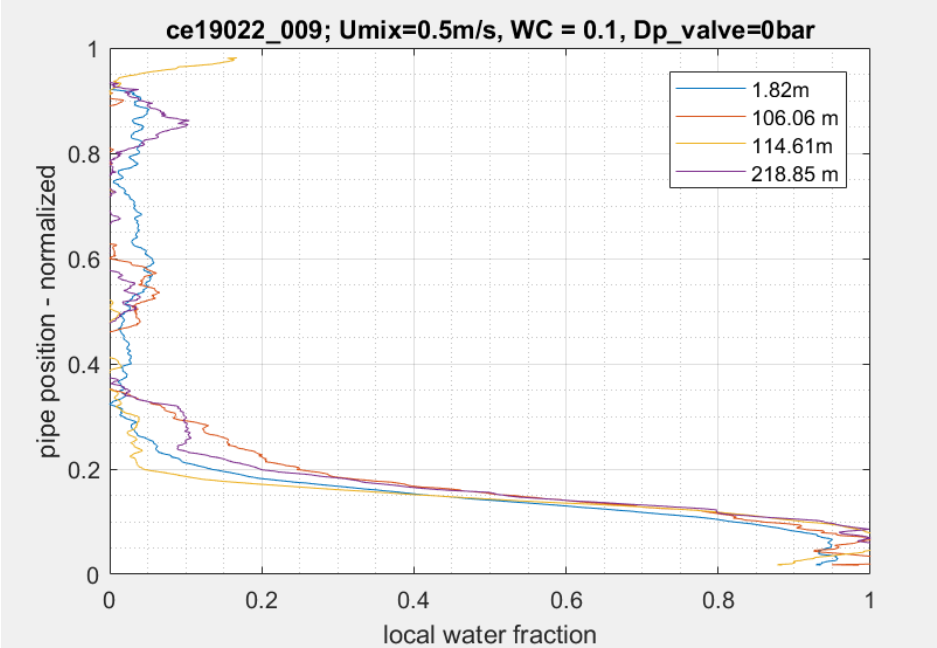

Figure 3.2: An example of a Phase fraction Profile produced from local Phase fraction data

3.2.4 CANTY InFlow Particle Sizer

Fluid samples were taken from the main stream in order to capture the images of droplets distribution in the flow. The flow was bypassed by a sample probe of 8 mm inner diameter that lead the mini flow to the particle sizing instrument known as CANTY InFlow Particle Sizer. The sample probe was considerably larger than the expected droplets sizes while at the same time the probe was small enough to not disturb the flow. CANTY InFlow analyzer has the very high resolution image sensor that provided droplet pictures for the size analysis with two dimensional video recordings.

Fluid samples were taken at 0.70 m, 106.51 m and 219.30 m from the inlet mixing valve. From the main stream at each stated position where the sample was collected, the sampling probe was varied at three different vertical position in a pipe cross-section to ensure that the variation of droplets distribution over three different sections is captured. The sampling probe was bent with its opening against the direction of flow at 3 cm, 6 cm and 8 cm from the bottom of the pipe. The sampling probe inside the flow can be seen in Figure 3.3.

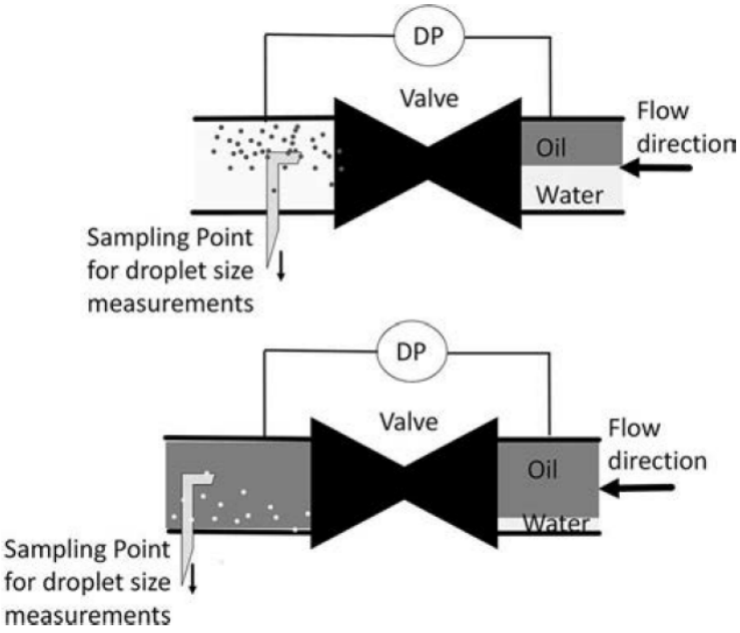

Figure 3.3: Positioning of a Sampling point at different water cuts(Fossen & Schümann, 2017)

3.3 Fluid System

The experiment conducted was mainly focused on the oil water flow under normal temperature conditions. The room temperature was 20° with small variations that were not taken in to account. $6m^3$ of MEDIUM mineral oil blend consisting of the two oils "Exxsol D60" and "Primol 352" type with a measured density of 850 kg/m^3 and a theoretical viscosity of 35 $mPaS$ at at experimental conditions was tested together with 4 m^3 of tap water that had a measured density of 999 kg/m^3 and viscosity of 1.0 $mPaS$. The densities of oil and water were measured with sigma 703D by KSV instrument at 20°C. Biocide IKM cc-80 at a concentration of 1000 ppm was added in water to prevent the organic growth.

3.4 Data Collection

A total of 71 data sets were obtained from the performed experiments. These data can be observed in Appendix A. The Provided data were the already processed data (sorted and filtered for noises) that could be used directly in the analysis of the experiment. Additional data that were provided apart from those seen in appendix A were the videos of the flow at the transparent sections of the pipe, droplets images from the CANTY InFlow particle sizer, and the gamma density profiles from gamma densitometers.

From 71 data sets, five experiments with a water cut (WC=0.2) and mixture velocity of 1m/s were analyzed for the effect of different mixing at the inlet valve. The pressure drops of 0.1, 0.2, 0.35, 0.5 and 1 bar across the mixing valve were analyzed to check the influence of mixing on the droplet size and the pressure drop downstream the test section. All data sets were also compared with the previous data of 2018 experimental campaign to evaluate the influence of increased viscosity on the flow pattern maps, pressure drop, droplet settling and

droplet growth. These data contained the same experimental setup with slightly different instrumentation where three traversing gamma densitometers were used to measure the local phase fraction of water. The type of oil used was also different and contained an "Exxon D60" type of oil with a viscosity of 1.43 cp. analyzed by Kivuyo & Issara (2018) These data were also used to test both the previous and the improved the 2-fluid model and the three layers model that were provided by SINTEF staff. The flow diagram for the test section can be found in appendix A

Chapter 4

Flow Characteristics

4.1 Identified flow patterns

Both the 2018 and 2019 experiments with low to medium oil viscosities respectively, showed fairly the same kinds of flow patterns. These flow Patterns were identified by Beatrice who was dealing with flow patterns and pressure drop for the data provided by SINTEF. Figure A.5 in appendix A shows the observed flow Patterns for 2019. The flow patterns from dispersed to stratified were identified. For simplification A homogeneous oil dispersion (Do-H) phase fraction is characterized by a fairly straight line as is seen in the Figure 4.1. That means the liquid fraction is the same throughout the cross-section of the pipe. In the image, the droplets are not clearly observed due to their large concentration and their small sizes.

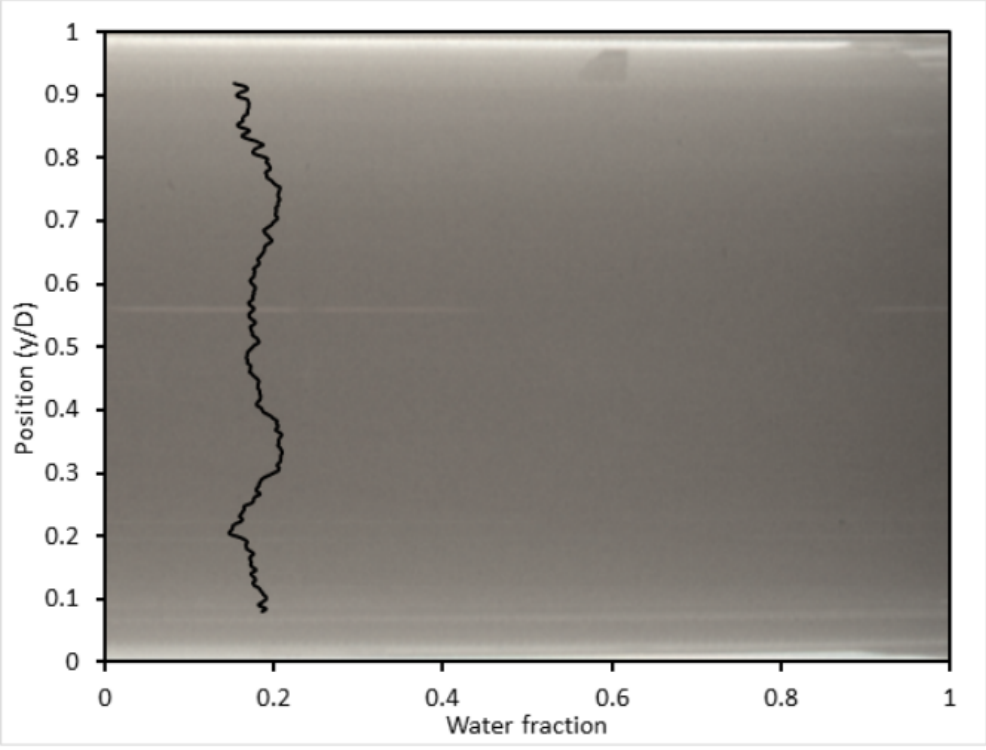

Figure 4.1: Homogeneous oil dispersion (Do-H)

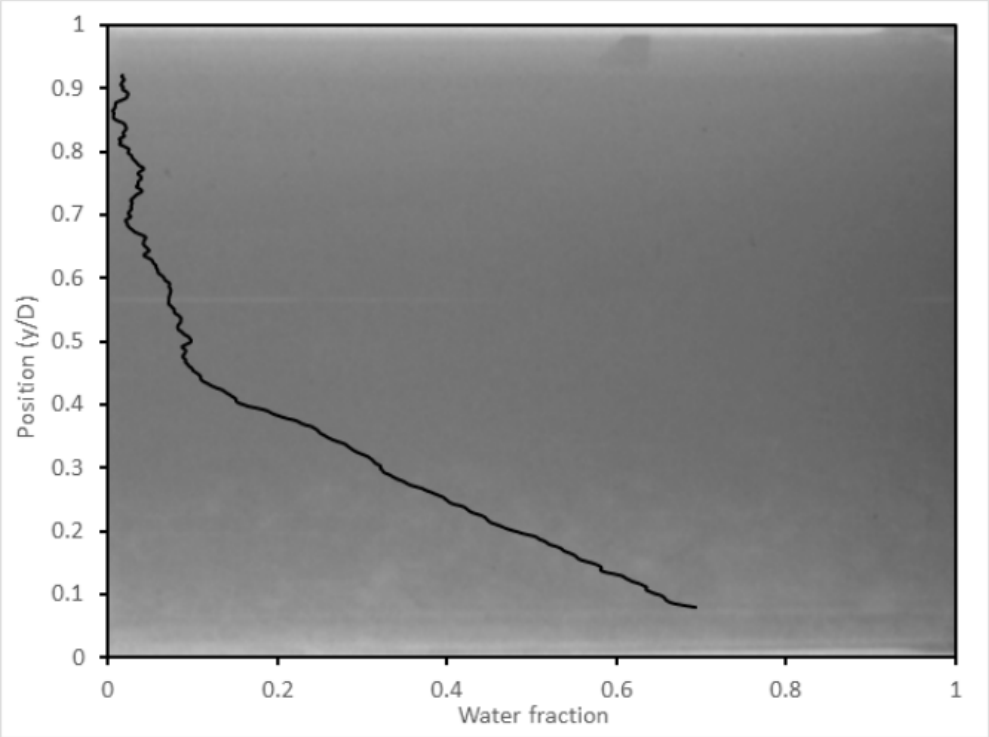

Figure 4.2: Inhomogeneous oil dispersion (Do-I)

The inhomogeneous oil dispersion (Do-I)was characterized by a fairly straight line at the top of the pipe and a steep gradient at the bottom of the pipe as seen in Figure 4.2. The figure shows the top part as if it appears without any droplets but the bottom of the pipe shows the presence of droplets because the larger droplets settle at the bottom together with the small droplets which are not visible. The water concentration being greater than zero at the top is proof that there is water in the form of small invisible droplets.
There is also inhomogeneous water dispersion observed where the oil droplets are contained in the water phase. Its phase fraction profile shows a line which at the top of the pipe approaches zero water fraction because of the oil droplets concentration; then has a steep slope toward 100% water fraction.

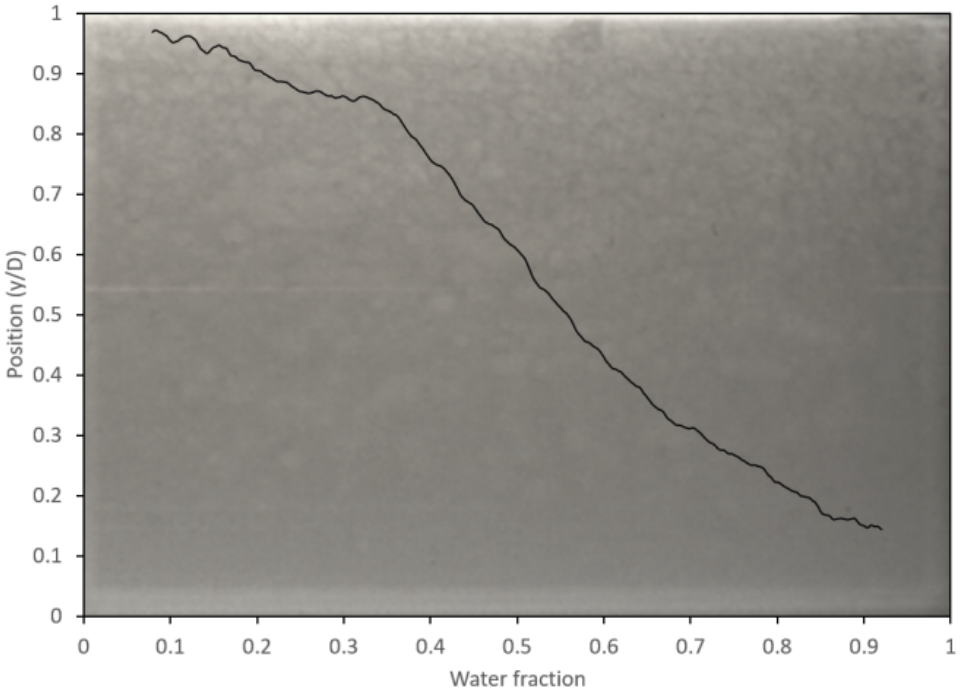

Figure 4.3: Inhomogeneous water dispersion (Dw-I)

Another flow pattern was observed to have oil dispersion with a dense packed layer of water droplets (Do-DP). From the visual seen in Figure 4.4, the flow looks like stratified flow but the phase fraction profile turn at the bottom suggests that the water is in form of densely packed droplets and that the continuous fluid is oil.

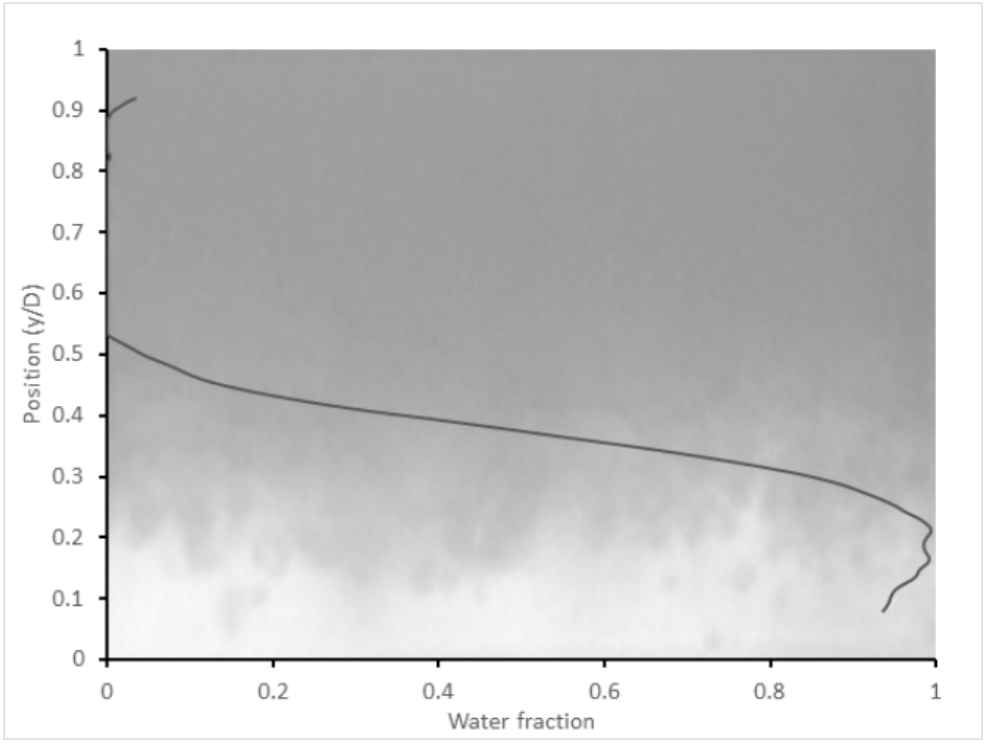

Figure 4.4: Oil continuos dispersion with a dense packed layer of water droplets (Do-DP)

The other identified flow pattern is the stratified mixed flow which is shown with both the oil and water as continuous phases separated by an interface containing droplets of both water and oil. For stratified mixed, the interface is not very clear since there are droplets of oil and water in the water phase and oil phase respectively. Its corresponding phase fraction profile shows a gentle slope on the interface and water concentration is almost one at the bottom of the pipe showing the continuous phase is water; see Figure 4.5.

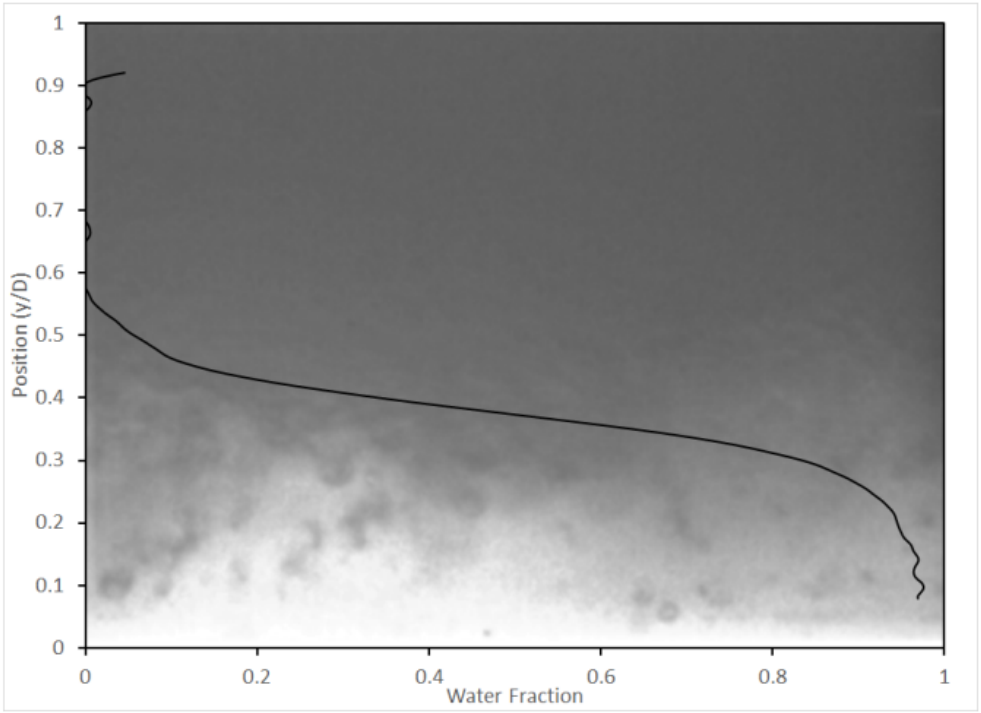

Figure 4.5: Stratified mixed flow with oil droplets in the water phase (SM)

Also there was stratified wavy flow which is shown with both the oil and water as continuous phases separated by an almost smooth interface containing droplets of both water and oil. Its corresponding phase fraction profile shows a gentle slope on the interface and almost clear phases at the bottom and top of the pipe. See Figure 4.6.

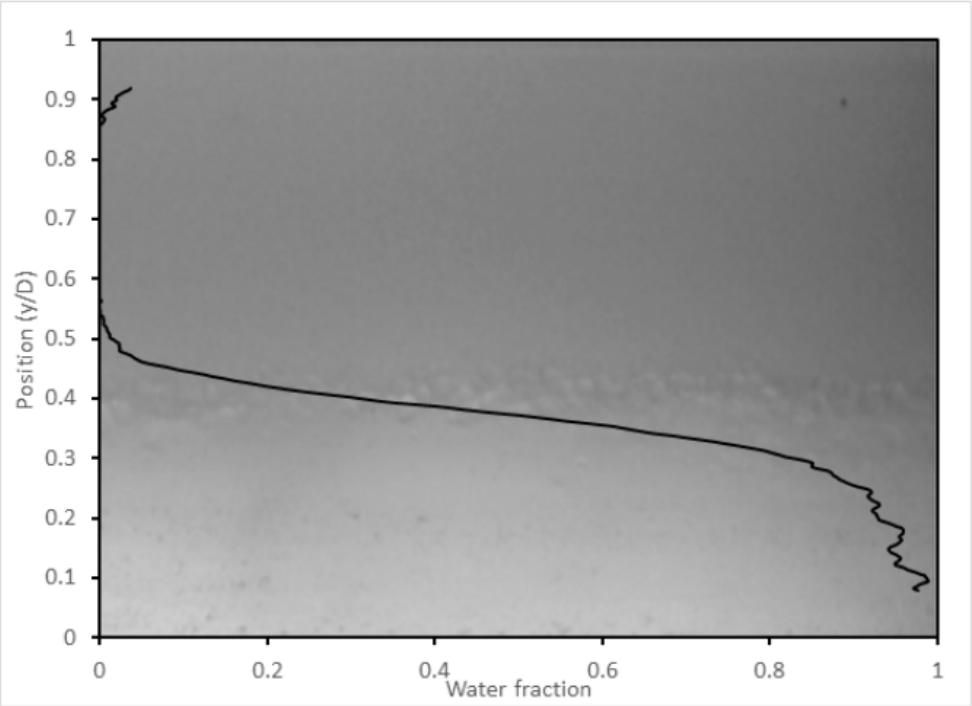

Figure 4.6: Stratified wavy flow (SW)

The last identified flow pattern was the oil dispersion with the dense packed layer plus water layer seen in figure 4.7. The phase fraction of this flow pattern looks a like an inhomogeneous dispersion but the water layer can be seen at the bottom of the pipe with very fine droplets of oil whose concentration increases to the top.

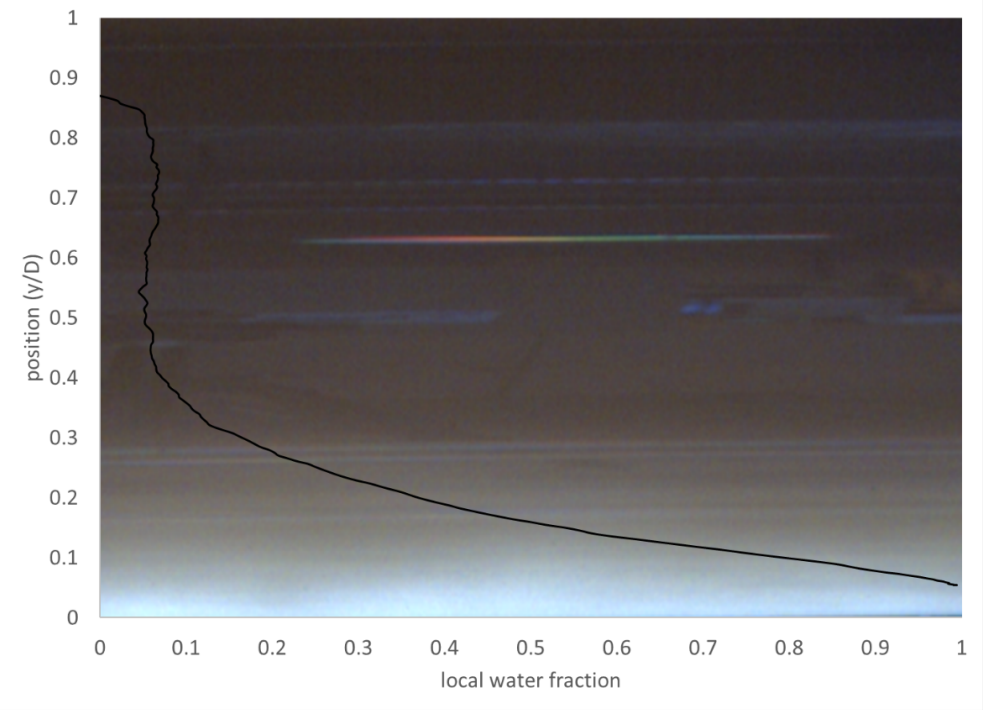

Figure 4.7: Oil dispersion with the dense packed layer plus water layer

4.2 Pressure drop

Pressure drop measurement were taken at different points along the test section. Pressure drop measurements were obtained as a result of variation of different parameters affecting the flow such as water cut, mixture flowrate and mixing at the inlet valve. In this section the pressure drop experimental results will be given in a nut shell for the 2019 experiments. Pressure gradient for the 2018 experimental results have been clearly illustrated by Kivuyo & Issara (2018) in their project report. Also enough information about the pressure gradient measurements for 2019 experiments can be found as explained Beatrice's thesis of 2019.

4.2.1 Effect of Pressure Drop Across the mixing valve

Generally the pressure drop along the test section was observed to decrease with increased distance along the test section. Increased pressure drop across the mixing valve also increased the measured pressure drop along the test section. figure 4.8 shows the effect of increased mixing at the inlet valve on the pressure gradient along the test section.

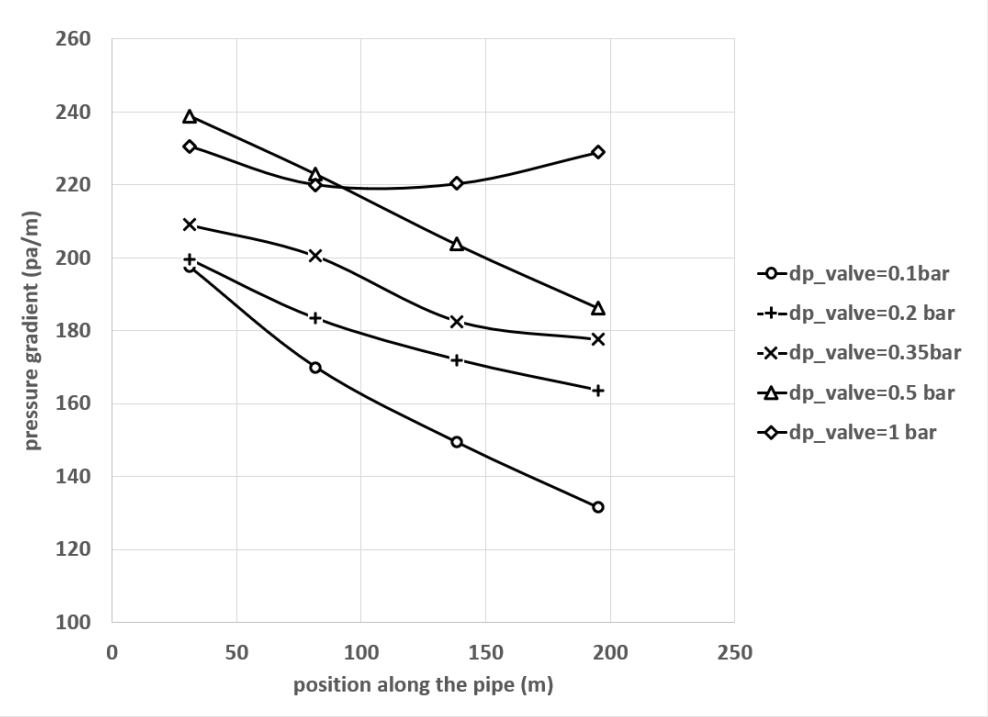

Figure 4.8: Effect of different mixing on the pressure gradient along the test section

4.2.2 Effects of Water Cut and Flowrate on the pressure gradient

Low water cuts were observed to cause a considerably higher drop in pressure especially at higher mixture velocity than the larger water cuts. At lower mixing velocities, it was observed from figure 4.9 that water cut had a very little influence on the pressure gradient along the test section. increased flowrate (mixture velocity) lead to a lazy increase in pressure gradient when the water cut was slowly increased until a peak was reached where further increase in water cut resulted in drop of pressure gradient. Further increase in flowrate lead to the rapid

increase in pressure gradient but the trend again reversed after the phase inversion point was reached see figure 4.9. This is because the most common flow pattern was the dispersed flow pattern which is associated with higher pressure drops compared to the stratified flow patterns. Abrupt decrease in pressure drop was observed after the kinds of dispersion were changed from oil continuous dispersions to water continuous dispersions.

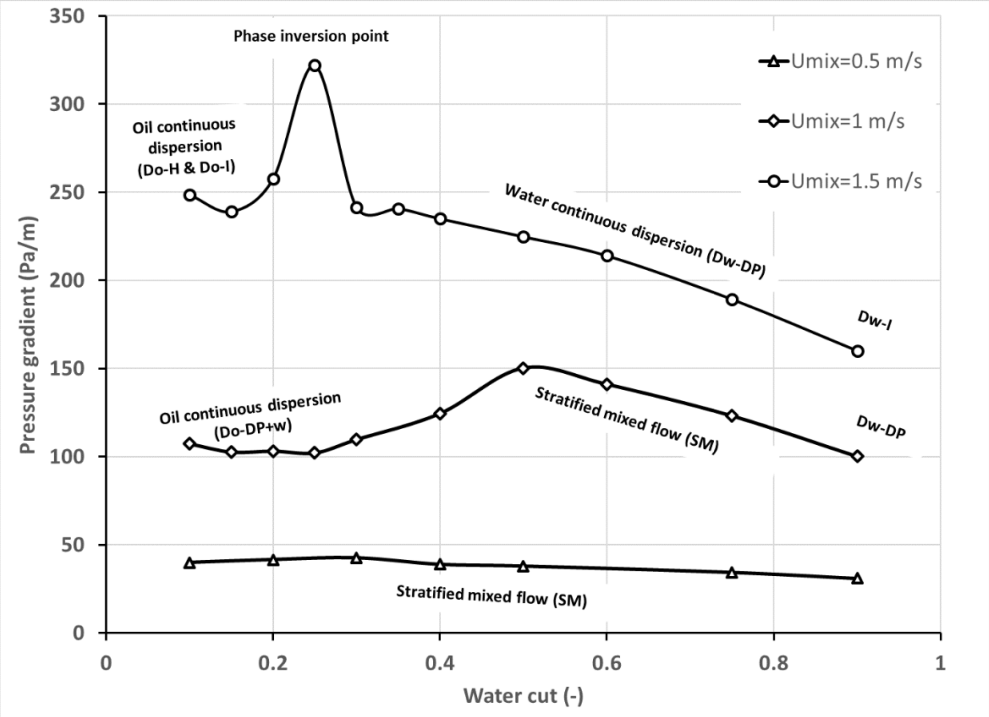

Figure 4.9: Oil dispersion with the dense packed layer plus water layer

Chapter 5

Oil Water Flow Modeling

5.1 Oil water flow modeling

The main objective of of this modeling work is to predict the Pressure drop along the pipe for the separated flows. Two models are presented here, the two fluid model and the three layers flow model. The Three layers flow model is the modified two fluid model that will include a third dispersed layer between the two continuous water and oil layers. These models were provided by SINTEF laboratory along with data to be used to test the models. Successful testing of the models gave a room to make some improvements that made a model to be more reliable and accurate for the prediction of pressure drop. Almost all the input data were obtained from the experiments performed in two different experimental campaign and some few were the calculated data which also used the experimental data. Details about the two model will be given in the next section. It is important to note that, there were no big improvements that were done to the models. Some improvements were attempted to be made to the three layers model but did not actually improve the model. Another important point to note is that despite attempting to test and improve the three layers flow model from the experiments performed, there were very few three layers flow pattern that were identified from the given data.

5.2 Two fluid model

The two fluid model performed in this work was from the modified Arirachakaran two fluid model. The model uses the fractions of pipe perimeters occupied by each phase to contribute for the total pressure gradient of the pipe. The main assumptions in the development of this model were:

- The model assumes that the flow has fully developed
- No relative motion nor mass transfer across the flowing phases
- No slip between the phases i.e no net shear force at the oil water interface

The two momentum balance equations for the two phases is presented below for the hori-

zontal flow

$$-A_o\left(\frac{dp}{dz}\right) + \tau_o S_o - \tau_{ow} Sow = 0 \tag{5.1}$$

$$-A_w\left(\frac{dp}{dz}\right) + \tau_w S_w + \tau_{ow} Sow = 0 \tag{5.2}$$

A_o and A_w are oil and water wetted areas, dp/dz is the pressure gradient, τ_o, τ_w and τ_{ow} are the oil, water and oil water interface shear stresses. The Blaussius equations were used to determine the closure relations for the wall and interface shear stresses in terms of average velocities and frictional factors. S_o, S_w, and S_{ow} are oil, water and interface perimeters wetted by each fluid phase. Upon elimination of pressure drop terms in equations 5.1 and 5.2and dividing by the total area A the following equation is obtained.

$$\tau_o S_o \varepsilon_w - \tau_w S_w \varepsilon_o + \tau_o w S_o w(\varepsilon_w + \varepsilon_o) = 0 \tag{5.3}$$

with ε_o and ε_w being insitu oil and water fractions respectively which are calculated as

$$\varepsilon_w = \frac{A_w}{A}\varepsilon_o = 1 - \varepsilon_w \tag{5.4}$$

These local fractions have been obtained straight from the experiment therefore the pressure gradient are calculated directly explicitly from the equations. For each phase flowing inside the pipe, the pressure drops of phases is calculated assuming they flow alone in a pipe with the same velocities. The total pressure gradient is then the summation of the pressure gradients calculated for each phase as indicated by equation 5.11. The pressure drop for each phase is calculated as indicated below

$$\left(\frac{dp}{dx}\right)_o = \frac{f_o \rho_o U_o^2}{2D} \tag{5.5}$$

$$\left(\frac{dp}{dx}\right)_w = \frac{f_w \rho_w U_w^2}{2D} \tag{5.6}$$

The densities used are for the pure oil and water and the friction factors were calculated by using the churchill equation for both phases using the overall diameter of the pipe and the hydraulic diameters.

$$f = 8\left[\left(\frac{8}{Re}\right)^{12} + \frac{1}{(\theta_1 + \theta_2)^{1}.2}\right]^{1/12} \tag{5.7}$$

with θ_1 and θ_2 given by

$$\theta_1 = \left[2.457 \ln\left(\frac{1}{\left(\frac{7}{Re}\right)^{0.9} + 0.27\frac{\in}{D}}\right)\right]^{16}$$

$$\theta_2 = \left(\frac{37530}{Re}\right)^{16}$$

$$Re = \frac{\rho U D}{\mu} \tag{5.8}$$

The Oil and water velocity are calculated from the superfacial oil and water velocity and the local oil and water fractions. The superficial oil and water velocities were obtained from the experimental data.

$$U_o = \frac{U_{so}}{\varepsilon_o} \tag{5.9}$$

$$U_w = \frac{U_{sw}}{\varepsilon_w} \tag{5.10}$$

The total pressure drop in the pipeline with two phases is then given by

$$\left(\frac{dp}{dx}\right)_{2phase} = \frac{S_o}{S}\left(\frac{dp}{dx}\right)_o + \frac{S_w}{S}\left(\frac{dp}{dx}\right)_w \tag{5.11}$$

Two different data from two different experiments with different conditions were used to test this model. The data from 2018 experiments presented by Kivuyo & Issara (2018) and the data from 2019 experiments located in Appendix A from figure A.1 to A.4 of this work. Both data showed that the model was working properly and the predictions were not bad. Figures 5.1 and 5.2, shows the comparison made between the measured experimental pressure gradient for the two experiments and the pressure gradient predicted by the two fluid model. The model predictions for these figures, used the whole pipe diameter to estimate the pressure gradient of each flowing phase.

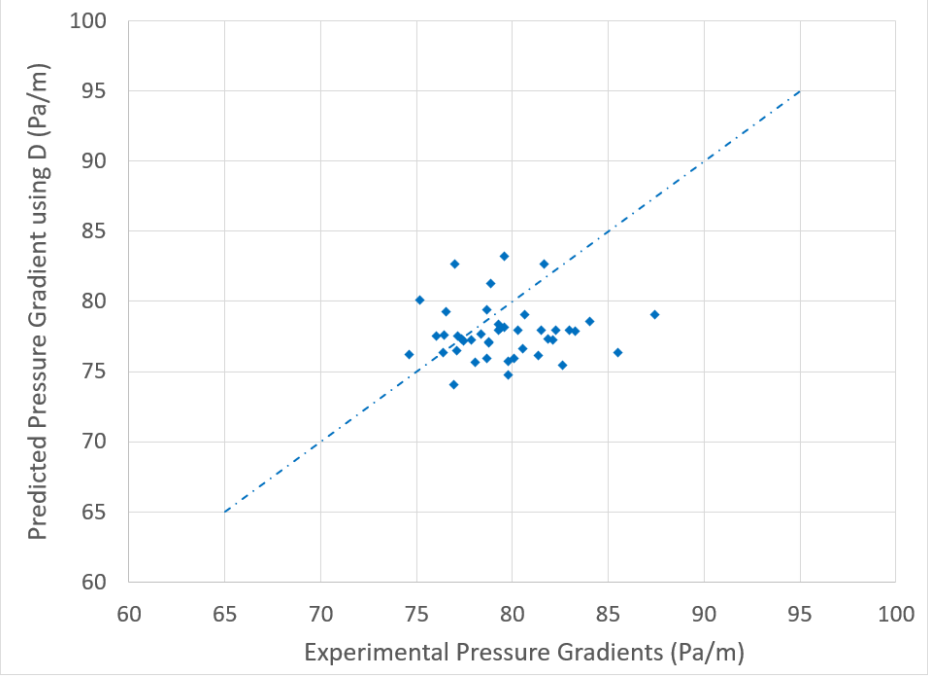

Figure 5.1: 2018 Experimental v/s model pressure gradient with pipe diameter used

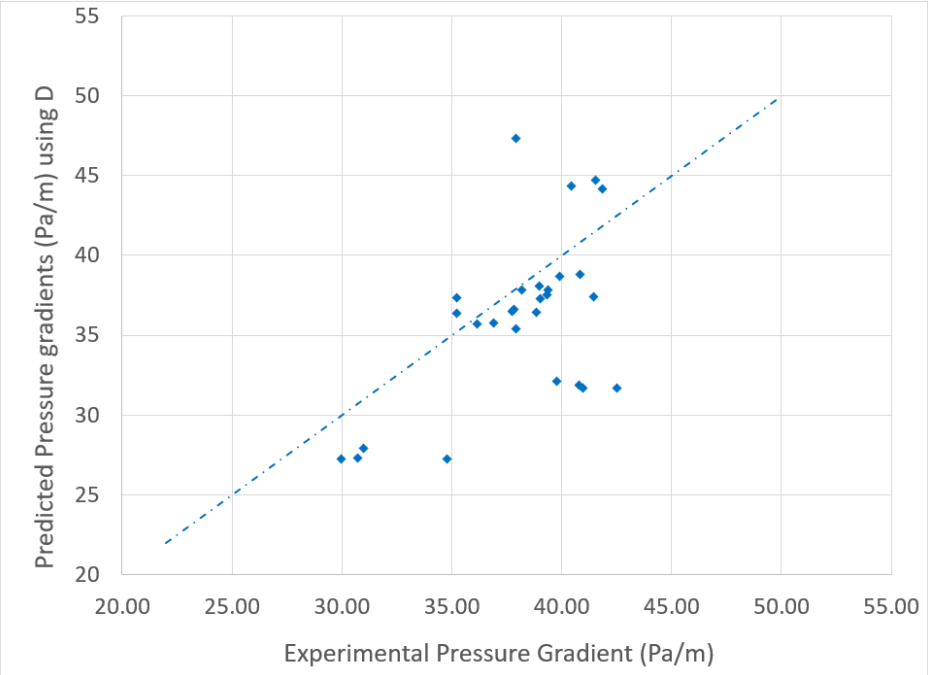

Figure 5.2: 2019 Experimental v/s model pressure gradient with the pipe diameter used

The results predicted by two fluid model were improved by using the hydraulic diameter proposed by Brauner (1991) in the estimations of pressure gradient of each flowing phase. The hydraulic diameter were defined according to the relative velocity of the phases Brauner (2002). The average absolute and relative errors were calculated and showed that, the use of hydraulic diameter improved the predictions made by two fluid model. The use of pipe diameter resulted in to an average absolute error of 1.78% and average relative error of 2.35%. For the hydraulic diameter, the model resulted an average absolute error of 1.64% and average relative error of 2.14%. Figure 5.3 and 5.4 shows the the experimental data versus the model prediction data when the hydraulic diameter was used for the experiments of 2018 and 2019.

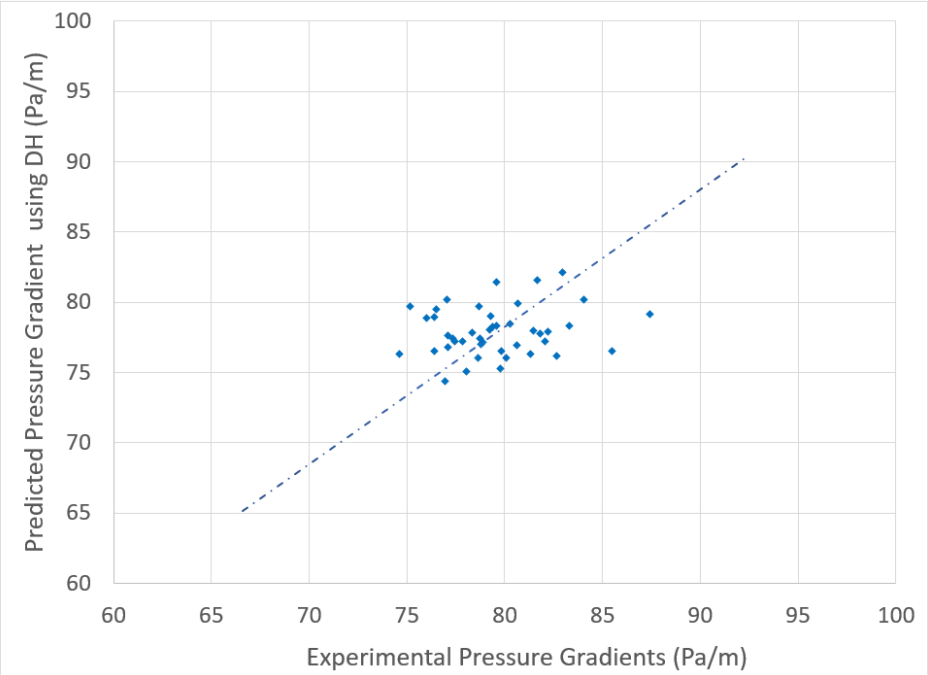

Figure 5.3: 2018 Experimental v/s model pressure gradient with hydraulic diameter used

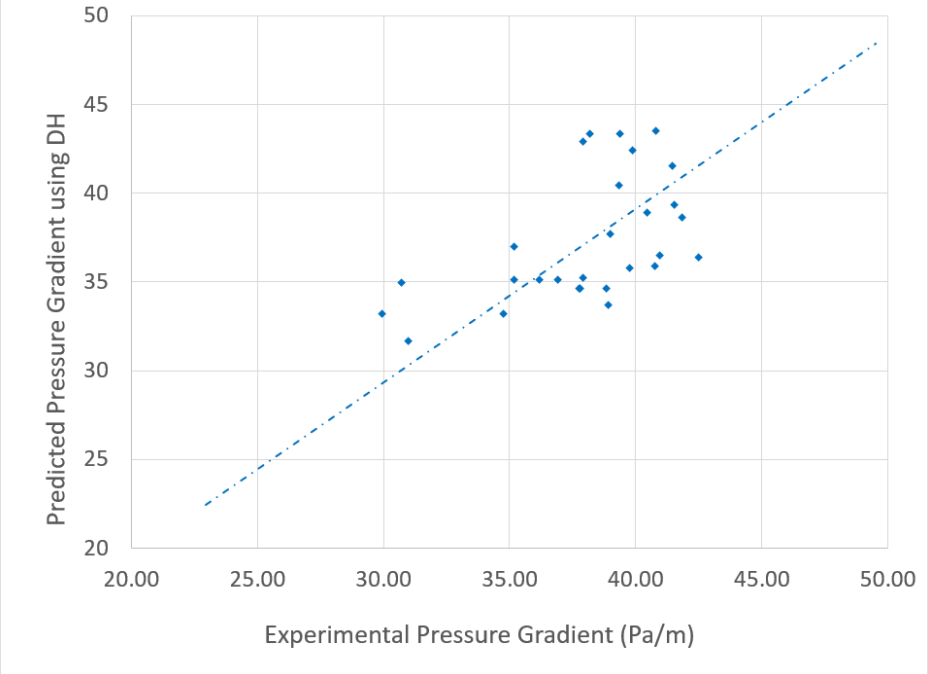

Figure 5.4: 2019 Experimental v/s model pressure gradient with the hydraulic diameter used

The effect of using hydraulic diameter can also be observed on the plots shown in the plots compared in figure 5.5 and 5.6

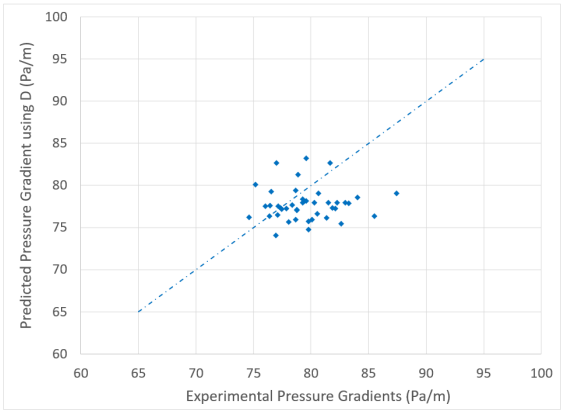

(a) model Vs 2018 experimental data using pipe diameter

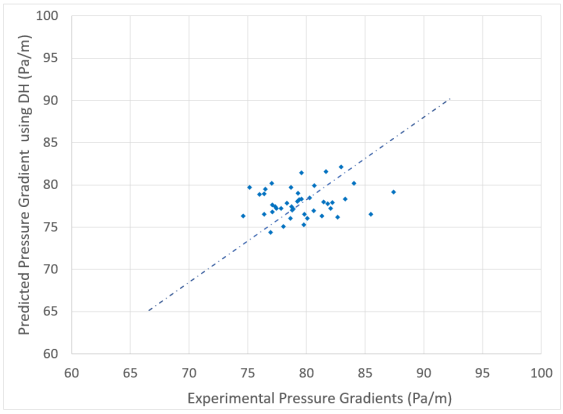

(b) model Vs 2018 experimental data using hydraulic diameter

Figure 5.5: Comparison of the models on the use of pipe diameter and hydraulic diameter

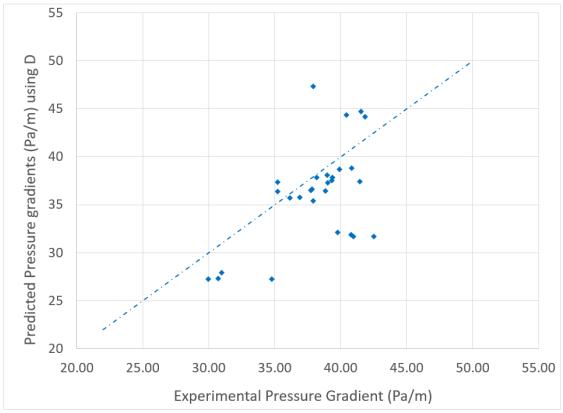

(a) model Vs 2019 experimental data with pipe diameter

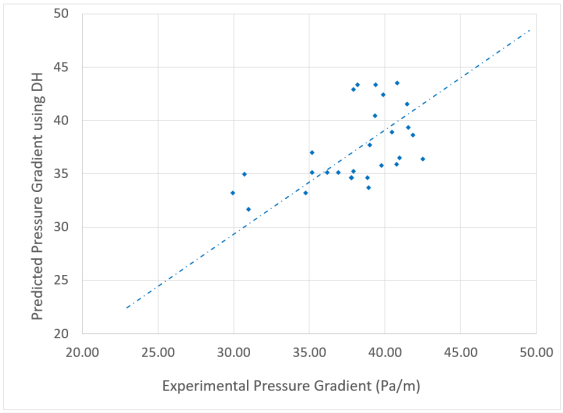

(b) model Vs 2019 experimental data with hydraulic diameter

Figure 5.6: Comparison of the models on the use of pipe diameter and hydraulic diameter

5.3 3 Layers model

From the 2 fluid model, the 3 layers model was developed by adding a homogeneous dispersed layer between the continuous oil and water layers. This layer was added to represent the dense packed layer of droplets that forms at the interface of the oil and water continuous layers, see figure 5.7. The dense packed layer is assumed to have a constant density, viscosity and a constant phase fraction across the whole layer. For the model to be independent of the type of dispersion, the phase fraction of the dense packed layer was assumed to be equal to the water cut at the phase Inversion point. Schümann (2016) and Smith et al. (2015) also applied this assumption in their models. The assumption of a smooth interface between the oil, the dense packed layer and water layer was applied in this model.

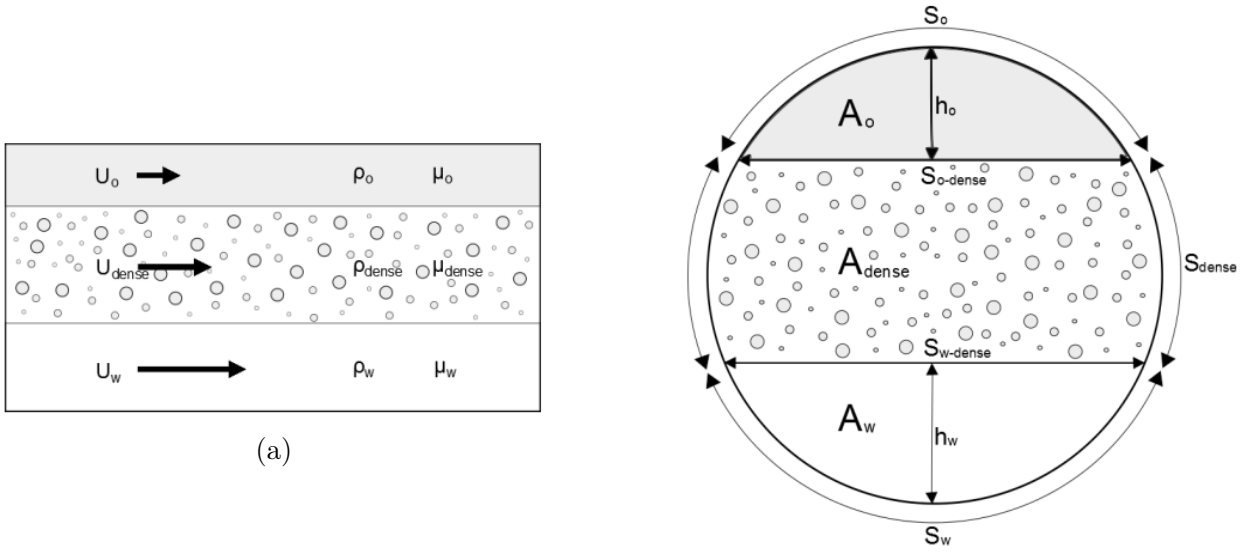

Figure 5.7: Three layers flow along and across the pipe

From figure 5.7, The distribution of phases can be observed in layers, with each layer defined by different fluid and flow properties. The computation of these layers, will assume that each layer is flowing separately in the pipe, and will later be combined to account for effects of presence of other fluids. The pressure gradient in the pipe is calculated as the summation of the individual pressure gradient calculated for each layer. Total pressure gradient for all phases is given by equation 5.12. The calculation of pressure gradient for oil and water layer is not different from the ones presented in the two fluid model, for the third dense packed layer however, the mixture properties such as density and viscosity which are constant at every point in that layer will be calculated as indicated in the homogeneous model presented at the literature review part. It is assumed that the water fraction at the dense packed layer is equal to the water cut at the phase inversion. Considering the perimeters of the pipe walls wetted by each phase, the total pressure drop for all the phases is calculated as

$$\left(\frac{dp}{dx}\right)_{3layers} = \frac{S_o}{S}\left(\frac{dp}{dx}\right)_o + \frac{S_m}{S}\left(\frac{dp}{dx}\right)_m + \frac{S_w}{S}\left(\frac{dp}{dx}\right) \tag{5.12}$$

where, the subscript m stands for the mixture layer or the dense packed layer containing a dispersed mixture of oil and water. The Pressure gradients for each phase k is calculated as

$$\left(\frac{dp}{dx}\right)_k = \frac{f_k \rho_k U_k^2}{2D} \tag{5.13}$$

For the dense packed layer, the mixture properties such as density, viscosity and mixture velocity will be calculated differently. The density of the dense packed layer is calculated as indicated in equation 5.14

$$\rho_m = \rho_w \alpha_w + \rho_o(1 - \alpha_w) \tag{5.14}$$

The mixture viscosity was calculated by using Pal & Rhodes(1989) model indicated in equa-

tion 5.15.

$$\mu_{mix} = \mu_c \left[1 + \frac{0.8415\phi/\phi_{\mu r=100}}{1 - 0.8415\phi/\phi_{\mu r=100}} \right]^{2.5} \tag{5.15}$$

The velocities of a dense packed layer and water layer were calculated based on the velocity of the oil layer. All these computations were implemented in MATLAB presented in appendix D. The initial guess was made for oil velocity and the rest of layers velocity were iteratively calculated . The dense packed layer and water velocities were calculated as follow

$$U_m = \frac{Q_o - U_o A_o}{Am(1 - WC_{inv})} \tag{5.16}$$

$$U_w = \frac{Q_w - U_m A_m WC_{inv}}{Aw} \tag{5.17}$$

Equations 5.16 and 5.17 requires A_o, A_w and A_m which are calculated based on the geometry of the phase distribution inside the pipe line. Figure 5.7b can be also represented in form of figure 5.8 on the left where the perimeters and areas of the wetting phases can be deducted from the geometric relations of the circle.

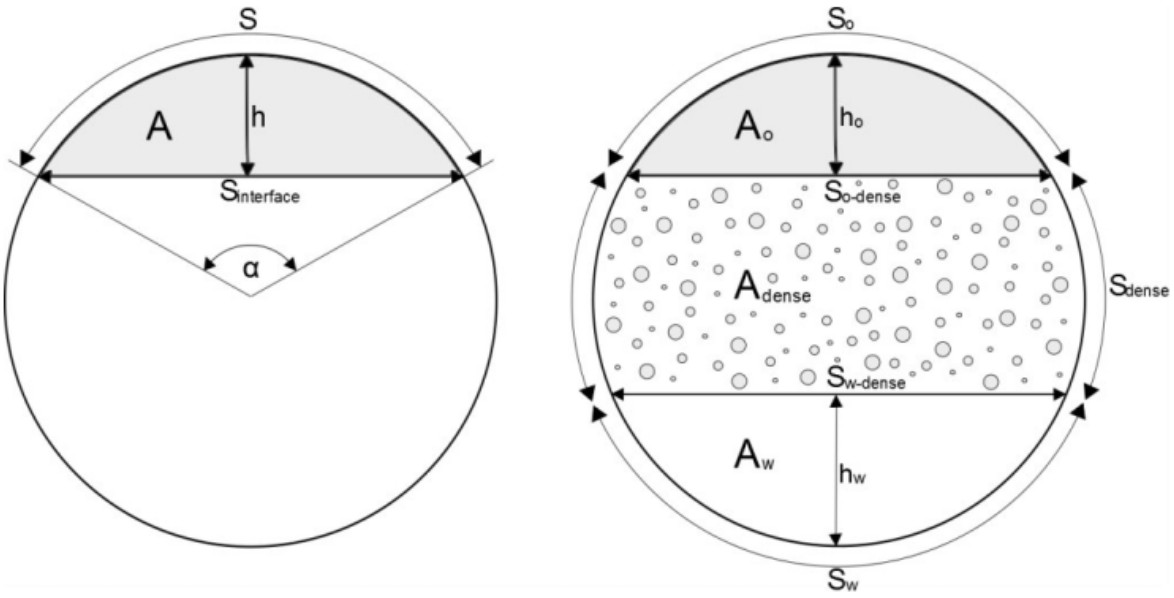

Figure 5.8: Relationship between the circle geometry and the pipe cross section occupied by 3 layers of phases

From figure 5.8 left, the areas and perimeters of each phase can be calculated as

$$A_o = R^2 arccos\left(1 - \frac{h_o}{R}\right) - (R - h_o)\sqrt{2Rh_o - h_o^2} \tag{5.18}$$

$$A_w = R^2 arccos\left(1 - \frac{h_w}{R}\right) - (R - h_w)\sqrt{2Rh_w - h_w^2} \tag{5.19}$$

$$A_m = A - A_o - A_w \tag{5.20}$$

$$S_o = R\alpha_o \tag{5.21}$$

where,

$$\alpha_o = 2arccos\left(1 - \frac{h_o}{R}\right)$$

$$S_w = R\alpha_w \tag{5.22}$$

where

$$\alpha_w = 2arccos\left(1 - \frac{h_w}{R}\right)$$

$$Sm = S - S_o - S_w \tag{5.23}$$

$$\tag{5.24}$$

The interface perimeters can also be calculated from equations 5.25 and 5.26

$$S_{om} = 2Rsin\left(\frac{\alpha_o}{2}\right) \tag{5.25}$$

$$S_{mw} = 2Rsin\left(\frac{\alpha_w}{2}\right) \tag{5.26}$$

From equation 5.18 to equation 5.22 the heights of the interfaces are needed to compute the areas and perimeters occupied by phases. These heights were obtained from the provided phase fraction profiles and the flow video recordings. Other inputs such as flow mixture velocity, input water cuts, pipe roughness and diameter, density and viscosities of phases were provided and were directly used in the model. The friction factor was calculated using the Churchill correlation in given in equation 5.7. and finally the pressure gradient for each phase and total pressure gradient were obtained.

5.3.1 Comparison of the Model and the Experimental Data

The model was tested by using different data provided by SINTEF. Unfortunately with the two experiments, both the 2018 and 2019 experiments, very few experiments gave out good predictions that were close to the measured experimental data. Both data from the two experiments were combined to test the model and figure 5.9 was produced to show the comparison made between the experimental pressure gradients and the predicted pressure gradient from the three layers flow model. From the model results, It was observed that the correct predictions appeared at higher water fractions which were very close to the water cut at the phase inversion of the dense packed layer. Figure 5.10shows the plot of pressure gradient versus water cut where the phase inversion point occurred at an average water cut of 0.5 for a mixture velocity of 1m/s where most of the three layers pattern were observed.

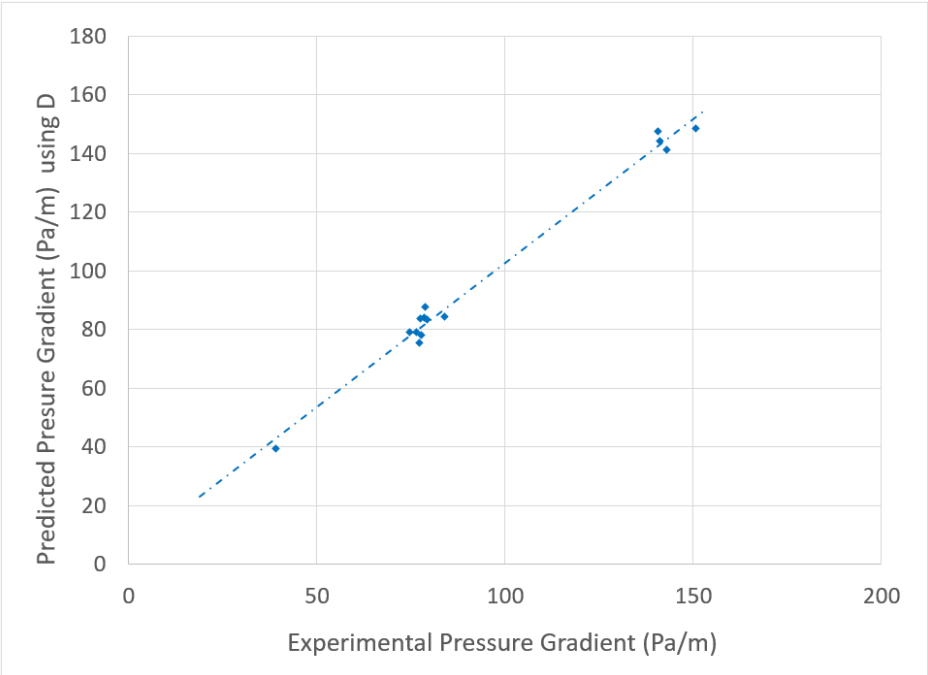

Figure 5.9: experimental v/s model prediction pressure gradient

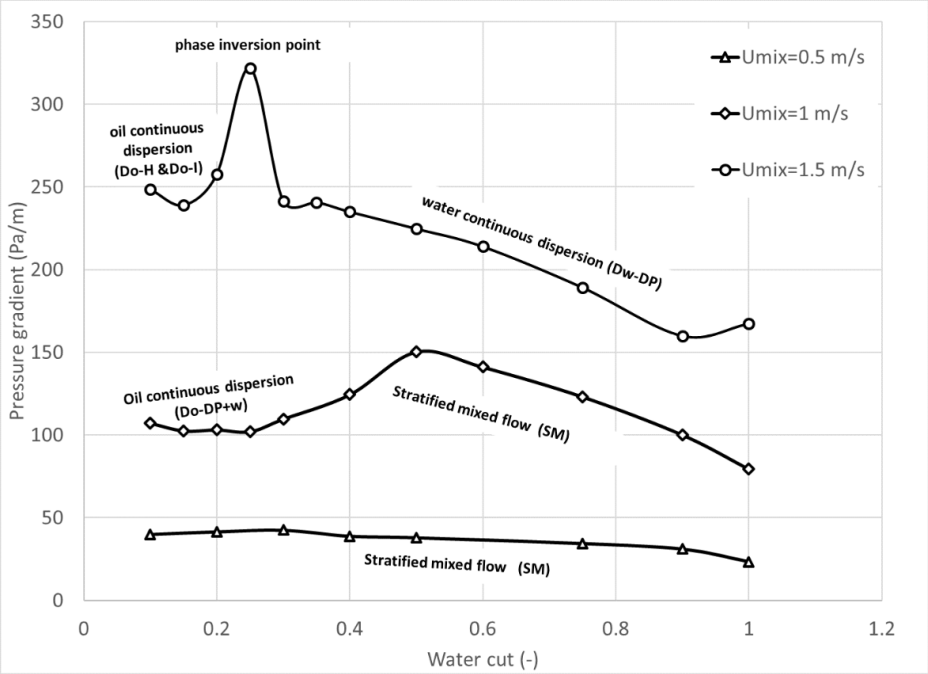

Figure 5.10: Pressure gradient versus input water fraction for different mixture velocities.

Both the pipe diameter and the hydraulic diameters were used in the computation of pressure gradient by the model. For this model however, the hydraulic diameter did not give good prediction results. Figure 5.11 shows the results of the model with pipe diameter and hydraulic diameter used. For the 2019 experiments, where the medium oil viscosity was used, the water fraction of between 0.3 to 0.4 gave out nice pressure drop predictions with the pipe diameter. for the low oil viscosity experiments, the water fraction of 0.4 to 0.6 gave out nice prediction results.

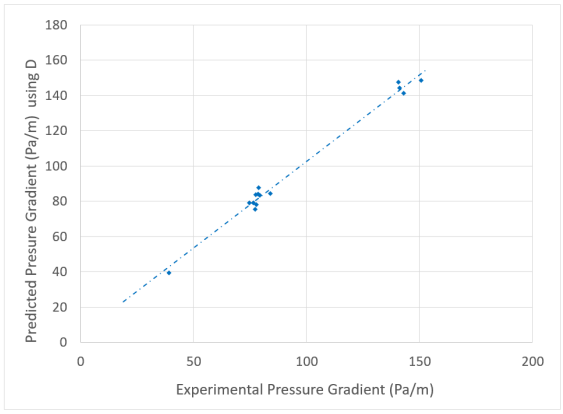

(a) model Vs experimental data with pipe diameter used

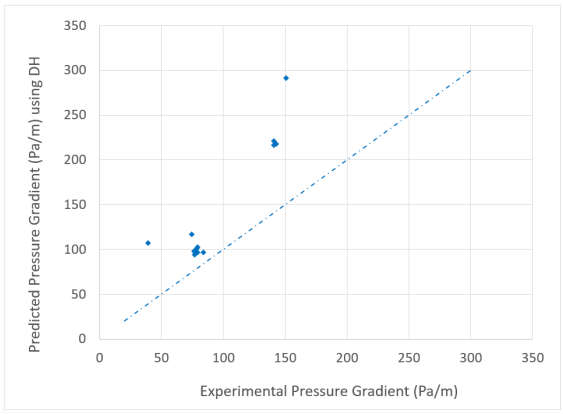

(b) model Vs experimental data with hydraulic diameter

Figure 5.11: Comparison of the models on the use of pipe diameter and hydraulic diameter

For the experiments that did not give good predictions of pressure gradient with the three layers flow model, they were tested with the two fluid model and resulted in to good predictions. It is possible that the two fluid model made good predictions because of the nature of the interface of such particular experiments. Different kinds of interfaces have been presented for example by Angeli & Hewitt (2000), Brauner (2002), Valle (1998) and Soleimani (1999) that might affects the prediction of pressure gradients by models that assume the smooth interface. It is also possible that most of three layers flow patterns did not give out good predictions because of the a sufficient deviation between the input phase fractions and insitu holdups. A large deviation in these two parameters is mostly attributed by the existing slip between the fluid phases. Angeli & Hewitt (2000) reported that slip is used to express the difference between the input phase ratios and the insitu phase fractions.

Also some experiment's flow patterns were not clearly identified to be belonging in a three layers flow pattern. These flows were tested with with the three layers model and were identified. For those in which the model predictions agreed with the measured pressure gradients, they were considered as the three layers flow patterns with the dense packed layer of droplets at the middle of oil and water continuous phases. This is to also add that the model could be used to identify the three layers flow pattern on top of phase fraction profiles and flow video recordings.

Chapter 6

Droplets Analysis

The effect of pressure drop across the mixing valve was tested to assess the droplets size distribution in the subsquent test section. Five experiments with the same water cut (WC=0.2), and mixing velocity (Umix=1m/s) were analyzed for pressure drop across the mixing valve (DP= 0.1, 0.2, 0.35, 0.5 and 1 (bar)). These test points were comparable with data from the 2018 experiments in terms of WC, flowrate and DPvalve. Also, the combination is relevant for real production systems, representing a typical situation for flow through a control valve or the choke upstream a separator.

6.1 Droplets Measurement

Droplets images covering three different positions along the pipe in flow direction were provided for all five experiments. The first position was 0.7m from the mixing valve and the remaining two were 106.5m and 219.3m from the mixing valve. In figure 6.2 and other related figures, the positions 1,3 and 4 corresponds to 0.7m, 106.5m and 219m from the mixing valve respectively. At every point along the test section, three different points inside the pipe cross section (top(8cm) , middle(6cm) and bottom(3)) were sampled to get a course distribution along the vertical direction in the cross section of the pipe. The droplets were then counted and measured from the provided images, by a special program known as Image j. The picture illustrating the manual counting and measurement can be seen in figure 6.1. During the process of measurement, the counted droplets were marked to avoid counting one droplet more than once and the distance which is measured in pixel is recorded in an excel file. At least 500 droplets were counted per measurement point in order to get a representative size distribution. Similar values were used by Fossen & Schümann (2017). In the process of counting, for most images with poor quality, measurements were also done if at least 3/4 of the droplets quality shape was seen. Droplets counts were further processed in order to calculate the mean sizes and to find maximum diameter for droplets at each position across and along the pipe. Plots of histograms and normal distribution were also produced and can be observed in appendix ...

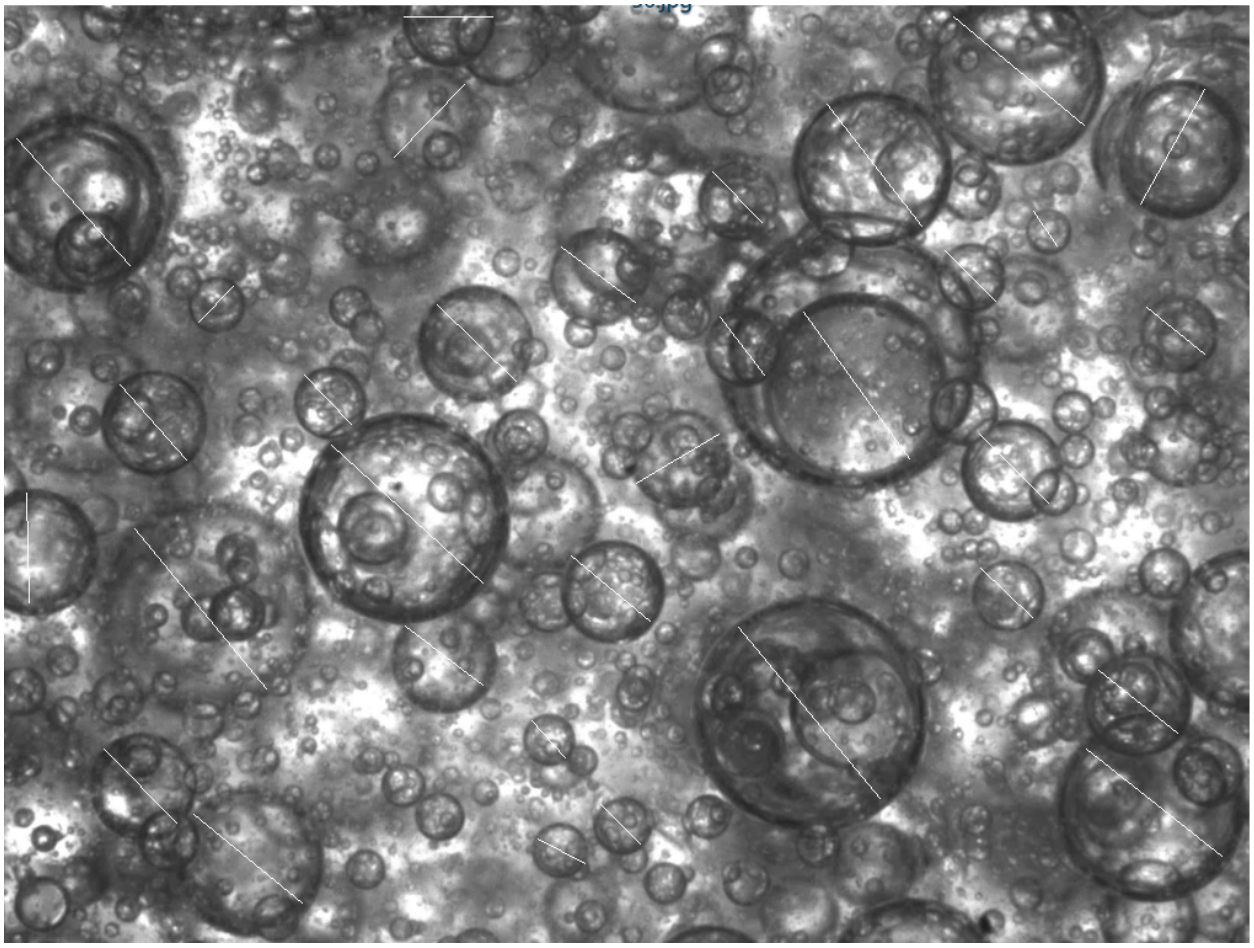

Figure 6.1: Manual counting of droplets by image j

6.2 droplets distribution and sizes

In figure 6.2 are the normal distribution curves that were plotted to assess the effect of pressure drop across the mixing valve on the size of droplets. Normally, the turbulent forces created by different mixing in the flow causes droplet's coalescence and droplets breakup. Low to medium turbulence may result into coalescence of droplets that aids the separation of phases as the flow continues Typhonix (2015). Increased mixing withing the flow itself increases the turbulence forces that results in the breakup of droplets which can also take longer time to separate. On the other hand, zones with strong mixing (like the valve) will lead to break up of droplets. The produced droplets will be considerably smaller than droplets that would have been produced by the turbulence in the flow itself. Therefore, we can expect the flow development in the pipe to be dominated by coalescence and settling of droplets leading to a gradual separation of the flow with distance from the valve. Such a behavior was clearly identified in the 2018 experiments for which a low viscosity oil was oil. This was however not observed from the behaviour of droplets seen in figure 6.2. From the figure there is no clear trend that showed the growth or breakup of droplet across and along the test section.

For increased pressure drop across the mixing valve the variation in droplets sizes was also not clearly deducted. A large decrease in droplets size was observed however, when pressure drop was changed from 0.1 to 0.2 but the trend was not observed in the remaining curves

where the pressure drop across the mixing valve increased. The decrease in size would be explained by the increased mixing but the trend was not observed for higher pressure drop across the mixing valve. The possible reason could be due to sampling procedures used as the similar case was observed by Fossen & Schümann (2017). Fossen & Schümann (2017) performed their experiments in the the same facilities and they observed a modest decrease in droplets sizes when they increased the flowrate for a given pressure drop across the mixing valve but the trend was different for other pressure drops. For lower pressure drops (0.05, 0.1 and 0.25) they observed a higher variation in flow rates but the trend was not observed in higher pressure drops. They explained this decrease to be due to sampling procedures if the sampling probe was placed far from the interface.

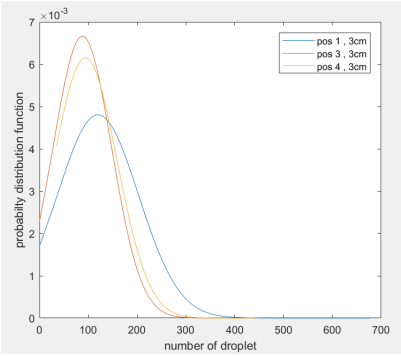

(a) Position 0.7, 106.5, 219m at 3cm for 0.1 bar DP

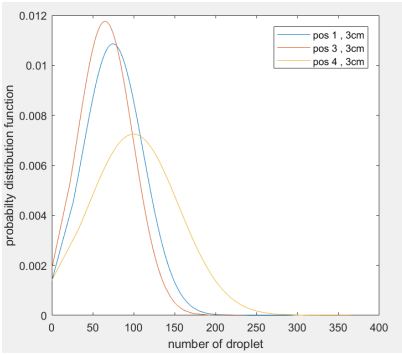

(b) Position 0.7, 106.5, 219m at 3 cm for 0.2 bar DP

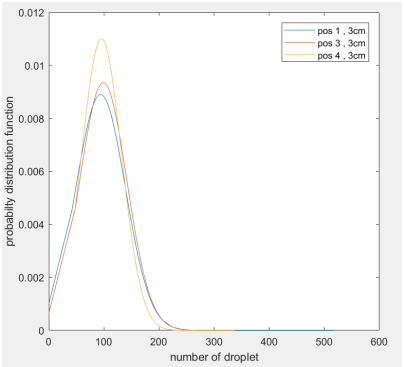

(c) Position 0.7, 106.5, 219m at 3cm for 0.35 DP

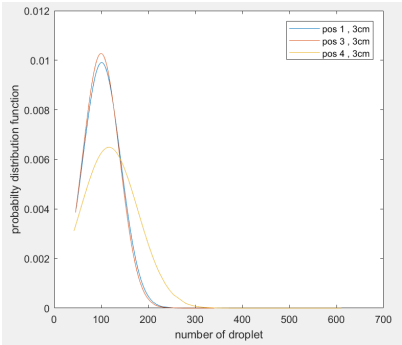

(d) Position 0.7, 106.5, 219m at 3cm for 0.5 bar DP

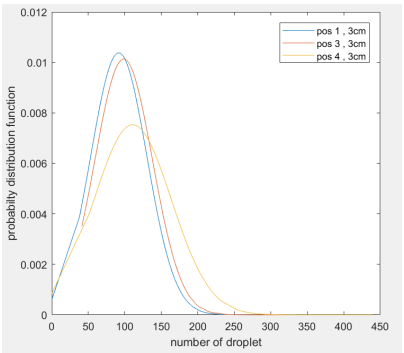

(e) Position 0.7, 106.5, 219m at 3cm for 1 bar DP

Figure 6.2: Normal distribution plots for Pressure drop of 0.1, 0.2, 0.35, 0.5 and 1 bar at the mixing valve respectively

The D32 were also calculated and plotted for different positions within the pipe cross section and along the pipe, see tables A.1, A.2, A.3, A.4, and A.5. As it can be observed in figure 6.3, the D32 results shows that the droplets were bigger at a pressure drop of 0.1 (occupying mean size of between 130 to 200 micrometer) and of smaller sizes at the remaining higher pressure drops across the mixing valve (roughly between 100 to 180 micrometer). From the pressure drop of 0.2, 0.35, 0.5 to 1 bar, the D32 shows a random distribution of droplets across the pipe cross section. The mean sizes do not show the clear trend if the droplets sizes are larger at the bottom and smaller at the top or vice versa. These results therefore shows that, increasing pressure drop across the mixing valve, also does not seem to clearly

increase or decrease the size of droplets across the pipe diameter.A very small decrease in size that falls within the uncertainty range is traced for these variations in pressure drop but this difference cannot really tell if the droplets were decreasing or not since the measurement errors are also considered.

Along the pipe however, a considerably small increase in size has been noticed for the pressure drops of 0.1, 0.2, 0.5 and 1.0 bar. This could possibly be the droplets growth process which is happening too slow. High viscosity means that there is large frictional force which is hindering the interaction of droplets within the flow. For this reason the droplets misses the collision and coalescence chances leading to a very slow or no growth of droplets sizes along the test section. The high viscous forces suspending a droplet are therefore keeping the droplet still and no free movement of a droplet within the flow except that caused by the flow itself. The above explained trend is for the plots of oil-water dispersion produced from oil of 35cp viscosity. The mini plots embedded in the big plots were produced from the data obtained when the oil viscosity of 1.43 cp was used and will be explained in the next section.

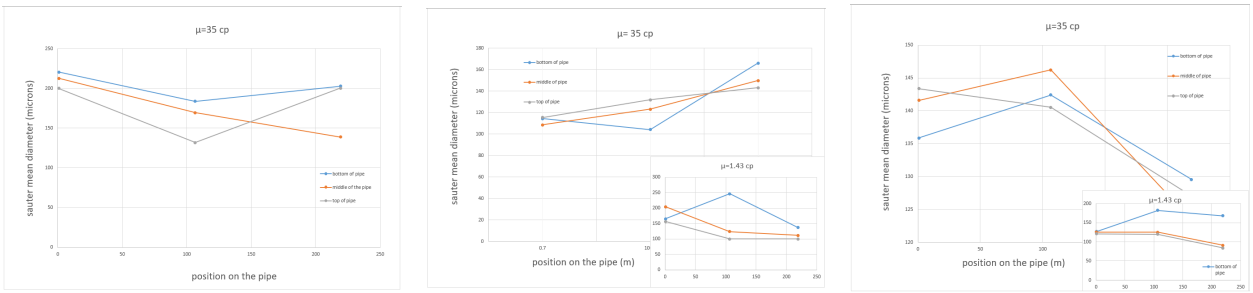

(a) D32 for 0.1 bar DP

(b) D32 for 0.2 bar DP

(c) D32 for 0.35 bar DP

(d) D32 for 0.5 bar DP

(e) D32 for 1.0 bar DP

Figure 6.3: The Sauter mean diameter for different oils and pressure drops across the mixing valve

6.2.1 Effects of Viscosity on droplets size

The size of droplets with the medium oil viscosity were then compared to the size of droplets for the experimental data where the low oil viscosity was used. The analysis of medium oil viscosity experiments can be observed in normal distribution plots in Appendix C, histograms located in appendix B, the Dmax and D32 tables of appendix A, together with figures 6.4 and 6.3. This analysis is compared with the analysis made by Kivuyo & Issara (2018) for experiments with low viscosity oil. Generally the size of droplets on the experiments

with medium oil viscosity was observed to be smaller compared to the size of droplets in the experiments with lower oil viscosity. The peaks in the histogram plots in appendix B, suggest that most droplets are of an average size below 70 micrometer for the medium oil viscosity. For the low viscosity oils, most droplets were observed to have an average size of above 70 micrometer Kivuyo & Issara (2018). The maximum sizes of droplets diameter as can be observed in figure 6.4 shows clearly that the sizes of droplets have dropped when the oil with medium viscosity was used. Figure6.4 (b) (c) and (d) shows the trend of maximum droplet's diameters with the low and medium oil viscosity used on the experiments with the same water cut, velocity and the same pressure drop across the mixing valve.

Pal (1996) noticed that the smaller droplets were associated with the higher emulsion viscosities when studying the effects of droplets size on the rheological behaviours of oil water flows. In this thesis work, the calculated effective/apparent viscosity oil water mixture with oil viscosity of 35 cp was higher compared to that of 1.43 cp. For this reason therefore, the smaller droplets sizes that were observed with an oil viscosity of 35 cp could be explained by the observation made by Pal (1996), that small droplets are associated with the higher oil viscosity and large droplets with lower oil viscosity. Kukizaki & Goto (2006) Also obtained the smaller droplets when they used higher oil viscosities. In their experiments they observed larger droplets with the low oil viscosity and smaller droplets with higher oil viscosity.

The settling of droplets was observed in the experiments of 2018 but not on the 2019 experiments. Due to the influence of gravity forces, Kivuyo & Issara (2018) and Fossen & Schümann (2017) found that for low viscosity oils, the droplets were growing and then settle down, with the bottom of the pipe being concentrated with larger droplets while the top part of the pipe remained with large concentration of smaller droplets. In the experiments of 2019, this behaviour was not observed. The droplets were being suspended over large distances without settling because the viscous forces overcome the gravitational forces.

6.2.2 Effects of Surfactants on Droplets Size

It has to be noted that there are other factors that might result in the existence of smaller droplets inside the flow. Once they have been formed, the smaller droplets could be stabilized by the presence of chemical surfactants and small solid fines that forms around the film of the droplets. Typhonix (2015) highlighted that the stability of emulsions/droplets increases as the droplets get smaller. Over long pipe distances, these droplets might be suspended in the flow without breaking or coalesce inside the flow as they have been kept stable by the added surfactant. Between the two experiments presented in this work, this case was not observed in the first experiments inlvolving low oil viscosities. In the low oil viscosity experiments, there was an addition of a known type and concentration of surfactant for the stabilization of dispersion but the droplets were observed to grow at different points along the pipe. With medium oil viscosities, the blended oils contained surfactants but the concentration were not identified. The surfactant seemed to stabilize the droplets in addition to the viscosity effect. Shi et al. (2000) found that the mixture of oil and water at lower input water cuts and higher superfacial velocities lead to easier mixing and production of emulsion but Surfactant addition resulted in a distribution of small droplets that occupied large surface area and preferred to stay in that state. This was because large mixing created smaller droplets whose interfaces were stabilized by the surfactant over time.

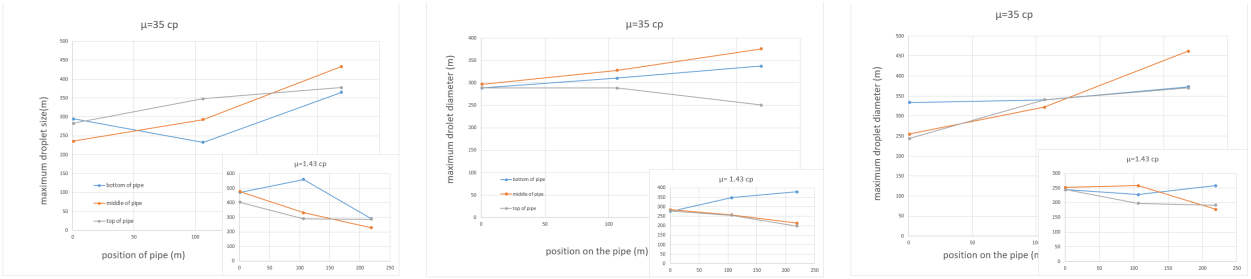

(a) Dmax with DP=0.2 bar (b) Dmax with DP=0.35 bar (c) Dmax with DP=0.5 bar

Figure 6.4: Maximum droplets diameter for different oil viscosities and Pressure drops across the valve

Chapter 7

Conclusion

Two different experiment were compared for their results in this thesis work. The difference in the experiments relied on the difference in the viscosities of oils used with 2018 experiments conducted with low oil viscosity while the new experiments of 2019 had a medium viscosity oil. 2019 data were analyzed for flow patterns identification and for the investigation and comparison of the distribution of droplets inside the flow when there are different mixing at the test section inlet. From other data obtained by these two experiments, two models were tested against the experimental data to see if the models worked properly and could be used in the prediction of pressure gradient along the pipe. Below were the findings:

- The identified flow Patterns from flow video recordings and phase fraction profiles for both experiments were Stratified Smooth, Stratified Wavy, Stratified Mixed, Homogeneous oil dispersion, Inhomogeneous oil dispersion, Homogeneous water dispersion, Inhomogeneous water dispersion, Oil dispersion with dense packed layer and Water dispersion with dense packed layer. An additional flow Pattern was observed in the experiments with high oil viscosities but not in the low oil viscosities. This flow pattern was Oil dispersion with dense packed layer plus water layer.
- From the 2019 experimental data, It was observed that the Pressure drop was higher for dispersed flows more than the stratified flows. Increased pressure across the mixing valve highly increased the pressure gradient along the test section since the most produced patterns were the dispersed flow patterns. Increased mixture flowrate also increased the pressure gradient and the flow took longer time to separate. Increased water cut also increased the pressure drop when the type of dispersion were water in oil dispersion but the pressure decreased after the phase inversion point where oil droplets were suspended in water.
- The two fluid model and the three layers models were both tested by using the experimental data and they both predicted well the pressure gradient along the pipe. Few data among the identified three layers flow pattern were well predicted by the three layers model gave out good predictions while some did not give good results. The predictions of the two fluid model were improved when the hydraulic diameter was used but for the three layers model the results were not improved by the hydraulic diameter.
- In the last part, the droplets sizes were counted measured and analyzed for their distribution in the flow. It was found out that the droplets from the low oil viscosity were growing and settle at the bottom of the pipe. However, for higher viscosity oils,

a considerably slow growth of droplets was observed but the droplets were not seem to settle nor break inside the flow. This was mentioned to be the attributed by the effect of higher viscosity, the type and the concentration of surfactant that was used in this experiments.

References

Al-Moosawy, A., Al-Hattab, T., & Al-Joubouri, T. (2008). Analysis of liquid–liquid two phase flow system. *Emirates J. Eng. Res*, *13*, 19–26.

Amundsen, L. (2011). *An experimental study of oil-water flow in horizontal and inclined pipes.*

Angeli, P., & Hewitt, G. (1999). Pressure gradient in horizontal liquid–liquid flows. *International journal of multiphase flow*, *24*(7), 1183–1203.

Angeli, P., & Hewitt, G. (2000). Flow structure in horizontal oil–water flow. *International journal of multiphase flow*, *26*(7), 1117–1140.

Arirachakaran, S., Oglesby, K., Malinowsky, M., Shoham, O., & Brill, J. (1989). An analysis of oil/water flow phenomena in horizontal pipes. In *Spe production operations symposium.*

Atkinson, D., & Strauss, W. (1978). Droplet size and surface tension in venturi scrubbers. *Journal of the air pollution control association*, *28*(11), 1114–1118.

Brauner, N. (1991). Two-phase liquid-liquid annular flow. *International journal of multiphase flow*, *17*(1), 59–76.

Brauner, N. (2002). Modelling and control of two-phase phenomena: liquid-liquid two-phase flow systems. *CISM Center, Udine, Italy*, 1–59.

Brinkman, H. (1952). The viscosity of concentrated suspensions and solutions. *The Journal of Chemical Physics*, *20*(4), 571–571.

Charles, M. E., Govier, G. t., & Hodgson, G. (1961). The horizontal pipeline flow of equal density oil-water mixtures. *the Canadian Journal of Chemical engineering*, *39*(1), 27–36.

Chesters, A. (1991). Modelling of coalescence processes in fluid-liquid dispersions: a review of current understanding. *Chemical engineering research and design*, *69*(A4), 259–270.

Elseth, G. (2001). *An experimental study of oil/water flow in horizontal pipes.* Fakultet for ingeniørvitenskap og teknologi.

Filippa, L., Trento, A., & Álvarez, A. M. (2012). Sauter mean diameter determination for the fine fraction of suspended sediments using a lisst-25x diffractometer. *Measurement*, *45*(3), 364–368.

Fossen, M., & Schümann, H. (2017). Experimental study of the relative effect of pressure drop and flow rate on the droplet size downstream of a pipe restriction. *Journal of Dispersion Science and Technology*, *38*(6), 826–831.

Hasan, S. W., Ghannam, M. T., & Esmail, N. (2010). Heavy crude oil viscosity reduction and rheology for pipeline transportation. *Fuel*, *89*(5), 1095–1100.

Hinze, J. (1955). Fundamentals of the hydrodynamic mechanism of splitting in dispersion processes. *AIChE Journal*, *1*(3), 289–295.

Ibarra, R., Markides, C. N., & Matar, O. K. (2014). A review of liquid-liquid flow patterns in horizontal and slightly inclined pipes. *Multiphase Science and Technology*, *26*(3).

Kivuyo, R., & Issara, B. (2018). Development of surfactant stabilized oil-water flow. *Masters Project, Norwegian University of science and Technology*.

Kukizaki, M., & Goto, M. (2006). Effects of interfacial tension and viscosities of oil and water phases on monodispersed droplet formation using a shirasu-porous-glass (spg) membrane. *Membrane*, *31*, 215–220.

Lignel, S., Salsac, A.-V., Drelich, A., Leclerc, E., & Pezron, I. (2017). Water-in-oil droplet formation in a flow-focusing microsystem using pressure-and flow rate-driven pumps. *Colloids and Surfaces A: Physicochemical and Engineering Aspects*, *531*, 164–172.

Liu, S., & Li, D. (1999). Drop coalescence in turbulent dispersions. *Chemical Engineering Science*, *54*(23), 5667–5675.

Lovick, J., & Angeli, P. (2004). Droplet size and velocity profiles in liquid–liquid horizontal flows. *Chemical engineering science*, *59*(15), 3105–3115.

Malvern. (2012). A basic guide to particle characterization. *MRK1806-01*.

Mooney, M. (1951). The viscosity of a concentrated suspension of spherical particles. *Journal of colloid science*, *6*(2), 162–170.

Nädler, M., & Mewes, D. (1995). The effect of gas injection on the flow of immiscible liquids in horizontal pipes. *Chemical Engineering & Technology: Industrial Chemistry-Plant Equipment-Process Engineering-Biotechnology*, *18*(3), 156–165.

Pal, R. (1988). *Emulsions: Pipeline flow behavior, viscocity equations and flow measurement.*

Pal, R. (1996). Effect of droplet size on the rheology of emulsions. *AIChE Journal*, *42*(11), 3181–3190.

Pal, R., & Rhodes, E. (1989). Viscosity/concentration relationships for emulsions. *Journal of Rheology*, *33*(7), 1021–1045.

Pergushev, L., & Tronov, V. (1998). Breakup of drops in a pipeline. *Journal of engineering physics and thermophysics*, *71*(3), 465–469.

Petrowiki. (2012). *Produced oil field water.* Retrieved 2018-01-15, from `https://petrowiki.org/Produced_oilfield_water`

Roumpea, E., Kovalchuk, N. M., Chinaud, M., Nowak, E., Simmons, M. J., & Angeli, P. (2019). Experimental studies on droplet formation in a flow-focusing microchannel in the presence of surfactants. *Chemical Engineering Science*, *195*, 507–518.

Schick, R. J. (1997). General guidelines on drop size measurement techniques and terminology. *Chemical Processing Industry Exposition*, *20*(7).

Schlumberger. (2016). *Liquid particle size analyzers.* Website. Retrieved from "https://www.jmcanty.com/product/liquid-particle-size-analyzers"

Schümann, H. (2016). *Experimental investigation of transitional oil-water pipe flow.* NTNU.

Shi, H., Cai, J., Gopal, M., & Jepson, W. (2000). The effect of surfactants on low water cut oil-water flows in large diameter pipelines. In *Bhr group conference series publication* (Vol. 40, pp. 91–114).

Smith, I. E., Nossen, J., Kjølaas, J., & Lund, B. (2015). Development of a steady-state point model for prediction of gas/oil and water/oil pipe flow. *Journal of Dispersion Science and Technology*, *36*(10), 1394–1406.

Soleimani, A. (1999). Phase distribution and associated phenomena in oil-water lows in horizontal tubes. *Ph. D. Thesis, Imperial College of Science, Technology & Medicine*.

Trallero, J., Sarica, C., & Brill, J. (1997). A study of oil-water flow patterns in horizontal pipes. *SPE Production & Facilities*, *12*(03), 165–172.

Typhonix. (2015). *The effect of shear on oil-water mixture.* Website. Retrieved from "http://www.lowshearschool.com/?page_id=16933",

Valle, A. (1998). Multiphase pipeline flows in hydrocarbon recovery. *Multiphase Science and Technology*, *10*(1).

Vedapuri, D. (1999). *Studies on oil-water flow in inclined pipelines* (Unpublished doctoral dissertation). Ohio University.

Vigneaux, P., Chenais, P., & Hulin, J. (1988). Liquid-liquid flows in an inclined pipe. *AIChE Journal*, *34*(5), 781–789.

Vuong, D. H., Zhang, H.-Q., Sarica, C., & Li, M. (2009). Experimental study on high viscosity oil/water flow in horizontal and vertical pipes. In *Spe annual technical conference and exhibition.*

Appendices

Appendix A

Useful Tables and Charts

Table A.1: Dmax and Sauter mean diameter: Umix=1m/s, WC=0.2, DP=0.1bar

Distributions	Pos 1,3cm	Pos 1,6cm	Pos 1,8cm	Pos 3,3cm	Pos 3,6cm	Pos 3,8cm	Pos 4,3cm	Pos 4,6cm	Pos 4,8cm
Dmax	435.0	382.1	460.0	383.3	427.2	347.2	440.8	384.2	433.6
D32	220.4	212.5	199.8	183.6	169.2	131.8	202.6	138.71	200.1

Table A.2: Dmax and Sauter mean diameter: Umix=1m/s, WC=0.2, DP=0.2bar

Distributions	Pos 1,3cm	Pos 1,6cm	Pos 1,8cm	Pos 3,3cm	Pos 3,6cm	Pos 3,8cm	Pos 4,3cm	Pos 4,6cm	Pos 4,8cm
Dmax	294.9	236.0	283.0	232.8	293.2	347.9	365.9	432.9	377.4
D32	114.3	108.4	115.5	104.1	123.1	131.8	165.9	149.7	143.1

Table A.3: Dmax and Sauter mean diameter: Umix=1m/s, WC=0.2, DP=0.35bar

Distributions	Pos 1,3cm	Pos 1,6cm	Pos 1,8cm	Pos 3,3cm	Pos 3,6cm	Pos 3,8cm	Pos 4,3cm	Pos 4,6cm	Pos 4,8cm
Dmax	288.5	297.0	289.2	310.5	328.0	288.7	337.4	375.7	250.6
D32	137.9	127.9	131.9	135.7	129.52	149.4	164.7	180.2	143.9

Table A.4: Dmax and Sauter mean diameter: Umix=1m/s, WC=0.2, DP=0.5bar

Distributions	Pos 1,3cm	Pos 1,6cm	Pos 1,8cm	Pos 3,3cm	Pos 3,6cm	Pos 3,8cm	Pos 4,3cm	Pos 4,6cm	Pos 4,8cm
Dmax	333.6	254.7	243.9	340.3	322.0	340.6	373.0	462.0	370.0
D32	114.3	108.4	115.5	104.1	123.1	131.8	165.9	149.7	143.1

Table A.5: Dmax and Sauter mean diameter: Umix=1m/s, WC=0.2, DP=1bar

Distributions	Pos 1,3cm	Pos 1,6cm	Pos 1,8cm	Pos 3,3cm	Pos 3,6cm	Pos 3,8cm	Pos 4,3cm	Pos 4,6cm	Pos 4,8cm
Dmax	268.3	333.6	284.7	323.1	275.8	334.1	439.6	378.4	386.3
D32	126.1	127.3	123/4	134.5	131.3	140.9	175.7	165.9	151.9

EXP_ID	Umix	WC	Uso	Usw	Usg	Dpvalve	Rho_w	Rho_o	Pgrad_1	Pgrad_2	Pgrad_3	Pgrad_4	Hw_1	Hw_2	Hw_3	Hw_4
	[m/s]	[-]	[m/s]	[m/s]	[m/s]	[bar]	[kg/m3]	[kg/m3]	[Pa/m]	[Pa/m]	[Pa/m]	[Pa/m]	[-]	[-]	[-]	[-]
ce19020_000	0.52	0.00	0.52	0.00	0.00	-0.06	999.76	849.61	49.35	50.18	50.20	50.94	0.00	0.00	0.00	0.00
ce19025_000	0.50	0.00	0.50	0.00	0.00	-0.06	1000.40	850.38	48.49	50.05	48.17	48.85	0.03	0.01	0.02	0.03
ce19026_000	0.49	0.00	0.49	0.00	0.00	-0.06	1000.40	850.57	49.45	50.11	48.17	47.99	0.00	0.00	0.00	0.00
ce19028_000	0.76	0.00	0.76	0.00	0.00	0.01	999.91	851.33	77.82	79.09	76.77	81.66	0.00	-0.01	0.01	-0.02
ce19028_001	0.00	0.53	0.00	0.00	0.00	0.00	999.92	842.96	-3.33	-3.80	-5.39	-4.60				
ce19025_001	1.01	0.00	1.01	0.00	0.00	-0.06	1000.4	850.30	124.50	106.26	103.09	106.00	0.02	0.01	0.02	0.02
ce19021_000	0.45	1.00	0.00	0.45	0.00	-0.06	999.63	846.79	21.08	20.97	19.87	18.63	1.00	1.00	1.00	1.00
ce19021_001	0.00	0.54	0.00	0.00	0.00	-0.06	999.53	845.44	32.94	19.69	8.10	14.27				
ce19029_000	0.50	1.00	0.00	0.50	0.00	0.01	999.81	846.69	23.87	24.07	21.02	26.63	1.00	1.00	1.00	1.00
ce19029_001	0.50	1.00	0.00	0.50	0.00	0.01	999.81	846.71	23.97	23.89	20.67	26.74				
ce19022_000	0.50	1.00	0.00	0.50	0.00	-0.06	999.74	842.42	24.89	24.38	23.12	21.86	1.01	1.00	1.00	1.01
ce19022_001	1.00	1.00	0.00	1.00	0.00	-0.06	999.57	844.83	82.78	83.22	78.65	80.97				
ce19022_002	1.50	1.00	0.00	1.50	0.00	-0.06	999.59	844.88	175.97	174.76	167.54	168.24				
ce19022_003	2.00	1.00	0.00	2.00	0.00	-0.06	999.35	844.90	299.88	298.53	284.35	284.18				
ce19022_004	0.50	0.00	0.50	0.00	0.00	-0.06	999.50	850.31	47.45	49.54	48.89	48.98	0.00	0.01	0.01	0.01
ce19022_005	1.00	0.00	1.00	0.00	0.00	-0.06	999.50	850.13	114.62	105.18	102.61	105.42				
ce19022_006	1.50	0.00	1.50	0.00	0.00	-0.06	999.53	849.78	346.16	341.34	338.46	338.50				
ce19022_007	1.74	0.00	1.74	0.00	0.00	-0.06	999.49	849.71	451.08	451.05	446.96	448.59				
ce19022_008	0.50	0.00	0.50	0.00	0.00	-0.06	999.52	849.46	44.46	44.98	45.04	46.75				

Figure A.1: 2019 experimental data

ce19022_009	0.55	0.09	0.50	0.05	0.00	-0.06	999.53	850.38	41.54	40.46	37.91	41.86	0.11	0.11	0.09	0.12
ce19022_010	0.50	0.10	0.45	0.05	0.00	-0.06	999.52	856.26	38.19	40.12	38.08	39.97				
ce19022_011	0.49	0.10	0.45	0.05	0.00	-0.06	999.54	857.29	39.91	39.41	38.20	40.82	0.14	0.17	0.14	0.13
ce19022_012	0.49	0.20	0.39	0.10	0.00	-0.06	999.54	859.53	39.33	39.00	38.96	41.56	0.25	0.26	0.23	0.26
ce19024_009	0.50	0.40	0.30	0.20	0.00	-0.06	999.41	856.32	37.82	37.73	35.19	38.85	0.39	0.40	0.36	0.40
ce19024_010	0.50	0.40	0.30	0.20	0.00	-0.06	999.40	854.79	37.12	37.06	34.35	37.28	0.39	0.41	0.36	0.38
ce19022_013	0.49	0.30	0.34	0.15	0.00	-0.06	999.43	864.73	40.96	40.77	39.77	42.52				
ce19022_014	0.50	0.50	0.25	0.25	0.00	-0.06	999.41	855.18	36.93	36.18	35.20	37.91	0.46	0.47	0.43	0.49
ce19022_015	0.50	0.75	0.12	0.37	0.00	-0.06	999.36	852.78	34.74	34.16	33.02	34.37	0.67	0.64	0.62	0.67
ce19022_016	0.50	0.90	0.05	0.45	0.00	-0.06	999.32	851.67	34.80	30.74	29.96	31.00	0.79	0.82	0.80	0.73
ce19022_017	0.50	1.00	0.00	0.50	0.00	-0.06	999.21	851.25	22.03	23.73	20.83	23.31				
ce19023_000	1.00	0.00	1.00	0.00	0.00	-0.06	999.87	849.88	124.66	103.27	100.39	102.84				
ce19023_001	0.98	0.10	0.88	0.10	0.00	-0.06	999.62	863.92	156.02	124.10	109.97	107.24	0.25	0.23	0.17	0.19
ce19025_002	0.97	0.10	0.88	0.10	0.00	-0.06	999.65	861.97	169.09	135.17	112.58	113.35	0.24	0.24	0.17	0.20
ce19025_007	0.98	0.10	0.89	0.10	0.00	-0.06	999.51	855.90	126.80	102.45	95.64	94.20	0.17	0.15	0.11	0.11
ce19026_002	0.97	0.09	0.88	0.10	0.00	-0.06	999.70	857.76	157.56	118.63	108.31	110.18	0.17	0.15	0.12	0.12
ce19025_006	0.98	0.15	0.83	0.15	0.00	-0.06	999.52	858.53	109.17	99.64	93.97	95.17	0.23	0.23	0.16	0.15
ce19026_003	0.98	0.15	0.83	0.15	0.00	-0.06	999.70	857.10	113.65	107.77	103.72	102.58	0.25	0.22	0.16	0.19
ce19023_008	0.97	0.21	0.77	0.20	0.00	-0.06	999.33	854.47	100.03	99.34	100.24	100.40	0.36	0.34	0.22	0.23
ce19025_004	0.97	0.20	0.78	0.20	0.00	-0.06	999.53	857.30	108.12	103.84	98.45	103.19	0.37	0.36	0.24	0.25
ce19026_001	0.85	0.06	0.80	0.05	0.00	-0.06	999.74	850.35	97.99	83.78	78.99	79.71	0.09	0.06	0.06	0.08

Figure A.2: 2019 experimental data

ce19025_005	0.98	0.25	0.73	0.25	0.00	-0.06	999.37	855.31	95.49	98.35	96.25	102.15	0.36	0.33	0.24	0.28
ce19026_004	0.99	0.25	0.74	0.25	0.00	-0.06	999.64	852.49	103.44	100.19	96.45	98.71	0.32	0.26	0.22	0.23
ce19023_007	0.99	0.30	0.69	0.30	0.00	-0.06	999.42	861.75	116.54	112.52	110.64	109.73	0.35	0.36	0.33	0.35
ce19023_006	0.99	0.40	0.60	0.40	0.00	-0.06	999.34	852.85	113.01	116.10	119.07	124.51	0.40	0.40	0.37	0.41
ce19023_005	1.00	0.50	0.50	0.50	0.00	-0.06	999.31	852.31	155.96	150.62	148.06	150.30	0.49	0.47	0.44	0.47
ce19023_004	1.00	0.60	0.40	0.60	0.00	-0.06	999.34	852.31	150.31	142.86	140.64	141.08	0.57	0.55	0.52	0.53
ce19023_003	1.00	0.75	0.25	0.75	0.00	-0.06	999.35	852.55	131.33	126.11	122.90	123.13	0.71	0.68	0.65	0.68
ce19023_002	1.00	0.90	0.10	0.90	0.00	-0.06	996.21	851.68	102.70	101.67	99.50	100.10	0.89	0.83	0.81	0.84
ce19024_000	1.00	1.00	0.00	1.00	0.00	-0.06	999.81	837.62	84.27	84.38	79.18	79.45	1.01	1.01	1.01	1.01
ce19028_002	1.50	0.10	1.34	0.15	0.00	0.03	999.65	856.77	265.51	254.55	244.42	248.63				
ce19028_003	1.46	0.14	1.26	0.21	0.00	0.03	999.64	860.29	293.05	277.85	276.12	239.04				
ce19024_007	1.47	0.20	1.17	0.30	0.00	-0.06	999.61	873.37	258.58	262.56	257.65	257.64	0.34	0.35	0.35	0.36
ce19026_005	1.47	0.20	1.17	0.30	0.00	-0.06	999.65	856.33	319.62	306.05	304.87	291.14	0.31	0.32	0.22	0.23
ce19028_004	1.46	0.20	1.17	0.29	0.00	0.03	999.65	863.43	312.11	320.94	316.76	294.80				
ce19028_005	1.48	0.25	1.11	0.37	0.00	0.03	999.48	860.18	240.03	296.85	357.45	321.93				
ce19024_008	1.47	0.30	1.03	0.45	0.00	-0.06	999.47	869.26	239.81	243.54	238.72	241.60	0.41	0.40	0.39	0.42
ce19028_006	1.48	0.30	1.03	0.45	0.00	0.03	999.29	853.91	219.72	251.13	262.09	274.17	0.42	0.37	0.30	0.31
ce19028_007	1.49	0.35	0.96	0.52	0.00	0.04	999.39	856.59	229.73	236.58	239.45	240.72				
ce19024_006	1.49	0.40	0.89	0.60	0.00	-0.06	999.56	857.85	234.80	236.61	231.95	235.03	0.44	0.44	0.43	0.44
ce19024_005	1.49	0.50	0.74	0.75	0.00	-0.06	999.54	855.73	227.97	227.10	222.46	224.76	0.53	0.51	0.51	0.51
ce19024_004	1.49	0.60	0.60	0.90	0.00	-0.06	999.53	854.91	218.09	216.88	212.34	213.99	0.62	0.60	0.58	0.59

Figure A.3: 2019 experimental data

ce19024_003	1.49	0.75	0.37	1.12	0.00	-0.06	999.36	855.08	189.73	188.83	184.78	189.23	0.77	0.75	0.73	0.75
ce19024_002	1.50	0.90	0.15	1.36	0.00	-0.06	995.97	850.98	175.14	170.23	161.84	160.01	0.89	0.90	0.88	0.90
ce19024_001	1.50	1.00	0.00	1.50	0.00	-0.06	998.33	837.60	179.43	179.01	168.80	167.31				
ce19027_002	0.96	0.20	0.78	0.20	0.00	0.09	999.61	854.72	197.65	170.12	149.48	131.58	0.31	0.31	0.21	0.16
ce19027_000	0.93	0.16	0.78	0.17	0.00	0.19	999.66	860.35	199.59	183.41	172.05	163.67	0.27	0.23	0.21	0.18
ce19027_001	0.95	0.18	0.78	0.19	0.00	0.31	999.70	854.13	209.05	200.51	182.63	177.55	0.29	0.25	0.21	0.19
ce19027_003	0.98	0.20	0.78	0.20	0.00	0.50	999.57	858.90	238.94	223.00	203.64	186.21	0.31	0.28	0.23	0.19
ce19027_004	0.98	0.20	0.79	0.19	0.00	0.89	999.54	851.12	230.65	220.13	220.35	228.89	0.26	0.19	0.21	0.19

Figure A.4: 2019 experimental data

Experimental ID	Umix	WC	DPvalve	Identified Flow Patterns			
	[m/s]	[-]	[bar]	1.6 m	106m	113.9m	218m
ce19022_009	0.55	0.1	0	SM	SM	SM	SM
ce19022_011	0.5	0.1	0	SM	SM	SM	SM
ce19022_012	0.5	0.2	0	SM	SM	SM	SM
ce19024_009	0.5	0.4	0	SM	SM	SM	SM
ce19022_013	0.5	0.3	0	SM	SM	SM	SM
ce19022_014	0.5	0.5	0	SM	SM	SM	SM
ce19022_015	0.5	0.75	0	SM	SM	SM	SM
ce19022_016	0.5	0.9	0	SM	SM	SM	SM
ce19023_001	1	0.1	0	Do-I	Do-I	Do-I	Do-Dp + w
ce19025_006	1	0.15	0	Do-I	Do-Dp + w	Do-Dp + w	Do-Dp + w
ce19023_008	1	0.2	0	Do-I	Do-Dp + w	Do-Dp + w	Do-Dp + w
ce19025_005	1	0.25	0	Do-I	Do-Dp + w	Do-Dp + w	Do-Dp + w
ce19023_007	1	0.3	0	Do-Dp + w	Do-Dp + w	Do-Dp + w	Do-Dp + w
ce19023_006	1	0.4	0	Dw-Dp	SM	SM	SM
ce19023_005	1	0.5	0	Dw-Dp	SM	SM	SM
ce19023_004	1	0.6	0	Dw-Dp	SM	SM	SM
ce19023_003	1	0.75	0	Dw-I	SM	SM	SM
ce19023_002	1	0.9	0	Dw-I	Dw-Dp	Dw-Dp	Dw-Dp
ce19028_002	1.5	0.1	0	Do-H	Do-H	Do-H	Do-H
ce19026_005	1.5	0.2	0	Do-I	Do-I	Do-I	Do-I
ce19028_005	1.5	0.25	0	Do-I	Do-I	Do-I	Do-I
ce19028_006	1.5	0.3	0	Do-I	Do-I	Do-I	Do-I
ce19028_007	1.5	0.35	0	Dw-Dp	Dw-Dp	Dw-Dp	Dw-Dp
ce19024_006	1.5	0.4	0	Dw-I	Dw-Dp	Dw-Dp	Dw-Dp
ce19024_005	1.5	0.5	0	Dw-I	Dw-Dp	Dw-Dp	Dw-Dp
ce19024_004	1.5	0.6	0	Dw-I	Dw-Dp	Dw-Dp	Dw-Dp
ce19024_003	1.5	0.75	0	Dw-I	Dw-Dp	Dw-Dp	Dw-Dp
ce19024_002	1.5	0.9	0	Dw-I	Dw-I	Dw-I	Dw-I
ce19027_002	1	0.2	0.1	Do-H	Do-H	Do-H	Do-H
ce19027_000	1	0.2	0.2	Do-H	Do-H	Do-H	Do-H
ce19027_001	1	0.2	0.35	Do-H	Do-H	Do-H	Do-H
ce19027_003	1	0.2	0.5	Do-H	Do-H	Do-H	Do-H
ce19027_004	1	0.2	1	Do-H	Do-H	Do-H	Do-H

Figure A.5: 2019 Identified Flow Patterns

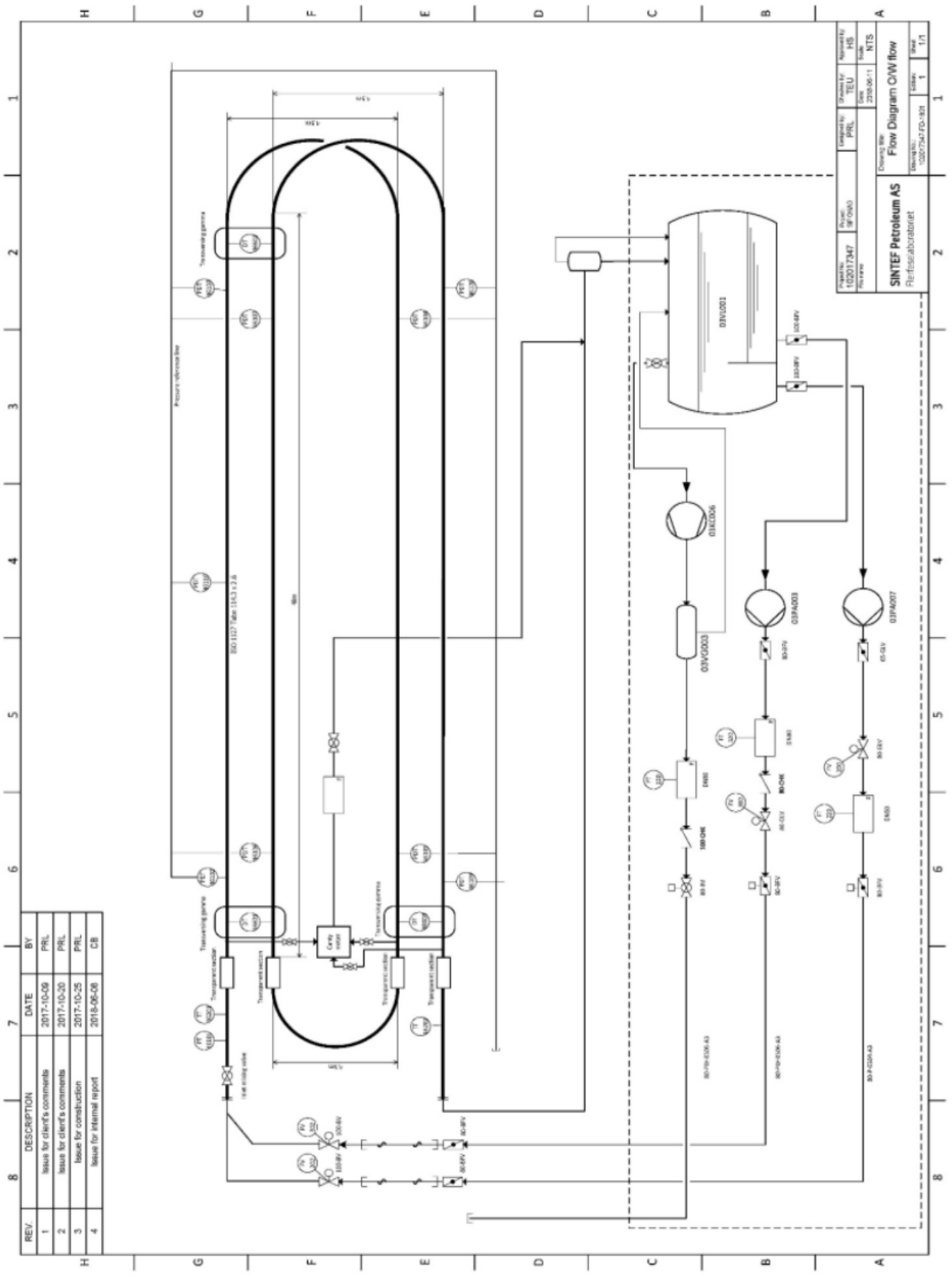

Figure A.6: Piping and instrumentation diagram

Appendix B

Histogram Plots

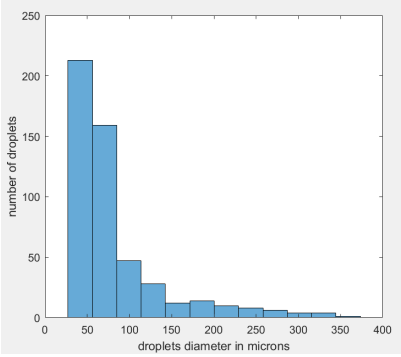

(a) Position 1, 8cm

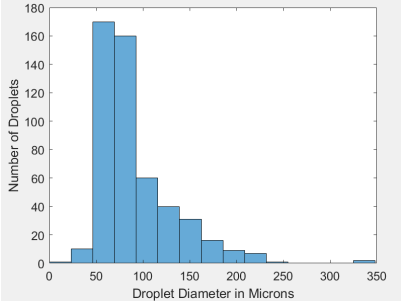

(b) Position 3,8cm

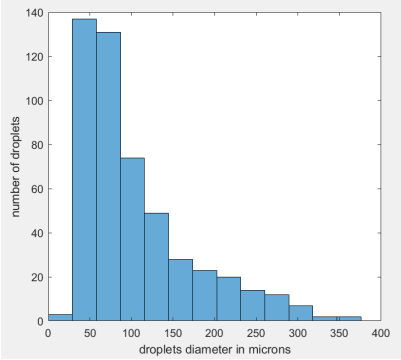

(c) Position 4, 8cm

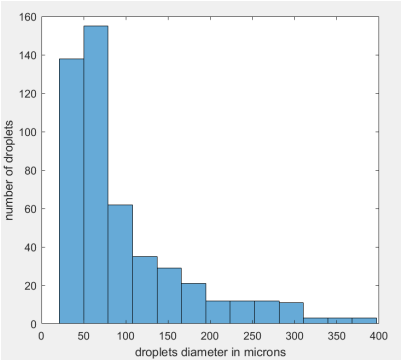

(d) Position 1, 6cm

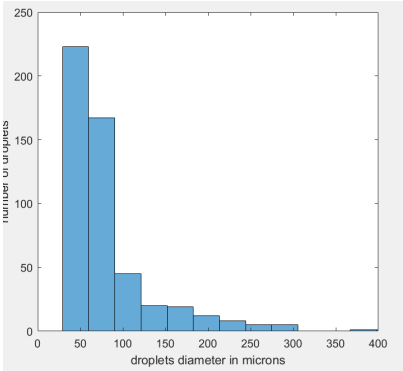

(e) Position 3,6cm

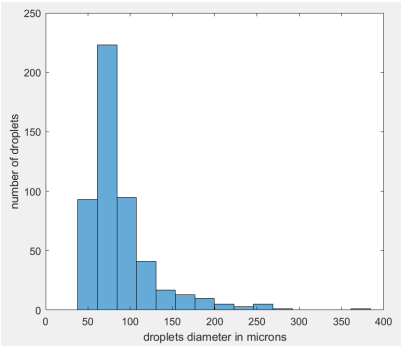

(f) Position 4, 6cm

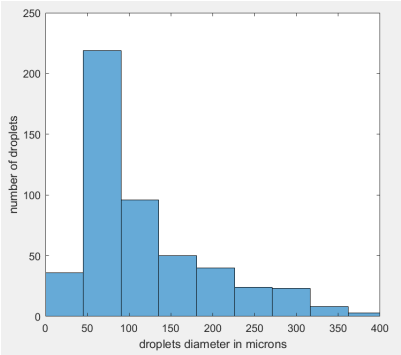

(g) Position 1, 3cm

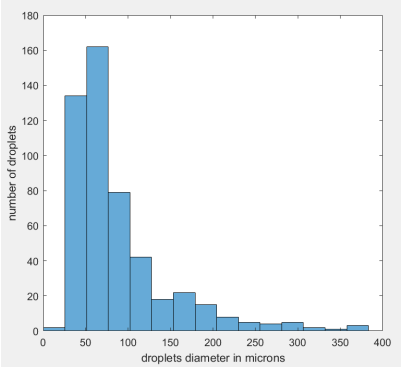

(h) Position 3,3cm

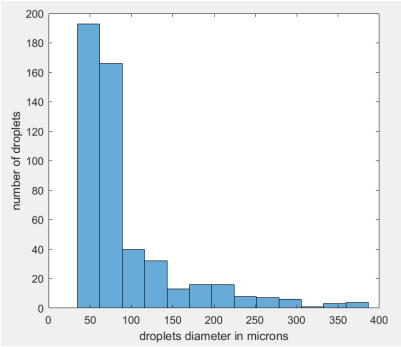

(i) Position 4, 3cm

Figure B.1: Histogram plots for experiment ce19027,002: WC=0.2, Umix=1m/s, DP=0.1 bar

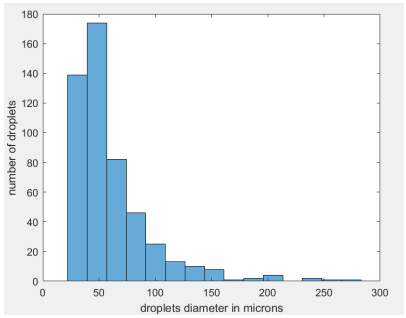

(a) Position 1, 8cm

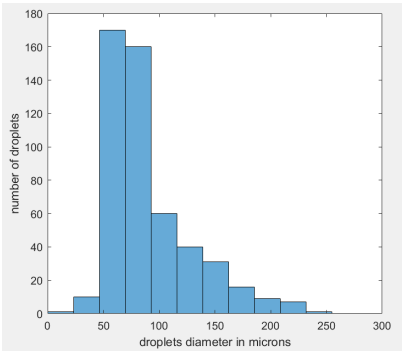

(b) Position 3,8cm

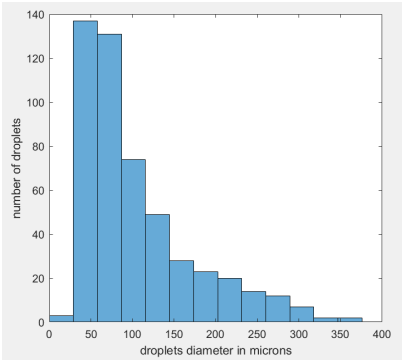

(c) Position 4, 8cm

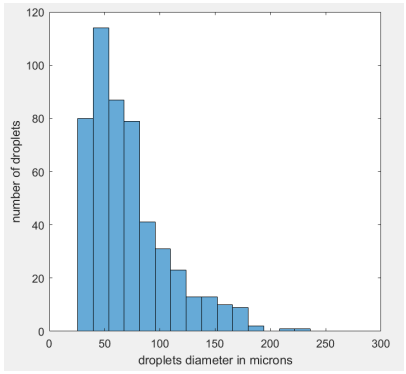

(d) Position 1, 6cm

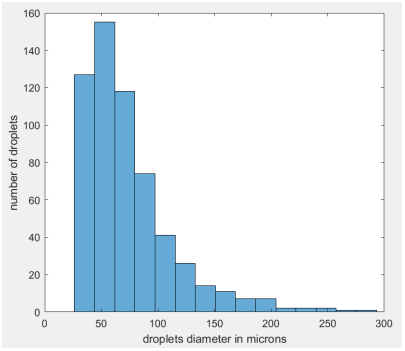

(e) Position 3,6cm

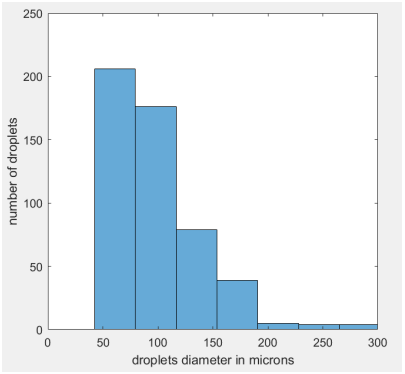

(f) Position 4, 6cm

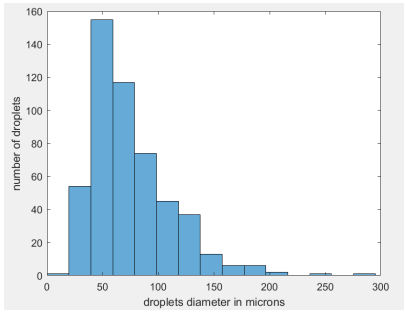

(g) Position 1, 3cm

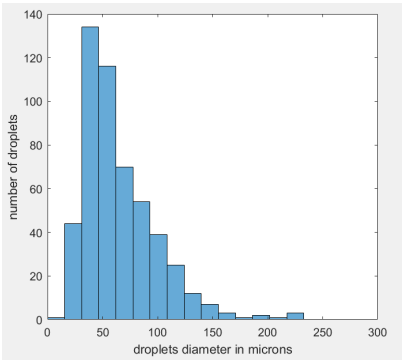

(h) Position 3,3cm

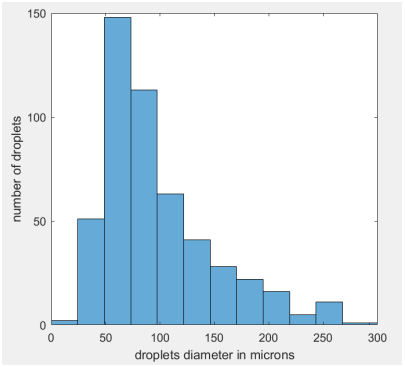

(i) Position 4, 3cm

Figure B.2: Histogram plots for experiment Ce19027,000: WC=0.2, Umix=1m/s, DP=0.2 bar

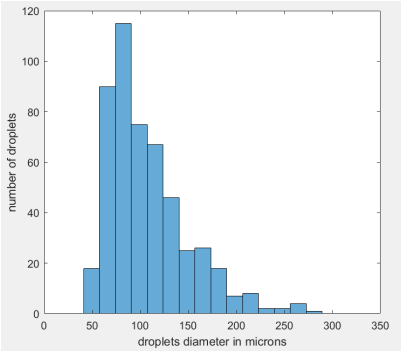

(a) Position 1, 8cm

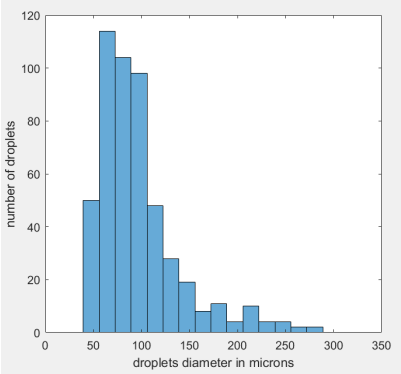

(b) Position 3,8cm

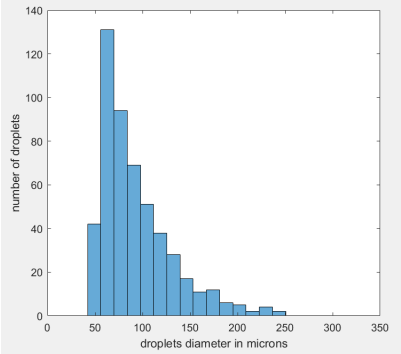

(c) Position 4, 8cm

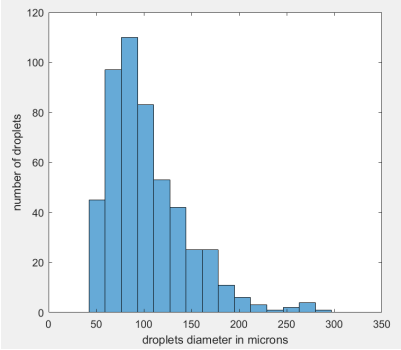

(d) Position 1, 6cm

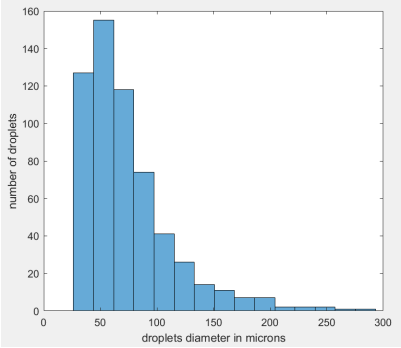

(e) Position 3,6cm

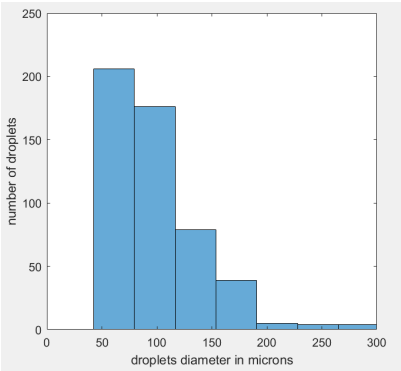

(f) Position 4, 6cm

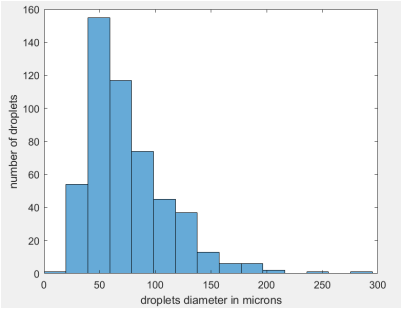

(g) Position 1, 3cm

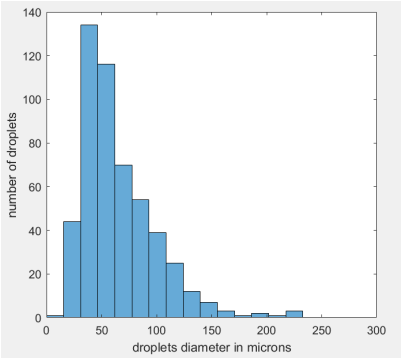

(h) Position 3,3cm

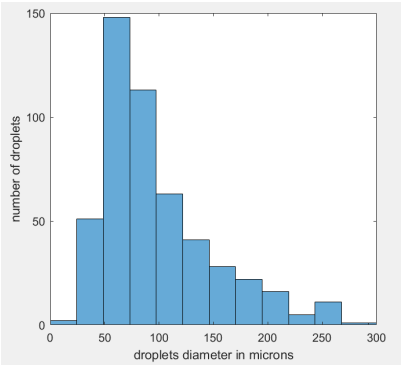

(i) Position 4, 3cm

Figure B.3: Histogram plots for experiment Ce19027,001: WC=0.2, Umix=1m/s, DP=0.35bar

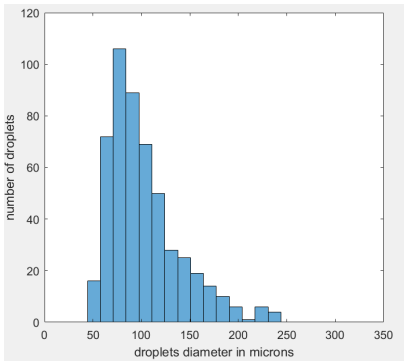

(a) Position 1, 8cm

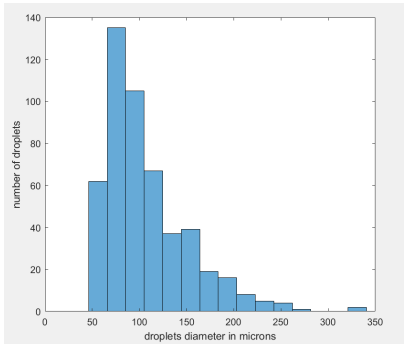

(b) Position 3,8cm

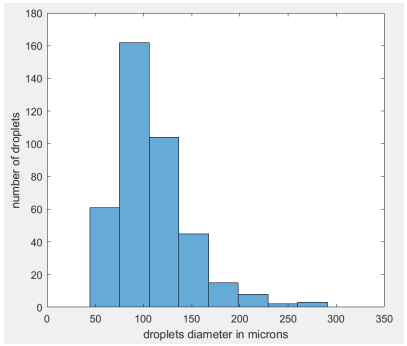

(c) Position 4, 8cm

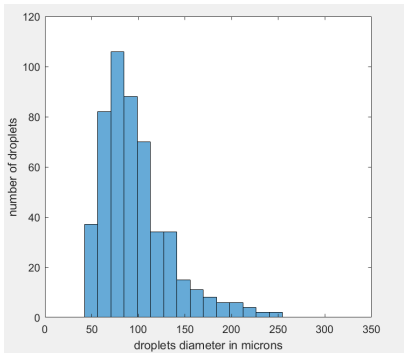

(d) Position 1, 6cm

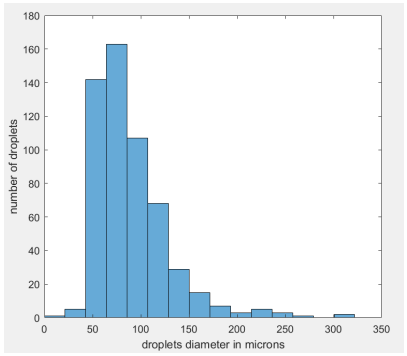

(e) Position 3,6cm

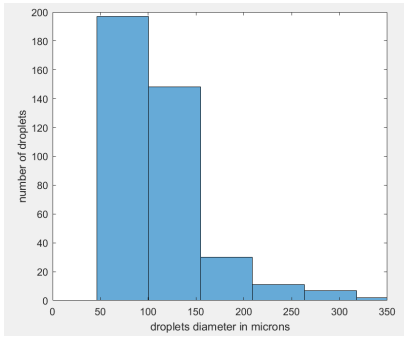

(f) Position 4, 6cm

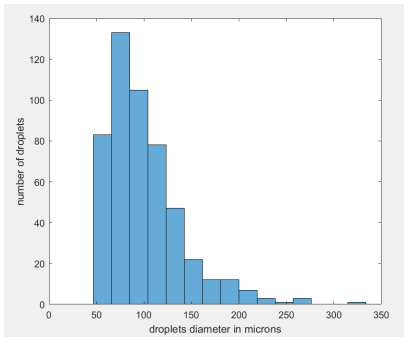

(g) Position 1, 3cm

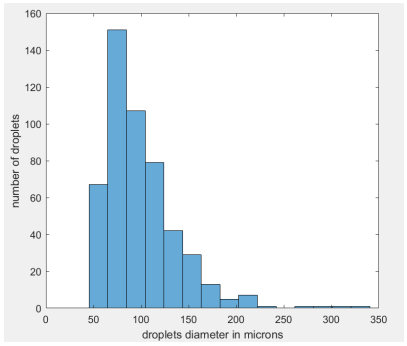

(h) Position 3,3cm

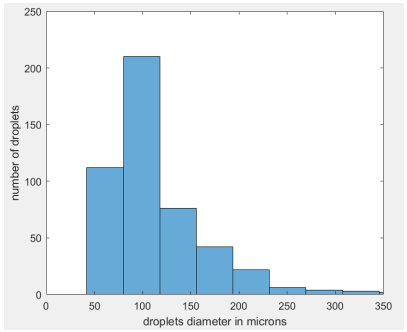

(i) Position 4, 3cm

Figure B.4: Histogram plots for experiment Ce19027,003: WC=0.2, Umix=1m/s, DP=0.5bar

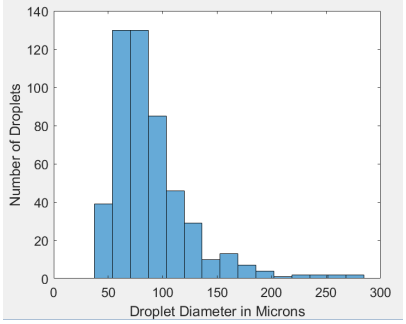

(a) Position 1, 8cm

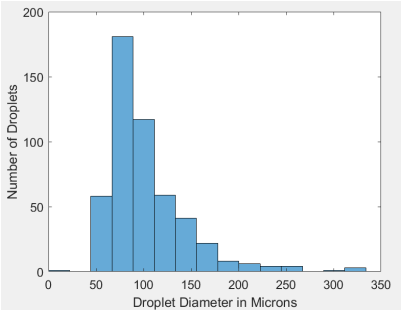

(b) Position 3,8cm

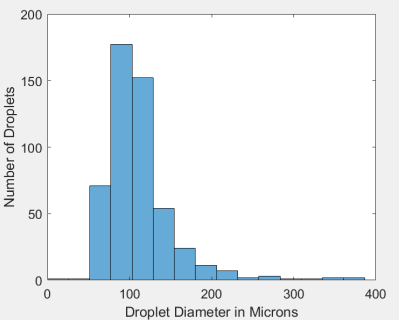

(c) Position 4, 8cm

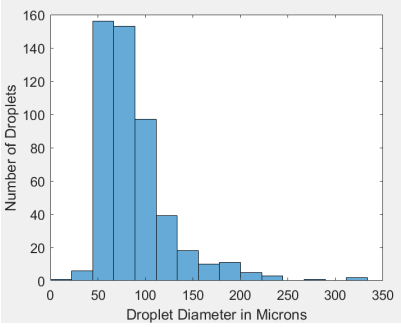

(d) Position 1, 6cm

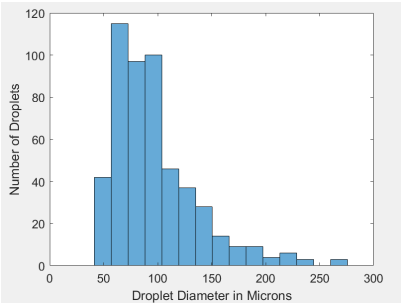

(e) Position 3,6cm

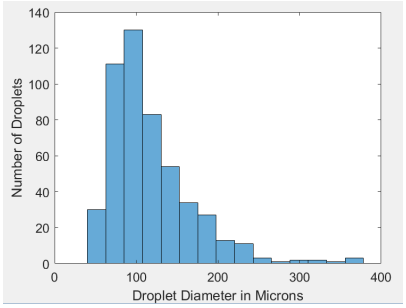

(f) Position 4, 6cm

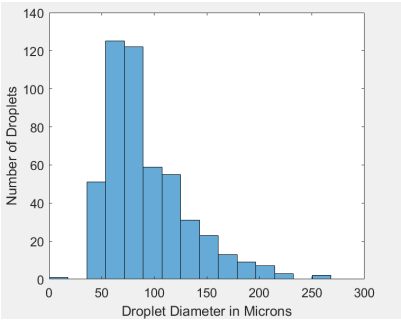

(g) Position 1, 3cm

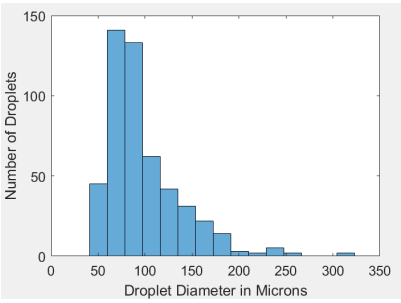

(h) Position 3,3cm

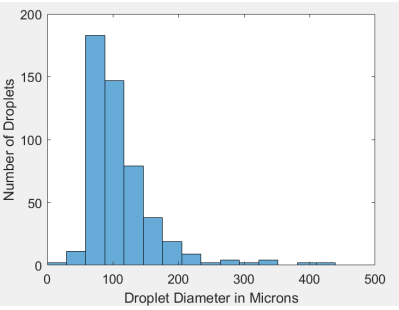

(i) Position 4, 3cm

Figure B.5: Histogram plots for experiment Ce19027,004: WC=0.2, Umix=1m/s, DP=1bar

Appendix C

Normal Distribution Plots

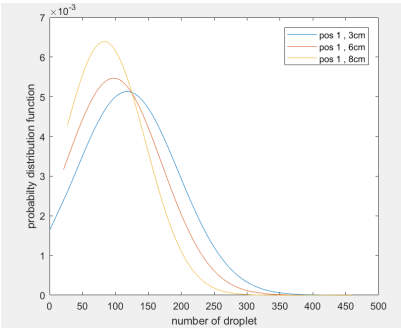

(a) Position 1 at 3,6,8cm

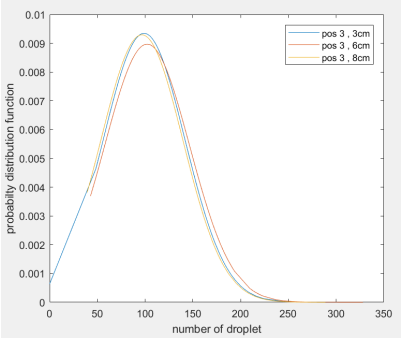

(b) Position 3 at 3,6,8cm

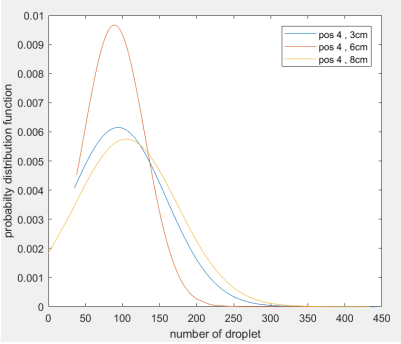

(c) Position 4 at 3,6, 8cm

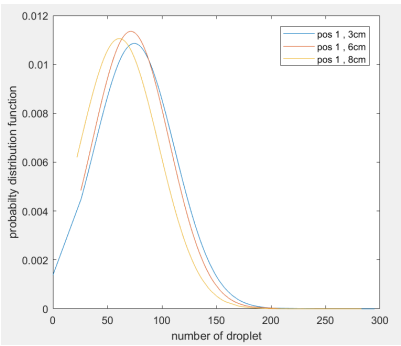

(d) Position 1 at 3,6,8cm

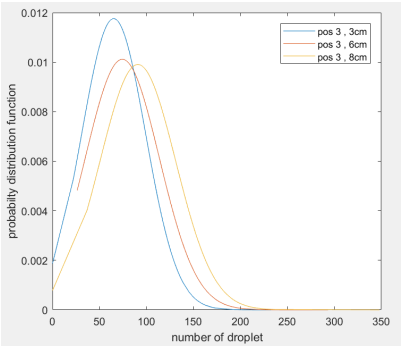

(e) Position 3 at 3,6,8cm

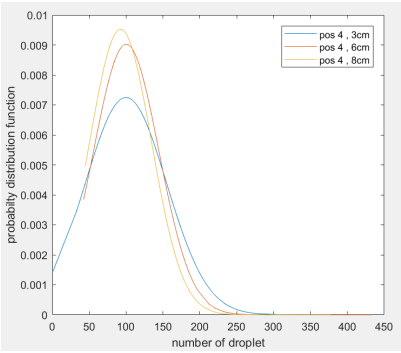

(f) Position 4 at 3, 6,8cm

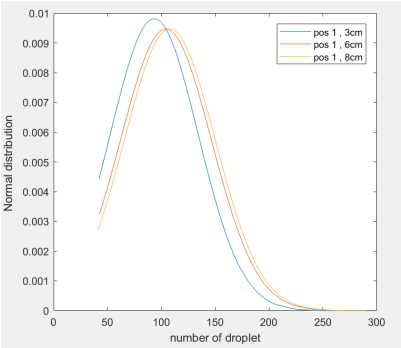

(g) Position 1 at 3, 6, 8cm

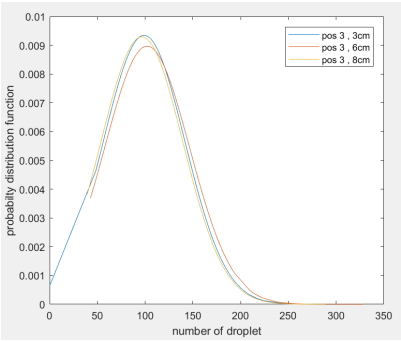

(h) Position 3 at 3,6,8cm

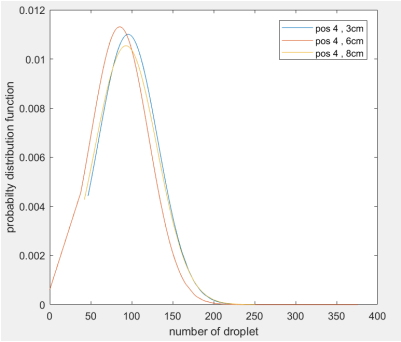

(i) Position 4 at 3, 6, 8cm

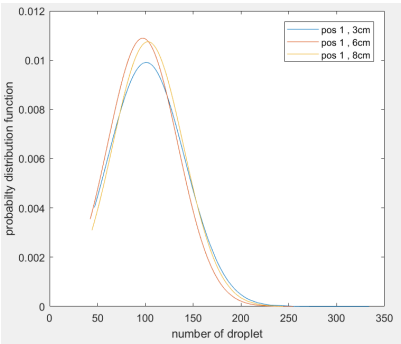

(a) Position 1 at 3,6,8cm

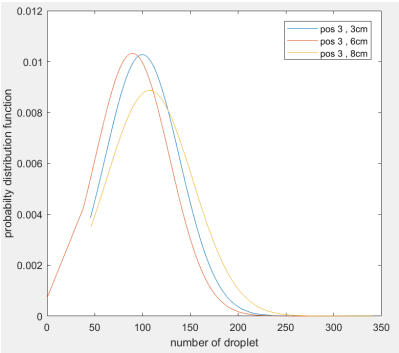

(b) Position 3 at 3,6,8cm

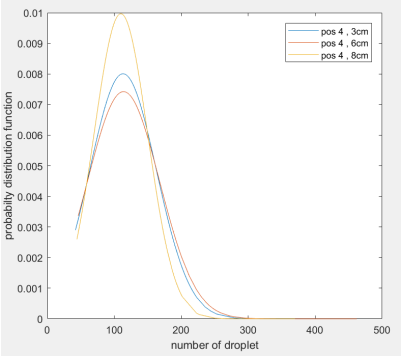

(c) Position 4 at 3,6,8cm

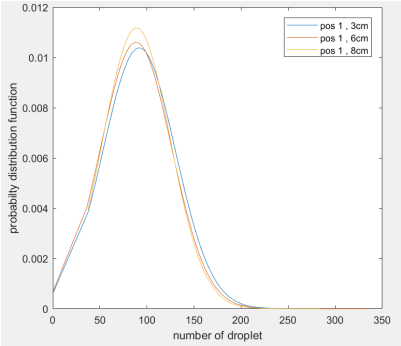

(d) Position 1 at 3,6,8cm

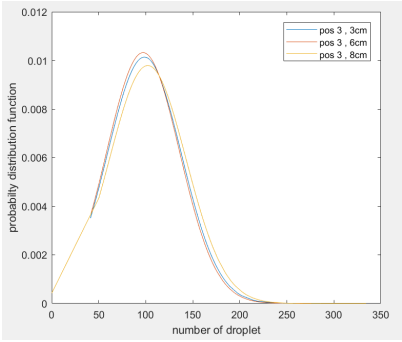

(e) Position 3 at 3,6,8cm

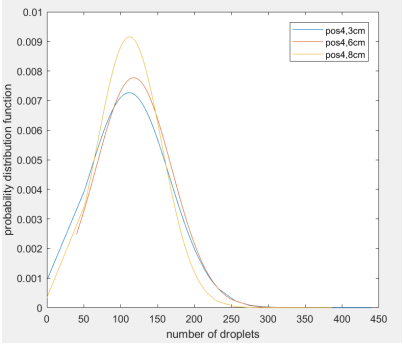

(f) Position 1 at 3,6,8cm

Figure C.2: Normal distribution plots for 0.1, 0.2, 0.35, 0.5 and 1 bar respectively

Appendix D

Matlab Codes

D.1 Three Layers flow

```
1
2 %This model model 3-layer flow consisting of a layer of pure oil, pure
3 %water and a dispersed layer in between.
4
5
6 %%%%%%%%%%%%%%%%%%%%%%%%%
7 % SINTEF DATA%%
8
9
10 %% Inputs
11 Umix=1.0;          %mixing velocity [m/s]
12 WC=0.3;            %input water fraction [-]
13 Hw=0.314666204;    %local water fraction [-]
14 D=0.1091;           %pipe diameter [m]
15 RHOoil=794.7;      %oil density [kg/m3]
16 RHOwater=999;      %water density [kg/m3]
17 MYoil=0.00143;      %oil viscosity [Pa*s]
18 MYwater=0.001;     %water viscosity [Pa*s]
19
20 Yoil=[0.05455, 0.003273];   %Position of the oil layer [Ystart, Yend]
21 Ywater=[ -0.0306727, -0.05455];%Position of the water layer [Ystart, Yend]
22
23 RElimit=2300;    %Reynoldsnumber for turbulent/laminar transition
24 eps=0.00001;     %surface roughness [m]
25
26 WCinv=0.6;       %input water fraction in dense packed layere56ir7
27
28 %% Compute the mixing viscosity at the phase inversion point (Model by Pal and Rhodes (1989))
```

```
phi100=0.765;   %dispersed phase fraction at a relative viscosity of 100
MYdisp=MYwater*((1+((0.8415*(1-WCinv)/phi100)/(1-0.8415*(1-WCinv)/phi100)))^2.5);    %we assume water continuous flow as the main part of the dispersed layer
%MYdisp=0.140;  %Set the dispersion viscosity directly
%% Computing phase areas and perimeters
R=D/2;
A=pi*R^2;
Aw=Hw*A;

%oil
h_oil=abs(Yoil(1)-Yoil(2));
Aoil=(R^2)*acos(1-h_oil/R)-(R-h_oil)*sqrt(2*R*h_oil-h_oil^2);    %Area oil
alpha_oil=2*acos(1-h_oil/R);
Poil=R*alpha_oil;    % Perimeter oil
Soildisp=2*R*sin(alpha_oil/2);  % Interface oil-dispersion

%water
h_water=abs(Ywater(1)-Ywater(2));
Awater=(R^2)*acos(1-h_water/R)-(R-h_water)*sqrt(2*R*h_water-h_water^2); %Area water
alpha_water=2*acos(1-h_water/R);
Pwater=R*alpha_water;    % Perimeter water
Swaterdisp=2*R*sin(alpha_water/2);

%dispersion
Adisp=A-Aoil-Awater;     %Area dispersion
Pdisp=pi*D-Poil-Pwater; %Perimeter dispersion

%% Pressure calculation with velocity-iterating

%Holdup test
Hwater=(Awater+Adisp*WCinv)/A;
Hoil=(Aoil+Adisp*(1-WCinv))/A;

Voil=Umix*A*(1-WC);
Vwater=Umix*A*WC;

%Initial guess
Uoil=0.0;
Udisp=(Voil-Uoil*Aoil)/(Adisp*(1-WCinv));
Uwater=(Vwater-Udisp*Adisp*WCinv)/Awater;
U=zeros(0,3);
DP_D=zeros(0,4);
DP_DH=zeros(0,4);
DP_DH_all=zeros(0,4);
Utest=zeros(0,1);
```

```
73
74 %looping through all possible velocity combinations
75 while Udisp >= Uoil %0.001
76
77     %velocities
78     Uoil=Uoil+0.001;
79     Udisp=(Voil-Uoil*Aoil)/(Adisp*(1-WCinv));
80     Uwater=(Vwater-Udisp*Adisp*WCinv)/Awater;
81     U=[U; Uoil Udisp Uwater];
82
83     %Approach by Arirachakaran(1989), friction factor by Churchill
         (1977)
84     %oil
85     REoil_D=RHOoil*Uoil*D/MYoil;                    %REoil based
         on pipe diameter
86     THETAoil1_D=(-2.457*log(((7/REoil_D)^0.9)+(0.27*eps/D)))^16;
87     THETAoil2_D=(37530/REoil_D)^16;
88     Foil_D=8*((((8/REoil_D)^12)+(1/((THETAoil1_D+THETAoil2_D)^1.5)
         ))^(1/12));   %Darcy friction factor
89     DPoil_D=(Poil/(pi*D))*(Foil_D*RHOoil*((Uoil)^2))/(2*D); %
         partial pressure gradient for the oil perimeter, based on
         REoil_D
90
91     %dispersion
92       RHOdisp=RHOwater*WCinv+RHOoil*(1-WCinv)
93 %       RHOdispsw=((RHOwater*Hw+RHOoil*(1-Hw))*Awater)/A
94 %       RHOdispsd=((RHOwater*Hw+RHOoil*(1-Hw))*Adisp)/A
95 %       RHOdispso=((RHOoil*Hw+RHOwater*(1-Hw))*Aoil)/A
96 %     RHOdisp=sum(RHOdispsw+RHOdispsd+RHOdispso)
97 %       RHOdisp=sum(RHOdisps)
98     REdisp_D=RHOdisp*Udisp*D/MYdisp;                %REdisp based
         on pipe diameter
99     THETAdisp1_D=(-2.457*log(((7/REdisp_D)^0.9)+(0.27*eps/D)))^16;
100    THETAdisp2_D=(37530/REdisp_D)^16;
101    Fdisp_D=8*((((8/REdisp_D)^12)+(1/((THETAdisp1_D+THETAdisp2_D)
         ^1.5)))^(1/12));   %Darcy friction factor
102    DPdisp_D=(Pdisp/(pi*D))*(Fdisp_D*RHOdisp*((Udisp)^2))/(2*D);%
         partial pressure gradient for the dispersion perimeter,
         based on REdisp_D
103
104    %water
105    REwater_D=RHOwater*Uwater*D/MYwater;            %REwater based
         on pipe diameter
106    THETAwater1_D=(-2.457*log(((7/REwater_D)^0.9)+(0.27*eps/D)))
         ^16;
107    THETAwater2_D=(37530/REwater_D)^16;
108    Fwater_D=8*((((8/REwater_D)^12)+(1/((THETAwater1_D+
         THETAwater2_D)^1.5)))^(1/12)); %Darcy friction factor
```

```
109     DPwater_D=(Pwater/(pi*D))*(Fwater_D*RHOwater*((Uwater)^2))/(2*
            D); %partial pressure gradient for the water perimeter,
            based on REwater_D
110
111     %Alternative computation based on the hydraulic diameter for
            oil and water as proposed by Brauner and Moalem
112     %Maron (1989). We set our condition C_DH to 20% difference in
            the layer
113     %velocities
114     C_DH=1.5;
115
116     if Uoil >= C_DH*Udisp
117         DHoil=4*Aoil/(Poil+Soildisp);
118         if Udisp >= C_DH*Uwater
119             DHdisp=4*Adisp/(Pdisp+Swaterdisp);
120             DHwater=4*Awater/Pwater;
121         elseif Uwater >= C_DH*Udisp
122             DHdisp=4*Adisp/Pdisp;
123             DHwater=4*Awater/(Pwater+Swaterdisp);
124         else
125             DHdisp=4*Adisp/Pdisp;
126             DHwater=4*Awater/Pwater;
127         end
128     elseif Udisp >= C_DH*Uoil
129         DHoil=4*Aoil/Poil;
130         if Udisp >= C_DH*Uwater
131             DHdisp=4*Adisp/(Pdisp+Soildisp+Swaterdisp);
132             DHwater=4*Awater/Pwater;
133         elseif Uwater >= C_DH*Udisp
134             DHdisp=4*Adisp/(Pdisp+Soildisp);
135             DHwater=4*Awater/(Pwater+Swaterdisp);
136         else
137             DHdisp=4*Adisp/(Pdisp+Soildisp);
138             DHwater=4*Awater/Pwater;
139         end
140     else
141         DHoil=Aoil/Poil;
142         if Udisp >= C_DH*Uwater
143             DHdisp=4*Adisp/(Pdisp+Swaterdisp);
144             DHwater=4*Awater/Pwater;
145         elseif Uwater >= C_DH*Udisp
146             DHdisp=4*Adisp/Pdisp;
147             DHwater=4*Awater/(Pwater+Swaterdisp);
148         else
149             DHdisp=4*Adisp/Pdisp;
150             DHwater=4*Awater/Pwater;
151         end
152     end
153
```

```
154     %oil_DH
155     REoil_DH=RHOoil*Uoil*DHoil/MYoil;                    %REoil based
            on DHoil
156     THETAoil1_DH=(-2.457*log(((7/REoil_DH)^0.9)+(0.27*eps/D)))^16;
157     THETAoil2_DH=(37530/REoil_DH)^16;
158     Foil_DH=8*((((8/REoil_DH)^12)+(1/((THETAoil1_DH+THETAoil2_DH)
            ^1.5)))^(1/12));    %Darcy friction factor
159     DPoil_DH=(Poil/(pi*D))*(Foil_DH*RHOoil*((Uoil)^2))/(2*D); %
            partial pressure gradient for the oil perimeter, based on
            REoil_DH
160
161     %oil_DH_all
162     THETAoil1_DH_all=(-2.457*log(((7/REoil_DH)^0.9)+(0.27*eps/
            DHoil)))^16;
163     THETAoil2_DH_all=(37530/REoil_DH)^16;
164     Foil_DH_all=8*((((8/REoil_DH)^12)+(1/((THETAoil1_DH_all+
            THETAoil2_DH_all)^1.5)))^(1/12));    %Darcy friction factor
165     DPoil_DH_all=(Poil/(pi*D))*(Foil_DH_all*RHOoil*((Uoil)^2))/(2*
            D); %partial pressure gradient for the oil perimeter, based
             on REoil_DH
166
167
168     %dispersion_DH
169     RHOdisp=RHOwater*WCinv+RHOoil*(1-WCinv);
170     REdisp_DH=RHOdisp*Udisp*DHdisp/MYdisp;                   %REdisp
            based on DHdisp
171     THETAdisp1_DH=(-2.457*log(((7/REdisp_DH)^0.9)+(0.27*eps/D)))
            ^16;
172     THETAdisp2_DH=(37530/REdisp_DH)^16;
173     Fdisp_DH=8*((((8/REdisp_DH)^12)+(1/((THETAdisp1_DH+
            THETAdisp2_DH)^1.5)))^(1/12));    %Darcy friction factor
174     DPdisp_DH=(Pdisp/(pi*D))*(Fdisp_DH*RHOdisp*((Udisp)^2))/(2*D);
             %partial pressure gradient for the dispersion perimeter,
            based on REdisp_DH
175
176     %dispersion_DH_all
177     THETAdisp1_DH_all=(-2.457*log(((7/REdisp_DH)^0.9)+(0.27*eps/
            DHdisp)))^16;
178     THETAdisp2_DH_all=(37530/REdisp_DH)^16;
179     Fdisp_DH_all=8*((((8/REdisp_DH)^12)+(1/((THETAdisp1_DH_all+
            THETAdisp2_DH_all)^1.5)))^(1/12));    %Darcy friction factor
180     DPdisp_DH_all=(Pdisp/(pi*D))*(Fdisp_DH_all*RHOdisp*((Udisp)^2)
            )/(2*D); %partial pressure gradient for the dispersion
            perimeter, based on REdisp_DH
181
182     %water_DH
183     REwater_DH=RHOwater*Uwater*DHwater/MYwater;              %
            REwater based on DHwater
```

```
184         THETAwater1_DH=(-2.457*log(((7/REwater_DH)^0.9)+(0.27*eps/D)))
                ^16;
185         THETAwater2_DH=(37530/REwater_DH)^16;
186         Fwater_DH=8*((((8/REwater_DH)^12)+(1/((THETAwater1_DH+
                THETAwater2_DH)^1.5)))^(1/12)); %Darcy friction factor
187         DPwater_DH=(Pwater/(pi*D))*(Fwater_DH*RHOwater*((Uwater)^2))
                /(2*D); %partial pressure gradient for the water perimeter,
                 based on REwater_DH
188
189         %water_DH_all
190         THETAwater1_DH_all=(-2.457*log(((7/REwater_DH)^0.9)+(0.27*eps/
                DHwater)))^16;
191         THETAwater2_DH_all=(37530/REwater_DH)^16;
192         Fwater_DH_all=8*((((8/REwater_DH)^12)+(1/((THETAwater1_DH_all+
                THETAwater2_DH_all)^1.5)))^(1/12)); %Darcy friction factor
193         DPwater_DH_all=(Pwater/(pi*D))*(Fwater_DH_all*RHOwater*((
                Uwater)^2))/(2*D); %partial pressure gradient for the water
                 perimeter, based on REwater_DH
194
195         %total pressure gradient
196         DPtotal_D=DPoil_D+DPwater_D+DPdisp_D
197         DPtotal_DH=DPoil_DH+DPwater_DH+DPdisp_DH
198         DPtotal_DH_all=DPoil_DH_all+DPwater_DH_all+DPdisp_DH_all
199
200         DP_D=[DP_D; DPoil_D DPdisp_D DPwater_D DPtotal_D];
201         DP_DH=[DP_DH; DPoil_DH DPdisp_DH DPwater_DH DPtotal_DH];
202         DP_DH_all=[DP_DH_all; DPoil_DH_all DPdisp_DH_all
                DPwater_DH_all DPtotal_DH_all];
203
204         Utest=[Utest; (Aoil*Uoil+Adisp*Udisp+Awater*Uwater)/A];
205
206 end
207
208 figure;
209 plot(U);
210 legend('Uoil', 'Udisp', 'Uwater');
211 ylabel('U [m/s]');
212 title('U');
213
214 figure;
215 plot(DP_D);
216 legend('DPoil', 'DPdisp', 'DPwater', 'DPtotal');
217 ylabel('DP [Pa/m]');
218 title('DP_D');
219
220 figure;
221 plot(DP_DH);
222 legend('DPoil', 'DPdisp', 'DPwater', 'DPtotal');
223 ylabel('DP [Pa/m]');
```

```
224 title('DP_D_H');
225
226 figure;
227 plot(DP_DH_all);
228 legend('DPoil', 'DPdisp', 'DPwater', 'DPtotal');
229 ylabel('DP [Pa/m]');
230 title('DP_D_H_a_l_l');
231
232 figure;
233 plot(Utest);
```

D.2 Two fluid Simple

```
1  % Simple two phase flow model to compute the presure gradient
       based on
2  % knowing mix, WC and Hw
3
4  %% inputs
5  Umix=1.0;          %mixing velocity [m/s]
6  WC=0.75;           %input water fraction [-]
7  hw=-3.32281;           %position of the interface [m]-I correceted
       this from the local water fraction to position of the interface
8  D=0.1091;          %pipe diameter [m] *(0.1091)
9  RHOoil=850;        %oil density [kg/m3] (2018-780, 2019-850)
10 RHOwater=990 ;     %water density [kg/m3]
11 MYoil=0.035;       %oil viscosity [Pa*s] *(adjust the viscosity to
       0.035-2019, 2018-0.0014)
12 MYwater=0.001;     %water viscosity [Pa*s]
13
14 RElimit=2300;      %Reynoldsnumber for turbulent/laminar transition
15 eps=0.00001;       %surface roughness [m] (
16
17 %% Model by Arirachakaran (1989)
18 % The model uses simple perimeter fractions occupied by the phases
       to
19 % compute the proportions each phase is contributing to the total
       pressure
20 % gradient.
21
22 %% phase velocities Uoil and Uwater
23 Uoil=Umix*(1-WC)/(1-hw);
24 Uwater=Umix*WC/hw;
25
26 %% Computing the center-perimeter angle alpha
27 R=D/2;
28 A=pi*R^2;
29 Aoil=A*(1-hw);
```

```
30 Awater=A*hw;
31
32 %solving nonlinear equation
33 syms alpha
34 f=((R^2)/2)*(alpha-sin(alpha))-Aoil;
35 soln=solve(f,alpha);
36 solnvalue=double(soln);
37 alpha=solnvalue;
38
39 %% Computing the oil and water perimeters Poil and Pwater and the
       interface Pinter
40 Poil=R*alpha;
41 Pwater=R*(2*pi-alpha);
42 Pinter=2*R*sin(alpha/2);
43
44 %% Hydraulic diameter for oil and water as proposed by Brauner and
       Moalem Maron (1989). We set our condition to 20% difference in
       the oil and water velocities
45 if Uoil >= 1.2*Uwater
46     DHoil=4*Aoil/(Poil+Pinter);
47     DHwater=4*Awater/Pwater;
48     PO=(Poil+Pinter);
49     PW=Pwater;
50 elseif Uwater>= 1.2*Uoil
51     DHoil=4*Aoil/Poil;
52     DHwater=4*Awater/(Pwater+Pinter);
53     option=2;
54     PO=Poil;
55     PW=(Pwater+Pinter);
56 else
57     DHoil=4*Aoil/Poil;
58     DHwater=4*Awater/Pwater;
59     option=3;
60     PO=Poil;
61     PW=Pwater;
62 end
63
64 %% Computing oil and water Reynolds numbers
65 REoil_DH=RHOoil*Uoil*DHoil/MYoil;              %based on
       hydraulic diameter
66 REwater_DH=RHOwater*Uwater*DHwater/MYwater;    %based on
       hydraulic diameter
67
68 REoil_D=RHOoil*Uoil*D/MYoil;                   %based on pipe
       diameter
69 REwater_D=RHOwater*Uwater*D/MYwater;          %based on pipe
       diameter
70
```

```
71 %% Check if turbulent/laminar flow (RElimit=2000) and compute oil
       and water pressure gradients
72 %here not needed as we use the Churchill equation
73
74 %% Compute oil and water pressure gradients directly with the
       Chruchill equation valid for laminar and turbulent flow:
       Churchill (1977)
75
76 %oil with REoil_DH
77 THETAoil1_DH=(-2.457*log(((7/REoil_DH)^0.9)+(0.27*eps/D)))^16;
78 THETAoil2_DH=(37530/REoil_DH)^16;
79 Foil_DH=8*((((8/REoil_DH)^12)+(1/((THETAoil1_DH+THETAoil2_DH)^1.5)
       ))^(1/12)); %Darcy friction factor
80 DPoil_DH=(Poil/(pi*D))*(Foil_DH*RHOoil*((Uoil)^2))/(2*D); %partial
        pressure gradient for the oil perimeter, based on REoil_DH
81
82 %water with REwater_DH
83 THETAwater1_DH=(-2.457*log(((7/REwater_DH)^0.9)+(0.27*eps/D)))^16;
84 THETAwater2_DH=(37530/REwater_DH)^16;
85 Fwater_DH=8*((((8/REwater_DH)^12)+(1/((THETAwater1_DH+
       THETAwater2_DH)^1.5)))^(1/12)); %Darcy friction factor
86 DPwater_DH=(Pwater/(pi*D))*(Fwater_DH*RHOwater*((Uwater)^2))/(2*D)
       ; %partial pressure gradient for the water perimeter, based on
       REwater_DH
87
88 %Original Arirachakarn approach with D instead of DH
89
90 %oil with REoil_D
91 THETAoil1_D=(-2.457*log(((7/REoil_D)^0.9)+(0.27*eps/D)))^16;
92 THETAoil2_D=(37530/REoil_D)^16;
93 Foil_D=8*((((8/REoil_D)^12)+(1/((THETAoil1_D+THETAoil2_D)^1.5)))
       ^(1/12)); %Darcy friction factor
94 DPoil_D=(Poil/(pi*D))*(Foil_D*RHOoil*((Uoil)^2))/(2*D); %partial
       pressure gradient for the oil perimeter, based on REoil_D
95
96 %water with REwater_D
97 THETAwater1_D=(-2.457*log(((7/REwater_D)^0.9)+(0.27*eps/D)))^16;
98 THETAwater2_D=(37530/REwater_D)^16;
99 Fwater_D=8*((((8/REwater_D)^12)+(1/((THETAwater1_D+THETAwater2_D)
       ^1.5)))^(1/12)); %Darcy friction factor
100 DPwater_D=(Pwater/(pi*D))*(Fwater_D*RHOwater*((Uwater)^2))/(2*D);
       %partial pressure gradient for the water perimeter, based on
       REwater_D
101
102 %% Total pressure gradient
103
104 DPtotal_DH=DPoil_DH+DPwater_DH      %based on DH
105 DPtotal_D=DPoil_D+DPwater_D         %based on D
106
```

```
107 %% Alternative with DH also for computing the friction factor
108
109 %oil with REoil_DH and DH
110 THETAoil1_DH_all=(-2.457*log(((7/REoil_DH)^0.9)+(0.27*eps/DHoil)))
    ^16;
111 THETAoil2_DH_all=(37530/REoil_DH)^16;
112 Foil_DH_all=8*((((8/REoil_DH)^12)+(1/((THETAoil1_DH_all+
    THETAoil2_DH_all)^1.5)))^(1/12)); %Darcy friction factor
113 DPoil_DH_all=(Poil/(pi*D))*(Foil_DH_all*RHOoil*((Uoil)^2))/(2*D);
     %partial pressure gradient for the oil perimeter, based on
    REoil_DH
114
115 %water with REwater_DH and DH
116 THETAwater1_DH_all=(-2.457*log(((7/REwater_DH)^0.9)+(0.27*eps/
    DHwater)))^16;
117 THETAwater2_DH_all=(37530/REwater_DH)^16;
118 Fwater_DH_all=8*((((8/REwater_DH)^12)+(1/((THETAwater1_DH_all+
    THETAwater2_DH_all)^1.5)))^(1/12)); %Darcy friction factor
119 DPwater_DH_all=(Pwater/(pi*D))*(Fwater_DH_all*RHOwater*((Uwater)
    ^2))/(2*D); %partial pressure gradient for the water perimeter,
     based on REwater_DH
120
121 DPtotal_DH_all=DPoil_DH_all+DPwater_DH_all
122
123 %The difference is very small for the friction factor. It is more
    important that the Reynolds
124 %number is based on the hydraulic diameter.
```

D.3 Histograms, Normal distribution and Mean Sizes

```
1  %loadin g the data
2  Data = xlsread ('C:\Users\rehem\Desktop\NTNU\Thesis\doplets\
     ce19027,000\4,8cm\results.csv');
3  A = Data(:,7);
4  int=(max(A)-min(A))/15;
5  bins=min(A):int:max(A);
6  % B=bins
7  % d32=sum(A.^3)/sum(A.^2)
8
9
10 figure(1)
11 histogram (A, bins)
12 % title('Cart esian Histogram ? Pos 1 ,3cm ')
13 xlabel('Droplet Diameter in Microns')
14 ylabel('Number of Droplets')
15 set (gca,'FontSize',12)
16
```

```
Mnot1=xlsread('C:\Users\rehem\Desktop\NTNU\Thesis\doplets\cw192027,004\4,3cm\4,3.csv')
M1=sort(Mnot1(:,7));
mu1=mean(M1)
sd1=std(M1)
X=normpdf(M1,mu1,sd1)
plot(M1,X)

hold on
Mnot2= xlsread ('C:\Users\rehem\Desktop\NTNU\Thesis\doplets\cw192027,004\4,6cm\4,6.csv')
M2=sort (Mnot2(:,7))
mu2=mean(M2)
sd2=std(M2)
X2=normpdf(M2,mu2,sd2)
plot(M2,X2)
%%
Mnot3=xlsread('C:\Users\rehem\Desktop\NTNU\Thesis\doplets\cw192027,004\4,8cm\4,8.csv')
M3=sort(Mnot3(:,7))
mu3=mean(M3)
sd3=std(M3)
X3=normpdf(M3,mu3,sd3 )
plot(M3,X3)
legend('pos4,3cm','pos4,6cm','pos4,8cm')
% title('Normal distribution curve')
xlabel('number of droplets')
ylabel ('probability distribution function')
```

NTNU
Norwegian University of
Science and Technology